PEOPLE'S DEMOCRATIC REPUBLIC OF ALGERIA

Ministry Of Higher Education and Scientific Research

University Larbi Ben M'hidi-Oum El Bouaghi-

Faculty of Sciences and Applied Sciences.

Department of Mechanical Engineering.

Specialty: Mechanical energetic Engineering.

Thesis Submitted in Fulfillment of the Requirements for the Degree of PhD.

Entitled:

NUMERICAL STUDY OF THE COMBUSTION OF LOW CALORIFIC VALUES (LCV) GAS MIXTURES

Submitted by: BOUSSETLA Salsabil

Committee members:

Prof. Rahmani Ahmed	University Oum El Bouaghi	President
Prof. Mameri Abdelbaki	University Oum El Bouaghi	Supervisor and reporter
Dr. Hadef Amar	University Oum El Bouaghi	Co-Supervisor
Prof. Aouachria Zeroual	University Batna 1	Examinator
Prof. Adouane Belkacem	University Batna 1	Examinator
Dr. Bouzid Sihem	University Oum El Bouaghi	Examinator

Defended the 16/01/2022

Abstract

The present study is designed to prevent pollution and to improve emission control technologies, it aims to reduce combustion pollutants especially CO_2 and NOx. The CO_2 can be avoided by using a biofuel that is neutral in terms of CO_2 emission. Whereas, the NOx emissions can be reduced by decreasing the combustion temperature. This is can be granted by the flameless combustion regime.

In this study, the effect of fuel mixture composition, oxygen concentration in oxidizer, injection velocity or strain rate, oxidizer temperature and pressure on the flame structure and emissions of the non-premixed MILD "Moderate or Intense Low-oxygen Dilution" combustion of the biogas-syngas mixture are simulated. NO emission from MILD combustion is deeply elucidated, five NO routes were considered, specifically: thermal, prompt, NNH, N_2O and reburning. Biogas is modeled by a mixture of methane and carbon dioxide; while, syngas is considered to be composed by hydrogen and carbon monoxide, this gives a fuel mixture of $CH_4/CO_2/H_2/CO$. Volume of methane and hydrogen are varied alternatively from 0% to 50% in fuel mixture. Oxidizer is composed by O_2/N_2 mixture where oxygen volume is increased from 4% to 21%. Injection strain rate is varied from apparition to vanishment of combustion. Injection temperature for oxidizer is varied from 900 K to 1500 K while for fuel is kept constant temperature of fuel equal to 300K. Finally, the ambient pressure varies from 1atm to 10 atm. Chemical kinetics of such complicated system is handled by a composed mechanism from the USC C_1-C_4 and the Gri 2.11 N-sub mechanism. The Chemkin software is used to achieve the computations.

Résumé

La présente étude a pour but de lutter contre la pollution et d'améliorer les technologies de contrôle des émissions, elle vise à minimiser les émissions nocives issues de la combustion ; particulièrement le CO_2 et les NOx. Le CO_2 peut être évité en utilisant un biofuel qui est neutre en termes de CO_2. Quant aux NOx peut être réduit en réduisant la température de la combustion, cela est garanti par le régime de combustion sans flammes.

Dans cette étude, l'effet de la composition du mélange combustible, de la concentration d'oxygène dans le comburant, de la vitesse d'injection ou du taux d'étirement, de la température d'injection de l'oxydant et de la pression sur la structure de la flamme et les émissions de la combustion non-prémélangée dans le régime MILD "Moderate or Intense Low-oxygen Dilution" du mélange biogaz-syngaz sont simulés. Les émissions d'oxydes d'azote de la combustion MILD sont profondément élucidées, cinq voies de formation de NO ont été considérées, en particulier : thermique, précoce, NNH, N_2O et reburning. Le biogaz est composé de méthane et de dioxyde de carbone ; alors que le syngaz est composé de monoxyde de carbone et de l'hydrogène, cela donne un mélange de combustible de $CH_4/CO_2/H_2/CO$. Les volumes de méthane et d'hydrogène varient alternativement de 0% à 50 % dans le mélange combustible. L'oxydant est composé d'un mélange O_2/N_2 où le volume d'oxygène est varié de 4% à 21 %. Le taux d'étirement est de l'apparition à la disparition de la combustion. La température d'injection de l'oxydant est variée de 900 K à 1500 K, celle de fuel est gardée constante et égale à 300K. Finalement, la pression ambiante varie de 1 atm à 10 atm. La cinétique chimique de ce système compliqué est décrite par un mécanisme composé de l'USC C_1-C_4 et du mécanisme Gri 2.11 N-sub. Le logiciel Chemkin est utilisé pour réaliser les calculs.

الملخص

تهدف هذه الدراسة لمكافحة التلوث وتحسين تقنيات التحكم في الانبعاثات، وتهدف إلى الحد من ملوثات الاحتراق خاصة ثاني أكسيد الكربون وأكاسيد النيتروجين. يمكن تجنب ثاني أكسيد الكربون باستخدام وقود حيوي محايد من حيث انبعاث ثاني أكسيد الكربون. بينما يمكن تقليل انبعاثات أكاسيد النيتروجين عن طريق خفض درجة حرارة الاحتراق. يمكن ضمان ذلك من خلال نظام الاحتراق الخالي من اللهب.

في هذه الدراسة، يتم محاكاة تأثير تركيب خليط الوقود، تركيز الأكسجين في المؤكسد، سرعة الحقن أو معدل الإجهاد، درجة حرارة المؤكسد والضغط على هيكل اللهب والانبعاثات للاحتراق الغير المخلوط مسبقًا والمخفف بالأكسجين المنخفض (المعتدل أو المكثف) لخليط الغاز الحيوي والغاز التخليقي. تم توضيح انبعاثات NO من الاحتراقMILD بشكل عميق، وتم النظر في خمسة مسارات لتشكيلNO، و بالتحديد: حراري، سريع، N_2O، NNH وإعادة الاحتراق. يتكون الغاز الحيوي من خليط الميثان وثاني أكسيد الكربون بينما الغاز التخليقي يتكون من الهيدروجين وأول أكسيد الكربون، وهذا يعطي خليط وقود مكون من CH_4 / CO_2 / H_2 / CO. يتغير حجم الميثان والهيدروجين بالتناوب من 0٪ إلى 50٪ في خليط الوقود. يتكون المؤكسد من خليط O_2/N_2 حيث يتغير حجم الأكسجين من 4 ٪ إلى 21٪. يتغير معدل إجهاد الحقن من ظهور إلى اختفاء الاحتراق. تتراوح درجة حرارة الحقن للمؤكسد من 900K إلى 1500K بينما يتم الاحتفاظ بدرجة حرارة ثابتة للوقود تساوي 300K. اخبرا، يتراوح الضغط المحيط من 1atm إلى 10atm. يتم وصف الحركية الكيميائية لهذا النظام المعقد بواسطة آلية مركبة تتكون من USC C_1-C_4 و Gri 2.11 N-sub. يستخدم برنامج Chemkin لإجراء الحسابات.

.

Table of Contents

List of Tables

List of Figures

Acknowledgements

Alhamdulillah, thank you Allah for all the blessing You had given me. The ability, courage, endurance, and patience You put inside me strengthening me in completing this study and research.

Firstly, I would like to express my special appreciation and thanks to my patient and supportive supervisor, Professor MAMERI Abdelbaki, you have been a tremendous mentor for me. I would like to thank you for encouraging my research and for allowing me to grow as a research scientist. Your advice on both research as well as on my career have been invaluable. Your wide knowledge and your logical way of thinking have been of great value for me.

I would also like to thank Dr. HADEF Amar for his instructions and pieces of advices throughout this research project.

My sincere thanks must also go to the members of my thesis advisory and exam committee: Professors Rahmani Ahmed, Aouachria Zeroual, Adouane Belkacem and Doctor Bouzid Sihem. They generously gave their time to offer me valuable comments toward improving my work.

A special thanks to my family for their continuous and unparalleled love, help and support. I am forever indebted to my parents for giving me the opportunities and experiences that have made me who I am. They selflessly encouraged me to explore new directions in life and seek my own destiny. This journey would not have been possible if not for them, and I dedicate this milestone to them. Finally, I have to thank my husband for keeping things going and for always showing how proud he is of me.

Nomenclature

a	Strain rate	s^{-1}
a_i	Planck mean coefficient for species i	
C	Total molar concentration	mol/m^3
C_k	Molar concentration of species k	mol/m^3
c_p	Heat capacity at constant pressure	J/kg.K
c_{p_k}	Heat capacity of species k at constant pressure	J/kg.K
c_v	Specific heat at constant volume	J/kg.K
d	Distance between the ducts	cm
D_k^H	Binary diffusion coefficient of k^{th} species in the mixture	m^2/s
D_{kj}	Binary diffusion coefficient	m^2/s
$D_{T,k}$	Thermal diffusion factor of k^{th} species in the mixture	m^2/s
$D_{T,kj}$	Thermal diffusion factor	m^2/s
E_i	Activation energy	J/mol
e	Specific internal energy	J/kg
f_k	External force per unit mass	N/kg
g	Relative velocity	m/s
H	Enthalpy of mixture	J
H_k	Molar enthalpy of species k	J/mol
H_P	Enthalpy of products	J
H_R	Enthalpy of reactants	J
h	Specific enthalpy of mixture	J/kg
$\overline{h_{f,k}^0}$	Enthalpy of formation of species k	J/mol
h_{fg}	Latent heat of vaporization	J/kg
h_k	Specific enthalpy of species k	J/kg
I	Unit matrix	
J	Number of chemical reactions in the reaction mixture	
k_B	Boltzmann constant	J/K
k_e	Equilibrium constant	

k_f	Rate constant for forward reaction	cm^3/mol.s
k_r	Rate constant for reverse reaction	cm^3/mol.s
m	Total mass	kg
m_k	Mass of species k	kg
m_{ki}^0	Initial mass of species k in reaction i	kg
m_{ki}	Mass of species k in reaction i	kg
N	Number of species in the reacting mixture	
n	Total number of moles	mol
n_k	Number of moles of species k	mol
n_k^0	Initial number of mole of species k	mol
$\bar{P}$	Pressure tensor	Pa
p	Pressure	Pa
p_{atm}	Atmospheric pressure	Pa
p_k	Partial pressure	Pa
q	Heat flux	W/m^2
Q_p	Heat of reaction at the constant pressure	J
Q_V	Heat of reaction at the constant volume	J
$\dot{Q}_r$	Radiative heat flux	W/m^2
R	Universal gas constant	J/mol.K
T	Temperature	K
T_{ad}	Adiabatic flame temperature	K
T_f	Far-field temperature	K
T_i	Activation temperature of ith reaction	K
T_{init}	Initial temperature	K
T_m	Intermediate temperature	K
T_0	Reference temperature	K
T_r	Temperature of the radiating substance	K
S_k	Molar entropy of species k	J/K.mol
s	Specific entropy of mixture	J/K.kg
s_k	Specific entropy of species k	J/K.kg

u	Axial velocity	m/s
v	Radial velocity	m/s
V	Velocity vector	m/s
V_T	Total volume of the mixture	m^3
V_{D_k}	Diffusion velocity of species k	m/s
v_c	Correction velocity	m/s
v_k	Ordinary diffusion vector	m/s
W	Molar mass of the mixture	kg/mol
W_k	Molar mass of species k	kg/mol
W_{kj}	Reduced mass of pair (k, j)	kg/mol
w_k	Thermal diffusion vector	m/s
$\dot{\omega}_k$	Mass production rate of species k	$kg/s.m^3$
$\dot{\omega}_{ki}$	Mass production rate of species k in reaction i	$kg/s.m^3$
X_k	Molar fraction of species k	
Y_k	Mass fraction of species k	

Greek symbols

γ'_{ki} , γ''_{ki}	Stoichiometric coefficients of k^{th} species in the i^{th} reaction	
λ	Thermal conductivity of mixture	W/m.K
λ_k	Thermal conductivity of mixture of species k	W/m.K
ν	Kinematic viscosity coefficient of mixture	m^2/s
ν_k	Kinematic viscosity coefficient of species k	m^2/s
ξi	Degree of advancement of reaction i	
Π	Viscous stress tensor	m^2/s^2
ρ	Volumetric mass density	kg/m^3
ρ_k	Density of species k	kg/m^3
σ_k	Collision diameter of interaction potential de Lennard-Jones	m
σ_{kj}	Diameter of species pair (k, j)	m
χ	Deflection angle of two molecules k and j after collision	
$\Omega^{(l,s)^*}$	Reduced collision integral	

Introduction

In the 19th century, and even more in the 20th century, combustion had many industrial applications (transportation, heating, industrial production, electricity production). However, it leads to a significant emission of various pollutants harmful to humans and nature, such as carbon oxides COx (CO, CO_2), sulfur oxides SOx (SO_2), nitrogen oxides NOx (NO and NO_2), unburned hydrocarbons and soot particles. Of these pollutants, NOx is increasingly subject to regulations as emissions of nitrogen oxides in the atmosphere pose serious health and environmental concerns. Indeed, emissions of nitrogen oxides cause respiratory problems for human beings and are the cause of acid rain, the formation of ground-level ozone resulting from photolysis of NO_2 ($NO_2 + hv = NO + O$ then $O + O_2 = O_3$) and the destruction of the ozone layer. A growing global population has amplified these effects, and this induced an increase in the consumption of fossil fuels and a reduction in the world stock. Two preventive alternatives exist: reduce the consumption of fossil fuels, and/or use alternative fuels containing a fewer carbon atoms, such as biomass fuels, particularly “biogas production”, or methane-hydrogen mixtures, or even hydrogen pure. Indeed, the only product of hydrogen combustion is water vapor. The use of hydrogen in combustion plants would significantly reduce greenhouse gas emissions, in the event that it is produced without carbon dioxide emissions. In recent years, studies have considered the use of syngas as a source of hydrogen. Indeed, syngas is a mixture of combustible gases consisting principally of hydrogen and carbon monoxide.

Fuel consumption can be significantly reduced by recovering the energy from the fumes to preheat the combustion air. However, preheating the combustion air leads to an increase in the adiabatic flame temperature and consequently higher nitrogen oxide emissions. Staged combustion (air or fuel staged combustion) is used to reduce NOx emissions through combustion zones that are generally at lower temperatures. For air staging, secondary injection is carried out in the downstream region of the first maximum temperature. In the case of fuel staging, the secondary fuel injection leads to an attack of nitrogen oxides by hydrocarbon radicals. The staged combustion allows the dilution of reactants before interacting. The radiation from the reaction zone becomes negligible compared to that from the walls of the furnace. That is why this regime is

called flameless combustion (or dilute combustion). In this configuration, NOx emissions are very low.

In industrial furnaces with high wall temperatures, the burners operating in flameless or MILD (Moderate or Intense Low-oxygen Dilution) combustion regime have shown a high efficiency in terms of energy efficiency, reduction in fuel consumption and pollutant emissions. This very specific combustion regime is achieved by using an original configuration of regenerative burner inducing very homogeneous combustion with very low nitrogen oxides. Many researches have been conducted to contribute to a better understanding this combustion regime.

The thesis presented here focuses on the study of the MILD combustion regime, carried out within the framework of the project "MILD combustion of the LCV fuels mixtures". The aim of this study is to investigate numerically the effect of (1) the composition, (2) the oxygen concentration, (3) the strain rate, (4) the oxidizer temperature and (5) the pressure on combustion structure and NO emission characteristics of laminar diffusion combustion of biogas (CH_4+CO_2)-syngas (H_2+CO) mixture. The opposed jet configuration is adopted. Several compositions, oxygen dilution level in the oxidizer stream, injection velocities, inlet temperatures and pressures are considered. Three chemical kinetic models, GRI-Mech 2.11, GRI-Mech 3.0 and USC-GRI-Mech 2.11 are examined. The USC-GRI-Mech 2.11 mechanism is found to agree best with the experimental data. The Chemkin code is used to achieve the computations.

This thesis is divided into six chapters:

- In the first chapter, the definitions and the basic concepts of the renewable energy sources, flameless combustion and a synthesis of the work were presented;
- The second chapter concerns the kinetics of NO formation in flames. The different NO formation pathways during combustion will be recalled before describing the detailed kinetic mechanisms used in this thesis, then the modeling tools used;
- In the third chapter, the technology known as Flameless Combustion will be discussed in more detail. In particular, we will focus on its different definition proposed in the literature and its characteristics;

- In the fourth chapter, definition, Characteristics and geometry of opposed-jet diffusion flame will be presented. The equations describing the gas reactive flows and some parameters used in combustion studies will be recalled;
- The fifth chapter is devoted to numerical simulation and interpretation of results;
- In the sixth and final chapter, the main conclusions from this work will be presented and explained.

Chapter I

Literature review

I.1. Energy overview

The history of humanity's existence and energy are inseparable. Initially, energy needs were modest and principally used for heating, cooking food, lighting…etc. After the industrial revolution, developing societies quickly began using other forms of energy. Mainly, to replace the human and animal force for building, transportation of various materials, movement, agriculture....

Until the end of 18th century, wood and plants represent the world's most-used energy sources, followed by human and animal power, hydraulics, and wind power. However, this development was not sustainable because it led to deforestation, which was avoided in Europe after the discovery of coal. With the industrial age, the introduction of machines has led to population growth and energy demand increase.

In the middle of the 19th century, the industrial revolution spread in the world by using machines and exploitation of new forms of energy such as steam energy (related to fire), electricity and fossil fuels (including coal, oil and natural gas). The latter is used to design autonomous vehicles transporting their energy source (locomotive, then cars and aircraft). In the second half of the 20th century, oil became the main source of energy, followed by natural gas. At the same time, nuclear energy and renewable energies have been developed.

However, at the dawn of the twenty-first century, the majority of primary energy comes from non-renewable energy stocks that are responsible for significant carbon dioxide emissions (**figure I.1**) [1]. Only 15.7% of primary energy comes from low-carbon sources. Among these low-carbon sources, 11.4% comes from renewable energies: hydropower (6.4%), wind power (2.2%), solar (1.1%), biofuels (0.7%) and other renewables (0.9%). The rest of low-carbon sources comes from nuclear (4.3%).

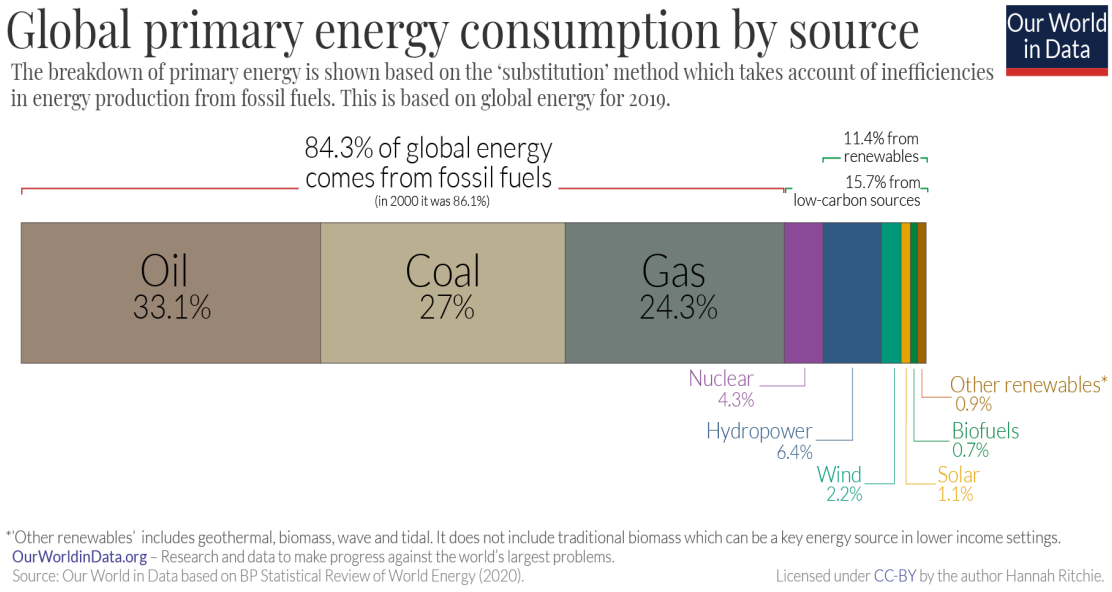

Fig. I.1: Global primary energy consumption by source [1]

I.2. Energy consumption and environmental impacts

From the beginning of 20th century until the present day, energy needs increase is almost exponential. Electricity has become the essential source for industrial and domestic uses. Fossil fuels are widely used despite their negative consequences on human health and the environment due to their harmful emissions, such as carbon dioxide (CO_2), sulphur oxides (SO_x), nitrogen oxides (NO_x) and other pollutants. Global energy demand in 2019 has increased by less than half the rate of growth in 2018, well below the average rate since 2010. This deceleration was due mainly to slower global economic growth and the impact of milder weather on heating and cooling (**Figure I.2**). There was, however, significant variation across energy sources, with coal showing an absolute decline and renewables a record increase. Electricity demand grew at the slowest rate since the financial crisis. Energy efficiency continued to improve but at levels well below those needed to meet the Sustainable Development Goals (**Figure I.3**).

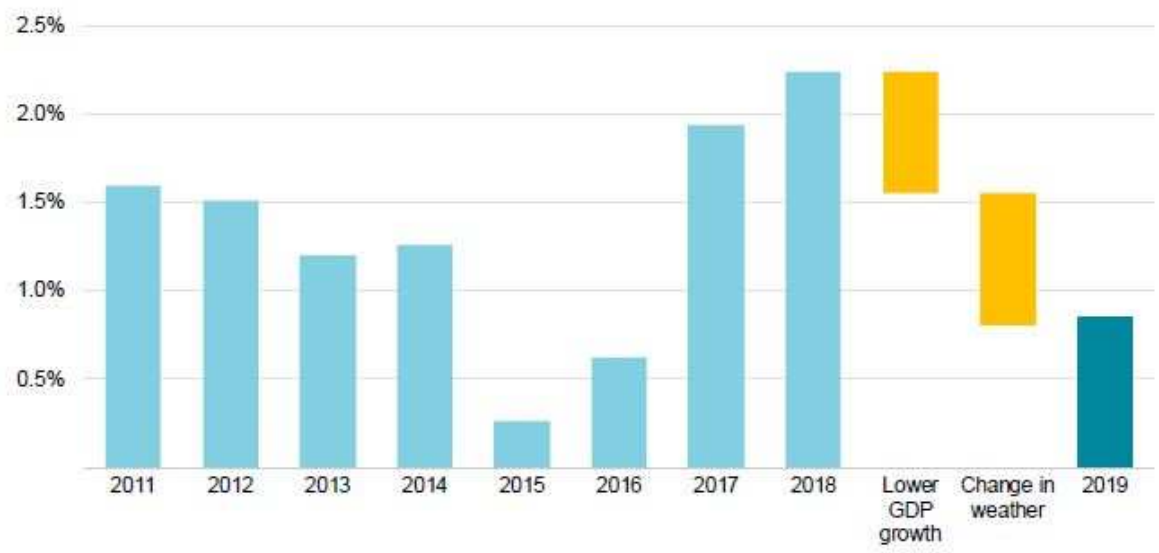

Fig. I.2: World energy demand growth rate, 2011-19 [2]

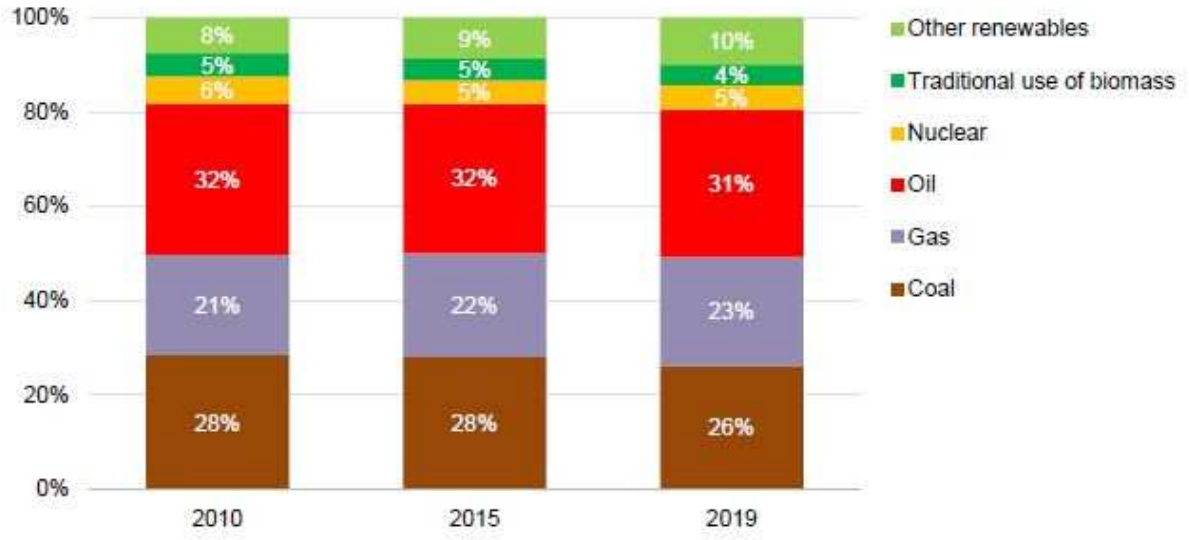

Fig. I.3: Share of total primary energy demand by fuel, 2010-19 [3]

Global energy-related CO_2 emissions remained little changed in 2019 at 33.2 gigatonnes (Gt), following two years of increases (**Figure I.4**). This stabilisation resulted mainly from a sharp decline in CO_2 emissions from the power sector in advanced economies. Power sector emissions fell thanks to the expanding role of renewable sources (mainly wind and solar PV), fuel switching from coal to natural gas, and higher nuclear power output.

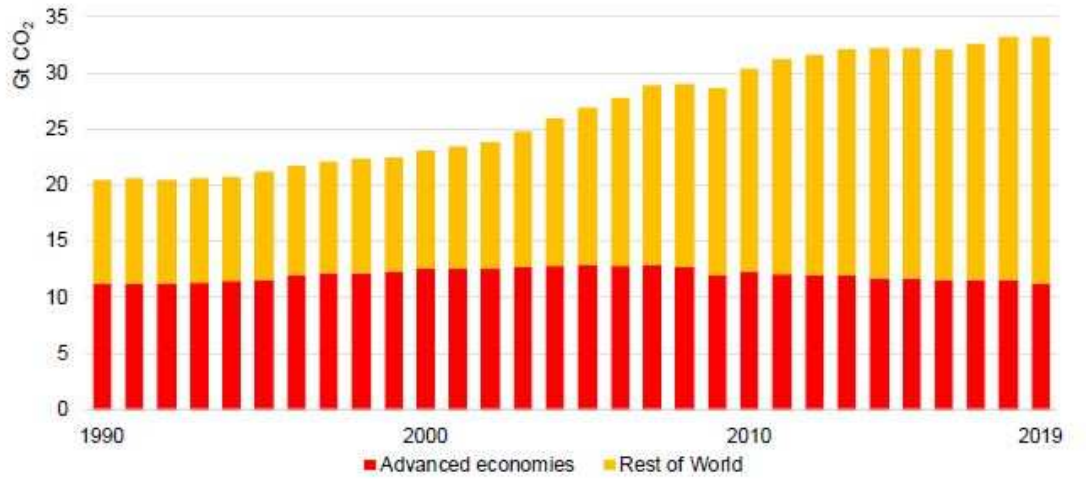

Fig. I.4: Energy-related CO2 emissions, 1990-2019 [4]

In fact, in ice age, CO_2 levels were 180 ppm and 280 ppm in the interglacial period. Since the beginning of the industrial age, the CO_2 concentration has increased to 375 ppm. It was established that the marked increase was the result of human activities. The increase of CO_2 levels in the air leads to an increase in the absorption of infrared radiation emitted by the sun and consequently an increase in temperature, which causes climate change.

Another important reason for turning to sustainable energy development is the problem of energy reserves. In 1973, it was predictable that oil reserves would last for another 30 years, and that today these reserves are still estimated at 30 years (despite 30 years consumption), these are, however, not inexhaustible. Since 1980, more oil is produced than is found each year. According to some scientific predictions, the world could reach its conventional oil production peak about 2035. This peak of production should lead to an inevitable rise in oil prices. Renewable energy sources will then become more competitive cost-wise.

I.3. Renewable energies

Energy sources are considered renewable to the extent that they can renew themselves quite rapidly. These energies are sometimes viewed as inexhaustible on a human timescale. There are six types of renewable energy.

I.3.1. Solar energy

It can be photovoltaic or thermal. This energy can be recovered from sunlight that is refracted on panels, thermal sensors which transmit it to metal plates, that would later heat a copper pipework systems.

a) Solar thermal energy:

To use thermal solar energy, solar panels must be installed on the home's rooftop. These panels would be able to refract the heat of the sun's rays to permit the heat of the carrier fluid. The heat is then transmitted to a buffer tank, which would enable the exchange with heating devices or domestic hot water.

b) Solar photovoltaic energy:

Photovoltaic solar energy is based on the photovoltaic effect, by which a photon (elementary particle of light) impacts a panel composed of semiconductors. Silicon is the main element in Semi-conductors. When the photon impacts semi-conductors it releases electrons. This reaction generates electricity through exposure to light. In photovoltaic energy solar panels, the semiconductors are shaped into thin layers that produce an electric current. These semiconductors comprise the core element of solar cells Semiconductors capture the electric current converting it into electricity for the house or business.

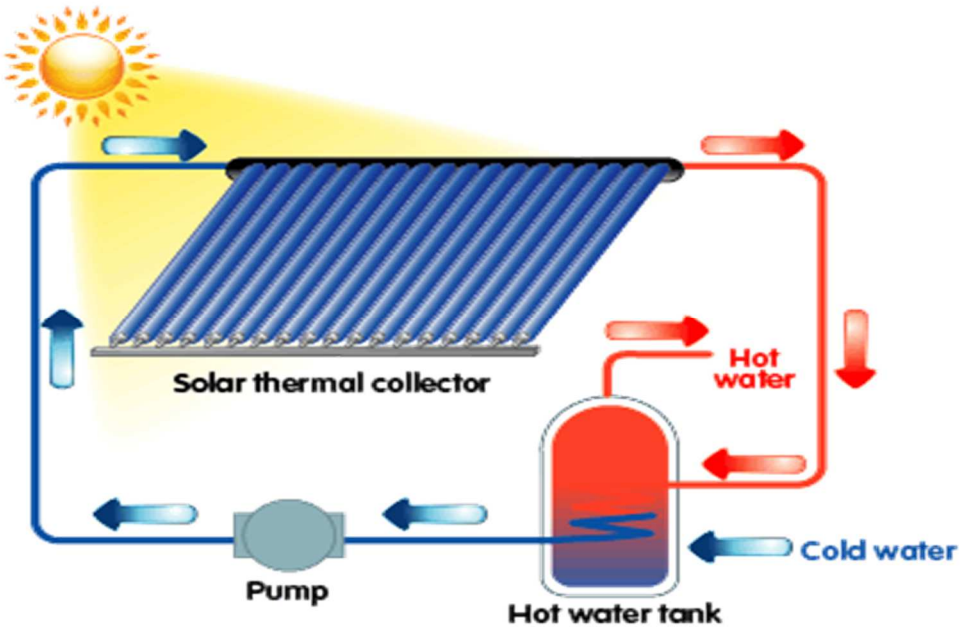

Fig. I.5: Solar energy power diagram [5]

➢ Advantages:

- Solar energy is a non-polluting source;
- Significantly reduces electricity bills with low maintenance requirements;
- An inexhaustible source of energy.

➢ Disadvantages:

- Solar energy is subject to climatic conditions. It offers good production in very sunny areas and summer, while electricity generation is very limited in winter and cloudy areas;
- A large area of photovoltaic panels is required to ensure good energy production;
- Solar panels provide optimal photovoltaic efficiency for 25 years. Beyond that, their efficiency decreases, and it is necessary to change them.

I.3.2. Wind energy

Wind energy, without a doubt, is the oldest energy used by man, for grinding wheat (mill) or sailing. A wind turbine allows recovering the kinetic energy of wind, converting it into mechanical energy and then into electricity.

Currently, wind turbines are grouped on wind farms of several dozen machines. Electricity is generated by using aero-generators that convert wind energy into mechanical energy and then into electricity.

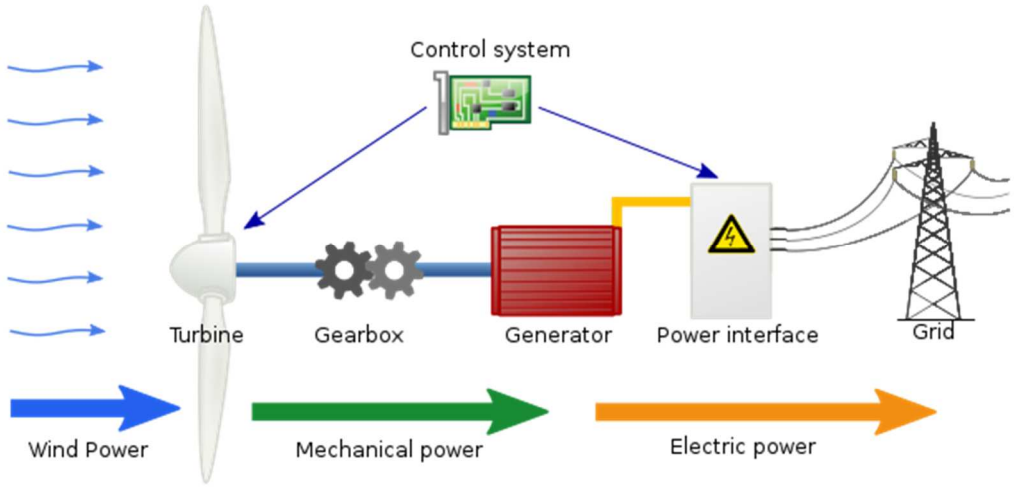

Fig. I.6: Wind energy power diagram [6]

- Advantages:
  - Inexhaustible energy;
  - Wind energy is a clean source.

- Disadvantages:
  - The most favorable areas for wind exploitation are in general, marine areas, coastal areas, some open plains, and some mountainous regions, so wind energy is unevenly distributed in the space;
  - The wind does not blow constantly, which makes wind power an intermittent energy source.

I.3.3. Geothermal Energy

Geothermal energy is the exploitation of heat stored in the sub-surface of the earth. The utilization of geothermal resources can be classified into two categories: electricity generation and heat generation. There are many applications, according to resources, to the technique used and to the needs. The criterion which serves as a guide to clearly define the sector is the temperature. Geothermal energy is defined as “high energy” (above 150°C), “medium energy” (from 90 to 150°C), “low energy” (from 30 to 90°C) and “very low energy” (below 30°C).

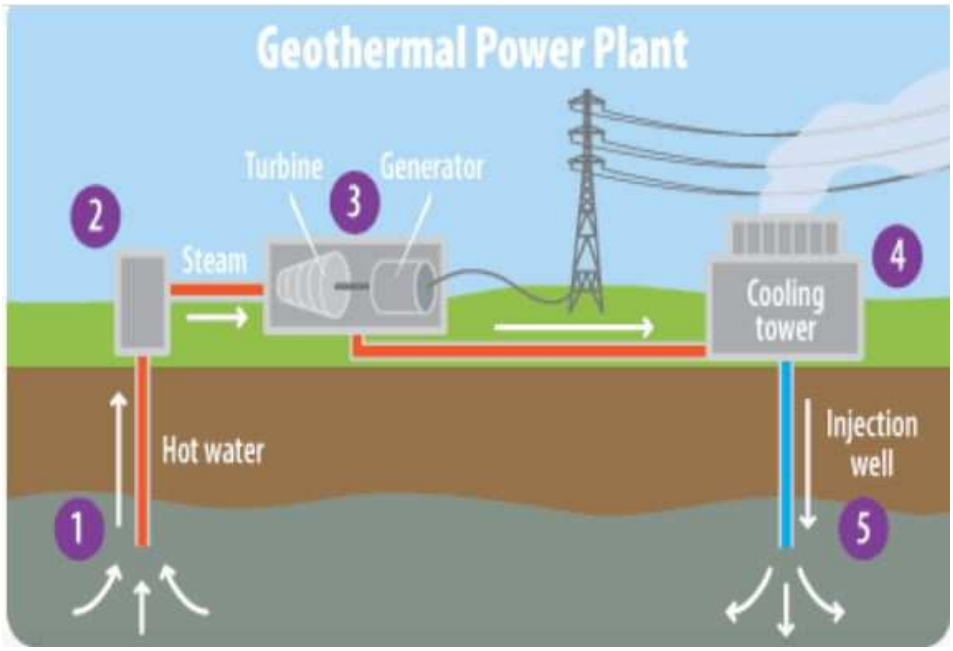

Fig. I.7: Geothermal Energy Power Plant Diagram [7]

- Advantages:
  - An economical heating mode;
  - It works anywhere on earth. Even if the volcanic areas produce more heat, geothermal energy is little influenced by the local weather, unlike solar energy for example;
  - Geothermal heating is environmentally friendly. Heat production generates very less greenhouse gas.

- Disadvantages:
  - Some rocky terrains are not eligible for geothermal energy;
  - Installing a geothermal system is expensive;
  - Horizontal geothermal requires large terrain while vertical energy capture requires deep drilling;
  - The profitability of the system may be observed from the 5th year.

I.3.4. Hydraulic energy

The first imperative is to have large amounts of water. The purpose of dams was to hold it. The dam impedes the natural water flow, except in the case of high flows, which allows water to flow. Large volumes of water collect and form an accumulation lake. When water is stored, only need to open valves to launch the electrical power generation cycle. Water flows into a penstock or gallery dug in the rock following installation and take the direction of hydropower plant located below.

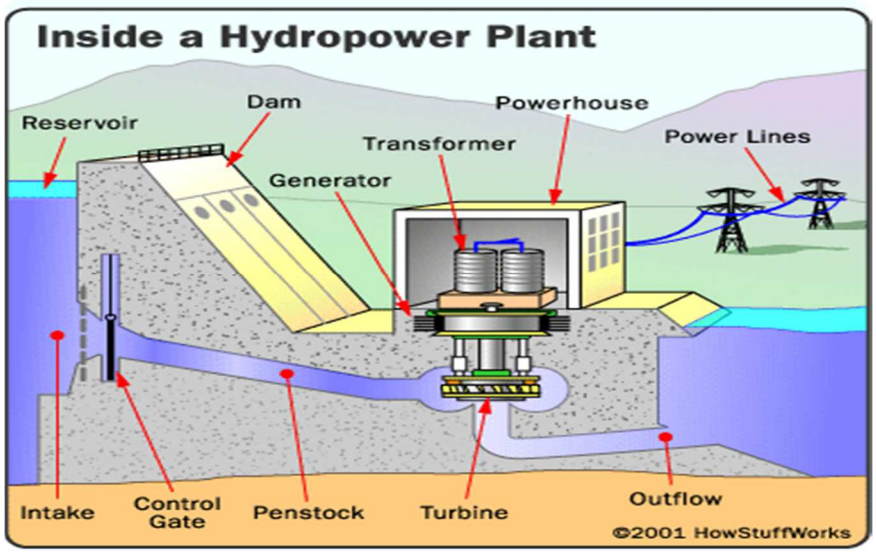

Fig. I.8: Hydraulic energy power diagram [8]

- Advantages:
  - The most controlled energy in the world. The fact that man has used it since ancient times to produce energy generally and electricity particularly;
  - Hydraulic energy is clean;
  - The dam's electrical output is quite large; it represents 16% of the world's energy production.

- Disadvantages:
  - The construction of a dam remains limited, requiring specific features of the land.
  - The construction of a dam has an impact on the population of areas where the dam is built, and it has an environmental impact;
  - The production depends on the amount of precipitation;
  - Even if it remains rare, the risk of dam failure exists, this would lead to a phenomenal flood that likely destroys everything downstream of the dam.

I.3.5. Biomass energy

It includes three major families:

- Energy wood or solid biomass;
- Biofuels;
- Biogas.

These are all bio-based materials used as fuels for heat production, electricity or transport fuels.

I.3.5.1. Bioenergy (solid biomass)

Solid biomass represents bio-based materials, which can be used as fuels for heat or electricity production. These are mainly woody resources (lignin-based) of forest-based, agricultural or urban origin, also known as wood energy.

Solid biomass is in favor of heat production for heating, steam production for industrial processes, drying. It is also possible to produce electricity, which can also be

sold to the grid: the steam generated drives stream turbines that generate electricity. However, Electricity generation from solid biomass has low operational efficiency. Therefore, cogeneration is mainly used to produce electricity in addition to heat.

Fig. I.9: Bioenergy production diagram [9]

- Advantages:
  - Wood fuel is easily available either in the form of firewood or wood wastes;
  - The cost of wood fuel is roughly 2-3 times cheaper than gas and fuel oil, it is not sensitive to currency and oil price fluctuations;
  - Wood energy technologies create local jobs because it requires about 5 times the labor needed for fossil energy-based technologies.
- Disadvantages:
  - Low benefits in terms of lowering carbon emissions;
  - To produce biomass energy, it is necessary to occupy arable land and therefore reduce agricultural production;
  - Water and soil pollution;
  - The impact of transportation costs;
  - The unsustainable use of biomass fuels can lead to substantial deforestation.

I.3.5.2. Biofuels

Biofuels are liquid or gaseous fuel, produced from non-fossil organic materials derived from biomass, e.g. vegetable materials produced by agriculture (beet, wheat, maize, rapeseed, sunflower, potato, etc.).

There are two types of first-generation biofuels:

- Bioethanol: was the first fuel of plant origin ever used. It is an ethyl alcohol resulting from fermentation of sugar or starch hydrolysis, and distillation. It can be mixed with petrol to increase its octane index and reduce pollutant emissions. However, plant cultivation requires large areas, the reason why some countries are driven to increase farmlands by deforestation. The reduction of polluting emissions through using ethanol is largely offset by deforestation, which did not solve environmental issues.
- Biodiesel: comes from oilseed (rapeseed, sunflower). After pressing and refining the seeds, the oil is mixed with methanol, to give properties close to gas oil (viscosity, stability, etc.). Commonly known as biodiesel. Its use cannot be extended to a large scale because the amount of oil available is still insufficient to cover all the needs.

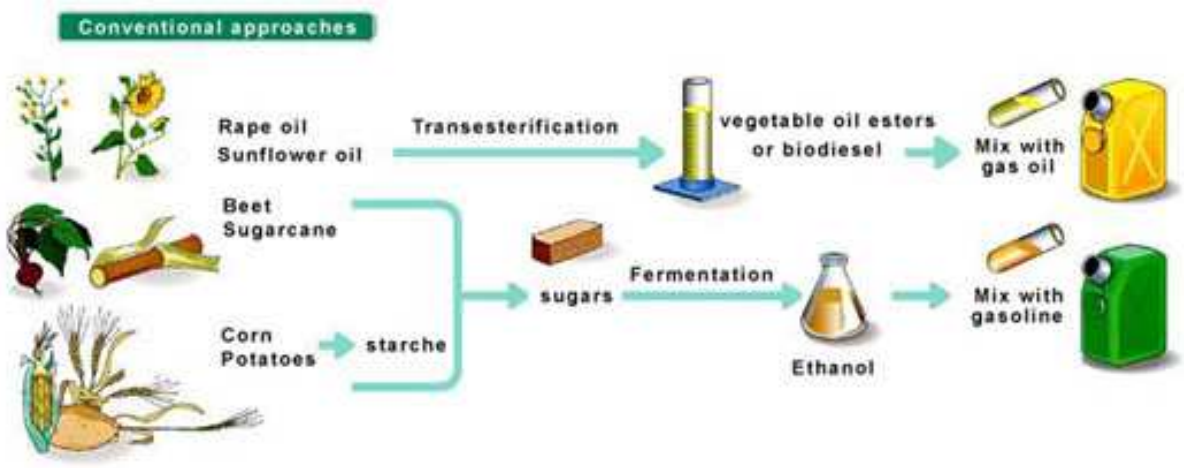

Fig. I.10: Production of first generation biofuels [10]

- Advantages:
  - The automobile is responsible for a significant part of air pollution in cities. Using biofuels will contribute to the reduction of greenhouse gas emissions;
  - They can be used without any adaptation of vehicles and engines.

- Disadvantages:

  - The production of sunflower oil is, on one hand, a waste of time, because the harvest will take place only once a year and on the other hand, only one part of the plant can be harvested, so large areas are needed in order to be able to harvest sufficient quantities.

  - Production costs are high. To quantify them, the costs of cultivation, collection, and processing must be taken into account. Eventually, biofuels cost twice as much as oil.

I.3.5.3. Biogas

Biogas is a combustible gas, a mixture of methane and carbon dioxide, with a few other components. The prefix “bio” (life) indicate where it comes from organic materials, which release biogas when decomposing through the fermentation process. Indeed, under ambient temperature and pressure, biogas is a gas. Chemically, it is primarily composed of methane (around two-thirds of the total volume) and one-third of carbon dioxide. Other substances are also present as traces (water, nitrogen, sulfur, oxygen, organo-halogenated elements), making it less pure and more corrosive than fossil natural gas. Finally, the composition of biogas varies in function of the nature of waste and fermentation conditions.

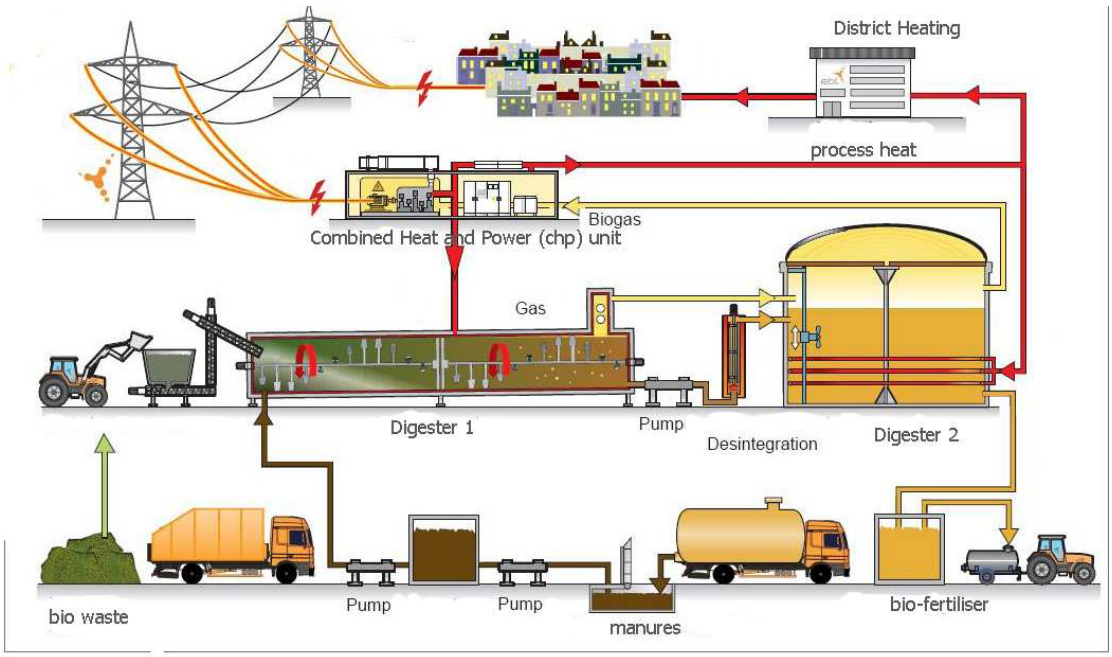

Fig. I.11: The industrial process scheme of a biogas plant [11]

➢ Why biogas?

The production of biogas and biomethane fits into the circular economy model and has positive knock-on effects: local energy production that cannot be moved elsewhere, job creation, an answer to the problem of how to manage agricultural co-products, the replacement of synthetic fertilizers etc. Here are the three direct advantages of mechanization:

- Repurposing of waste

  Mechanization provides a use for organic waste, producing renewable energy and organic fertilizer. It allows the processing of oily or very wet non-compostable organic waste. It is also a way of achieving a reduction in the quantity of organic waste requiring treatment in other sectors.

- Reduction in greenhouse gases

  According to "Methanisation in 10 questions" from Ademe, every kWh of biomethane injected into the gas grid could avoid 200 g of CO2 equivalent. There are two reasons for this positive impact:

  - Methanisation allows the methane produced naturally by the breakdown of organic matter – particularly livestock effluents – to be captured and utilised.
  - Biogas and biomethane can replace fossil fuels such as oil, coal and natural gas, because they can be transformed into heat, electricity or renewable fuel (BioNGV).

- Digestate: a natural fertilizer

  Digestate is the portion of the waste that remains at the end of the methanisation process. It can be exploited as natural fertiliser, as a substitute for chemical fertilisers. To optimise its use, a digestate phase separator can be used. In fact, the liquid and solid phases do not have the same properties: the one is a fertiliser, the other is a soil improver.

➢ Disadvantages:

- The investment cost presents the biggest obstacle that effects biogas production.

- This energy is very promising but methanisation techniques are still unknown so there is a need to raise public awareness.

➢ Sources

Substrates for anaerobic digestion are mainly, manure, municipal wastewater, organic fraction of household waste and Agri-food waste.

➢ Fermenters

These are the facilities where the methanisation takes place. It is usually constituted by a closed tank, airtight, and preferably thermally isolated from the outside wherein microorganisms coexist for chemical and biological degradation of organic liquid waste and producing biogas. The choice of digester varies depending on the type of waste and application.

Fixed-culture digesters are particularly suitable for liquid waste. They allow bacteria to attach to movable support (fluidized bed) or static support and therefore increase their population.

The infinitely mixed digesters homogenize the substrate using mechanical mixing or gas (biogas is reinjected into the tank base). They are used to treat substrates containing more dry matter than fixed-culture digesters.

Plug flow reactors are horizontal cylindrical digesters. The substrate is introduced from one side and slowly moves out while decomposing. These digesters allow operation with more dry matter than infinitely mixed reactors.

➢ Methanisation

Methanisation is a natural biological process of degradation of organic material under anaerobic conditions. It leads to the formation of methane-rich gas: biogas.

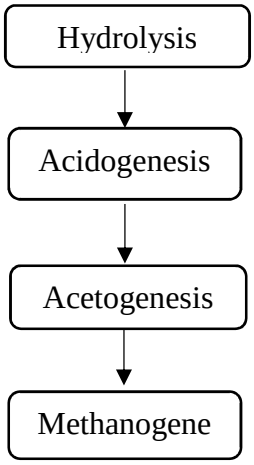

Fig. I.12: The four steps of methanisation [12]

Organic matter consists principally of proteins, carbohydrates and lipids. This complex source is initially hydrolysed into simple molecules (amino acids, sugars and fats). These intermediate products are then transformed into organic acids, such as propionic acid, butyric acid… Alcohols, hydrogen, carbon dioxide and water are also formed. This is the acidogenesis step.

The acetogenesis step allows the transformation of compounds previously formed into methane precursors, acetic acid, carbon dioxide, and hydrogen. Methanogenesis is then insured by two routes.

- From hydrogen and CO_2 using hydrogen bacteria.
- From acetate with acetotrophic bacteria.

It is estimated that 70% of methane production comes from acetates. The first two steps of fermentation are made by anaerobic and aerobic bacteria. On the other hand, methanogenesis is strictly anaerobic.

The temperature affects the rate of decomposing the organic matter: the higher it is in digester, the faster the biological process of methanisation proceeds rapidly. There are three temperature levels: the psychrophile, the mesophile and the thermophile.

- The ancient techniques used psychrophile fermentation, below 25°C. These unheated installations are no longer used because they require very long retention times.
- Between 25 and 45°C, mesophilic fermentation allows residence times of about 40 days.
- Between 45 and 55°C, thermophilic fermentation allows fast decomposition of the substrate and high gas yield.

➢ Biogas composition

Biogas mainly contains methane and carbon dioxide. The proportion of these two gases depends on the nature of substrate, and more specifically on the proportion Carbon - Hydrogen - Oxygen - Nitrogen (CHON). A substrate rich in C and H produces a high proportion of methane. A medium-rich substrate, such as cellulose, produces biogas that typically contains 55% methane and 45% carbon dioxide. The content of methane in biogas varies between 25 and 70%.

Biogas production is given by the classical equation of BUSWELL [13]:

$$C_nH_aO_b + \left(n - \frac{a}{4} - \frac{b}{2}\right)H_2O \rightarrow \left(\frac{n}{2} + \frac{a}{8} - \frac{b}{4}\right)CH_4 + (\frac{n}{2} - \frac{a}{8} + \frac{b}{4})CO_2$$

Thus, for carbohydrates (generic formula CH_2O), the equation gives:

$$2CH_2O \rightarrow CH_4 + CO_2\ (50\%\ of\ methane)$$

On the other hand, for fatty substance:

$$2C_9H_{20}O_2 + 6H_2O \rightarrow 13CH_4 + 5CO_2(72\%\ of\ methane)$$

In addition to methane and carbon dioxide in varying proportions, biogas contains small amount of sulfur compounds (H_2S, mercaptans) and nitrogen compounds (ammonia, nitrogen) (<1000 ppm). Traces of hydrogen, intermediate fermentation products (alcohols, acids, esters, etc.), siloxanes and organochlorines are also present in biogas. This means that biogas needs to be treated before using it as a fuel.

The composition of biogas may vary depending on the composition of starting substrate, type of fermentor, and fermentation time. **Table. I.1** illustrates the composition of different biogas according to their origin. It should be noted that the

source has a much stronger influence on the quality of biogas with a methane concentration varying between 30 and 75%.

Table. I.1: Biogas composition according to the source.

	Household waste	Sewage sludge	cattle and sheep manure in fermenters	Distillery
CH_4 (%)	50-60	60-75	60-75	68
CO_2 (%)	38-34	19-33	19-33	26
N_2 (%)	0-5	0-1	0-1	-
O_2 (%)	0-1	<0,5	<0,5	-
H_2O (%)	6	6	6	8
H_2S (mg/m3)	100-900	1000-4000	3000-10000	400

- Biogas properties

Calorific value of biogas

The calorific value of the fuel is the amount of heat released from its complete combustion. If the water obtained from combustion condenses, the HHV (High Heating Value) is defined. Whereas, when the water leaves in vapor form, the LHV (Low Heating Value) is defined. It is obvious that the HHV and LHV of the biogas are proportional to its content of methane, i.e. biogas contains 70% of methane at 15°C and normal atmospheric pressure the LHV is equal to $9.42 \times 0.7 = 6.59$ kWh / m^3 [14, 15]. Illustratively, 1 m^3 of methane is equivalent to 1 liter of gasoline in terms of energy. Methane emits less CO_2 than gasoline or oil because it has the highest H/C ratio.

Adiabatic flame temperature of biogas

The adiabatic flame temperature (the maximum temperature that can be reached in the combustion process) of the biogas combustion is proportional to its LHV, the latter is proportional to methane contained in biogas. That means that high-quality biogas, high methane content, with higher LHV gives important adiabatic flame

temperature. For biogas, the adiabatic flame temperature can vary between 800°C and 1100°C [15] according to methane concentration in biogas. Biogas containing 50 percent methane has a flame temperature of 870°C [16].

- Recovery method of biogas

Biogas may be reclaimed in the form of thermal, electrical energy, or biofuel. It can also be injected into the natural gas grid.

Heat recovery: combustion is the most effective process to reclaim biogas. Combustion heat of biogas can be used to generate hot water, steam, or heat furnaces. It is a simple process, which does not require many investments and that therefore pays off rapidly. However, the consumer using biogas should be placed in locations close to the source. Plants treating frequently use a fraction of biogas produced to maintain the temperature of the fermenters.

Electricity recovery with or without cogeneration: biogas can be used to power an engine or gas turbine that produces electricity. It may be then be reinjected into the power grid. Cogeneration produces electricity and heat that may be used to heat fermentors or for other purposes.

Biogas fuel: Biogas may also be used as a fuel. Its use is currently limited to captive vehicle fleets such as intercity buses or garbage trucks.

Biogas injection into the natural gas grid: the solution which offers the best energy yield, if the grid is close enough to generation point. The injected gas should be odorized and undergo some pre-processing to remove CO_2, H_2S, O_2, H_2O and halogenated compounds.

I.3.6. Hydrogen-based fuels

Currently, hydrogen-based fuels are a very important alternative. Unlike fossil fuels, they could not aggravate some environmental problems such as the greenhouse effect because they emit insignificant amounts of carbon dioxide. They are used particularly in various energy generation systems such as gas turbines. They can be in the form of pure hydrogen as in fuel cells or the form of hydrogen-containing gas mixtures.

I.3.6.1. The syngas

Syngas, or synthesis gas, is part of hydrogen-based fuels, which is not a primary energy source such as natural gas or oil but can be produced from a wide range of raw materials containing carbon and hydrogen. It is a combustible gas mixture created either by gasification of plants biomass or waste products (carbon-based) pyrolysis. It is lean gas (two times less on energy than natural gas), dirty, toxic, corrosive acid if it has not been carefully purified. It is derived from a complex chemical reaction, characterized by the first step of gasification by pyrolyzing organic matter (wood or coal), in presence of an oxidizing agent introduced in insufficient quantities, enough to allow combustion, a little bit just to be complete. This reaction produces a gas consisting of a mixture of condensable and non-condensable gases, a type of residual wood charcoal; the marketed synthesis gas is produced by the second phase of thermal decomposition.

- Why syngas

The syngas has several advantages:

- It can be produced from a solid or gaseous raw material;
- It is renewable;
- It allows to get rid of waste instead of storing them;
- It can be used in centralized or decentralized energy generation systems and cogeneration systems;
- It releases less pollution than conventional fuels;
- Finally, several derived products can be obtained from syngas, such as methanol, ethanol, hydrogen, lubricants and even pharmaceuticals and wax.

- Syngas production

Syngas can be produced from many sources, explain that production does not necessarily depend on fossil material; it may also be produced from waste materials or biomass gasification. It will only be generated from renewable resources in the future. The syngas is produced by different process namely: partial oxidation, gasification and auto-thermal reforming (ATR). These methods employ as feedstocks petroleum residues, coal or biomass. The choice of syngas production process depends on H_2/CO

ratio at the outlet of the reactor, purity of product, the capacity of plant, availability of resources, and cost.

- Gasification

Gasification is a thermochemical transformation that consists the heat decomposing of carbonaceous solid fuel (coal, biomass) in the presence of gaseous reactant (carbon dioxide, water vapor then oxygen/air) to obtain a combustible gas mixture. The gasification reaction occurs under very high temperature conditions (over 1000°C). The synthesis gas obtained at the end, called "syngas", is mainly a mixture of two combustible gases: carbon monoxide (CO) and hydrogen (H_2).

- Principle of biomass gasification

There are four main stages in the gasification process:

Drying phase, integrated or not in gasification reactor,

Pyrolysis phase, which produces volatile materials (CO, CO_2, H_2, CH_4, H_2O_{vap} and hydrocarbons gas called "tars") and coal, under the effect of heat and in the absence of an oxidizing agent,

Combustion phase, also called partial oxidation, which by injection of oxidizing agent (air, O_2, H_2O_{vap}) oxidizes the volatile substances, produced during the pyrolysis phase, and sometimes part of coal. This phase produces the heat required for the whole process and destroys the tar fraction.

Gasification phase, also called reduction, is closely linked to the combustion phase, which converts, by complex thermochemical reactions, coal (carbon) into fuel gas rich in CO and H_2 called "synthesis gas" or "syngas".

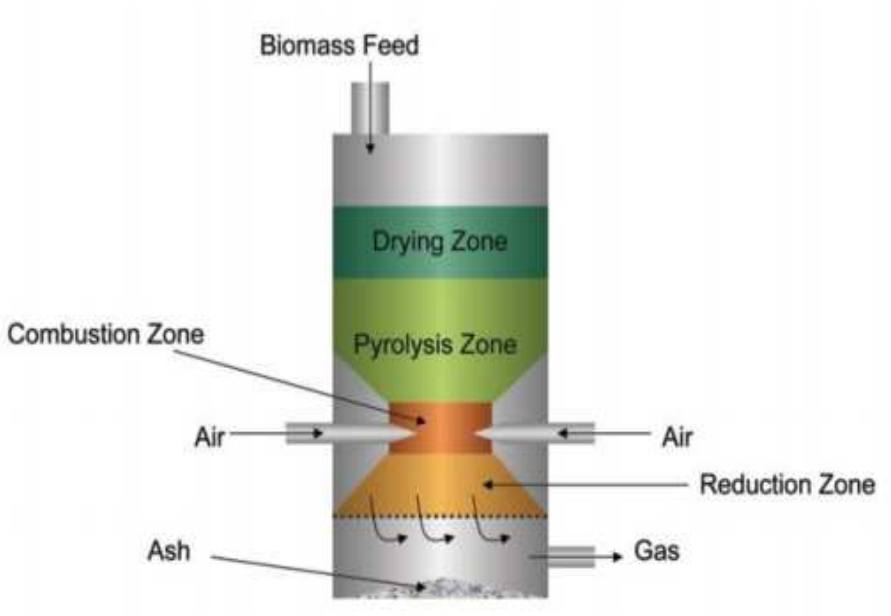

Fig.I.13: Downdraft fixed bed gasifier [17]

- Syngas composition

The following table shows composition of syngas

Table.I.2: Syngas composition.

Substance	Composition (%)
H_2	20-40
CO	35-40
CO_2	25-35
CH_4	0-15
N_2	2-5

- Recovery method of syngas

There are different operating modes are possible in gasification:

- Generation of heat in afterburning boiler and electricity in a turbo alternator group (integrated gasification or first generation process),

- Production of synthetic gas as a substitute for natural gas or industrial gases, in furnace systems (dryer, cooking oven, etc.),
- Production of purified synthesis gas cogeneration in thermal engines or gas turbines, for optimizing the generation of electricity (second generation processes).

To achieve characteristics compatible with the gas supply constraints of internal combustion devices. In the latter two cases, the syngas produced should be cooled and purified before being using as fuel for engines or gas turbines.

I.4. Flameless combustion overview

The use of hydrocarbons is expected to continue to increase, despite its disadvantages, because of its benefits and plurality applications. Combustion installations are key sources of greenhouse gas emissions and diverse types of air pollutants such as carbon monoxide (CO) which can cause harmful effects on human health (difficulty breathing, dizziness, tiredness…), nitric oxides (NO), which is toxic at low doses (mucosal irritations) and may be combined with water to form nitric acid (HNO_3), responsible for acid rain. While nitrous oxide (N_2O) is one of the major greenhouse gases. During the combustion of hydrocarbons, NO is formed according to three main mechanisms, namely: thermal-NO, which is the main formation pathway for temperature above 1700 K; Fenimore-NO, also called prompt NO, active at lower temperatures and fuel-NO which is related to the presence of nitrogen in some fuels [18].

In every combustion system, the main objectives are to reduce harmful emissions, improve efficiency, decrease fuel consumption and find a clean renewable, sustainable and low-cost replacement. Such targets can only be met by using forms of available renewable energy produced from biomass. The latter is found abundantly in nature and can substitute traditional energy sources in the future [19]. It has long been known that mud swamps generate combustible gas (a mixture of methane, hydrogen sulfide, and carbon dioxide). In 1630, Van Lemon found that fermentation of organic matter could emit flammable gases. In the 18^{th} century, Volta identified methane as a fuel component. In Europe, the first applications of anaerobic digestion appeared in the mid-nineteenth century with the first purification stations. Major problem linked to

biofuel combustion is their LCV (Low Calorific Value) [20, 21], which gives a weak and unstable flame [22]. Unfortunately, the biofuels upgrading process by removing impurities such as CO_2 and H_2S remains very costly [23]. However, all these issues can be bypassed by applying flameless or MILD (Moderate or Intense Low-oxygen Dilution) combustion technology [24]. The latter can be easily powered by LCV biofuels and oxidizers diluted by carbon dioxide since it is naturally present in biofuels [25].

MILD combustion is one of the new technologies designed to increase thermal efficiency, it is stable with low temperature and species gradients [26] and emitting very few pollutants (CO and NO). It reduces fuel consumption and emissions such as nitrogen oxides, carbon monoxide and unburnt hydrocarbons [27, 28, 20]. In MILD combustion mode, reagents are diluted by combustion products in a high-temperature environment [29, 30]. This technology is also known by FLameless OXidation (FLOX) [31] and Colorless combustion [32] since no flame is visible. To obtain FLOX regime it is necessary to dilute fuel and / or oxidant jets by a strong recirculation of flue gas before reaction [33-36]. Besides, for the MILD regime, reactants injection temperature should be higher than the auto-ignition temperature of the mixture. Also, the maximum temperature increase due to combustion must be lower than the auto-ignition temperature of the mixture [37]. This can be operated by the recirculation of hot combustion gases to preheat reactants and dilute oxidizer [26]. Flameless combustion has been mostly applied in furnaces and boilers for industrial use, particularly in the metallurgy field [38, 39].

Several studies were attracted by flameless or MILD combustion of biofuels. In a lab-scale furnace, Hosseini et al. [20] pointed out that to meet flameless mode, the walls of the combustion chamber should be heated up firstly by high calorific value fuel such as CH_4 and then the system can be switched to biogas flameless combustion mode. It is noticed that in biogas flameless combustion, the temperature inside the furnace is uniform and lower than the traditional mode of CH_4. Indeed, hot spots are eliminated, CO and NO_x formation recorded are very low, and thermal NO_x suppressed. For high concentrations of CO_2 in biogas, flameless combustion products, heat capacity, rate of radiation, and absorption capacity are enhanced. To show different priorities of biogas flameless combustion compared to conventional mode, Hosseini et al. [40] investigated numerically effects of oxidizer temperature and oxygen concentration on non-premixed turbulent biogas flameless combustion. A tridimensional CFD study has been

performed, k-ε model was used to model turbulence, Eddy Dissipation Model (EDM) to handle turbulence-combustion interaction and a two steps global mechanism of Westbrook and Dryer to describe combustion kinetics. The biogas was composed of a volume of 60% CO_2 and 40% CH_4. It was found that NO_x formation is reduced in flameless mode due to the elimination of hot spots and a low level of oxygen. In addition, entropy generation was minimized since the temperature was uniform inside the furnace. The effect of dilution agent on biogas oxy-fuel combustion performance was considered by Liu et al. [41]. Two diluents were compared namely: CO_2 and H_2O with various oxygen concentration and preheated temperature of oxidant. It has been found that it is prudent to sustain the MILD oxy-fuel combustion regime under CO_2 moderation condition than H_2O moderation. In addition, performances of such combustion regime under the H_2O moderation operation was more sensitive to oxidizer preheating temperature and oxygen concentration. In the same context, Mehregan et al. [42] considered numerically the effect of oxygen concentration, preheating diluted oxidizer temperature, and type of diluting species on NO_x emission of biogas flameless combustion in non-premixed configuration. Biogas was formed by volumes of 60% CH_4 and 40% CO_2, whereas oxidizer (composed by 5%, 7% and 10% of oxygen) was diluted simultaneously by N_2, CO_2 and preheated (to 900 K, 1100 K and 1300 K). It has been found that an increase of NO_x emission is more sensitive to oxygen concentration than preheating air temperature. NO_x emissions were slightly influenced by dilution species, whereas, it was reduced by N_2 dilution rather than CO_2. Under distributed combustion conditions, Murat S. [43] has numerically investigated thermal field distributions and pollutant levels of the non-premixed biogas flames. Predictions were based on PDF/mixture fraction combustion model, k-ε standard turbulence model and P-1 radiation model. It has been shown that NO_x and CO emission levels were reduced by both high mixture temperature and decrease of oxygen concentration in the oxidizer. It was also demonstrated that a more uniform thermal field emerged when oxygen concentration decreases.

Several research studies demonstrated that the addition of hydrogen to methane, biogas, and other C_1-C_4 hydrocarbon fuels enhances flame stretching resistance, enlarges stability limits, increases flame temperature and total heat transfer rate. Under MILD conditions, the effect of hydrogen addition on turbulent non-premixed CH_4-H_2 jet flame was numerically studied by Mardani et al. [44]. Three fuel mixtures were

considered (5%H_2-95%CH_4, 10%H_2-90%CH_4 and 20%H_2-80%CH_4). The combustion kinetics were described by the DRM-22 reduced mechanism and the Grimech 2.11 full mechanism. The Eddy-Dissipation-Concept model was used to handle turbulence-chemistry interaction. Results showed that an increase of hydrogen in fuel decreases the mixture fraction, strain rate, and radial velocity. The addition of hydrogen to methane increased mixture ignitability, enhanced the rate of heat release, and led to an elevated level of OH, CH_2O, HCO, and higher reaction intensities. At constant co-flow oxygen level, hydrogen addition to methane increases both turbulent kinetic energy decay along the flame axis and flame entrainment. In contrast, for a constant hydrogen volume, an increase of co-flow oxygen level decreases flame entrainment and turbulent decay. Sheng et al. [25] studied the effect of hydrogen addition to biogas under MILD oxy-fuel combustion in counter flow configuration. Oxygen concentration and preheating temperature in the oxidizer stream were varied. It was shown that the addition of high amounts of hydrogen was not necessary into fuel blends under MILD oxy-fuel combustion using small LCV biogas, which mostly consists of CO_2. A lower preheating temperature and oxygen concentration in the oxidizer flow are better to sustain the MILD regime for hydrogen-enriched biogas combustion. In an experimental study, hydrogen addition's effect on combustion stability, adiabatic temperatures, soot emission, and impingement heat transfer of biogas in counter-flow diffusion flame have been investigated by Zhen et al. [45]. Different compositions of biogas under different levels of hydrogen addition (5% to 10%) were considered. Results show that the flame stability of biogas can be enhanced by the addition of a small amount of hydrogen to fuel. Comparison of CH_4-CO_2 and CH_4-N_2 flames at the same H_2 concentration indicates that biogas flame shows a lower stability limit due to the presence of CO_2. Under identical volumetric flow rate, the CH_4-N_2 mixture has higher flame temperatures and greater soot emission than biogas flame. Heat transfer at the stagnation point is increased by hydrogen addition, due to a high flame temperature at a higher level of hydrogen addition. While the total heat transfer rate is lowered because hydrogen has lower energy content per unit volume than the substituted biogas. Effects of CH_4 content in biogas, H_2 volume and O_2 enrichment levels on heat release characteristics of non-premixed biogas flames were studied by Jun li et al. [46]. It was found that maximum combustion temperature and net reaction rate of biogas increase with increasing CH_4 content in biogas, hydrogen volume, and oxygen levels. Mameri et al. [47] studied numerically the effects of biogas composition, hydrogen enrichment

and oxidizer dilution on flame structure and emissions in counter-flow diffusion flame under the MILD regime. It has been stated that hydrogen enrichment and oxygen reduction in the oxidizer decrease H_2O, CO, OH and NO emissions. The flame temperature and species production, excepting CO, are decreased by the chemical effect of CO_2 available in the oxidizer stream. For high amounts of CO_2 in the oxidizer, the chemical effect of CO_2 becomes negligible.

Recently, syngas consisting principally of hydrogen and carbon monoxide was used as renewable and sustainable hydrogen sources [48, 49]. Synthesis gas is a mixture of combustible gases; it is characterized by short ignition delay time, high burning velocity, and adiabatic flame temperature [48]. Som et al. [50] studied numerically and experimentally the effects of fuel composition, pressure, and strain rate on combustion and NO_x characteristics of syngas non-premixed and partially premixed counterflow flames. Results show that stable flame can be formed over wide ranges of strain rate, syngas compositions and equivalence ratio in a counterflow configuration. Safer et al. [51] investigated numerically the structure of syngas diffusion flame and NO formation pathways over a wide range of hydrogen volume, scalar dissipation rates, and operating pressure from 1 to 10 atm. It has been noticed that from hydrogen-lean syngas to hydrogen-rich syngas fuels, maximum flame temperature increases for scalar dissipation rate values lower than the intermediate value whereas decreases at higher values. In addition, thermal NO is found to be the principal source of NO formation. The latter increase with increasing hydrogen content and pressure. Also, at a lower strain rate, the authors found that hydrogen-rich syngas flames produce more NO while NO levels increase towards hydrogen lean syngas flames at higher strain rates. Investigation of oxygen-enriched syngas laminar counter-flow diffusion flames showed that flame temperature and NOx formation were augmented by increasing oxygen volume [52].

In the MILD combustion regime of syngas, Huang et al [53-55] investigated the effect of fuel injection velocity, air preheating temperature, and pressure in an axially staged combustor. It was found that higher secondary fuel injection velocity was beneficial for rapid fuel-oxidizer mixing, flame lift-off height increasing, flame temperature lowering, more uniform thermal field, and lower NO_x emissions, but higher pressure drop and CO formation [53]. Moreover, higher air preheating temperature increase flame peak temperature and NO_x formation but decrease CO emissions. While the increase of equivalence ratio resulted in higher NO_x but lower CO emissions [54].

They also investigated numerically the effect of fuel type and pressure on threshold gas recirculation ratio, before designing the MILD combustor. Results show that pressure has only a slight influence on inlet temperature and self-ignition temperature of MILD combustion of the mixture. In addition, an increase of pressure decreases OH mole fraction, resulting in a delay in the oxidation process [55]. Mardani et al. [56] performed a numerical simulation to clarify the effect of hydrogen concentration in two fuel mixtures of syngas and methane/hydrogen mixtures, the oxygen concentration in the oxidizer stream, and the velocity of the fuel jet. The RANS approach was adopted with EDC combustion model using Grimech 3.0 and DRM-22 chemical mechanism. Results show that the volume of the high-temperature combustion region increases with hydrogen addition. While low oxygen concentration in the oxidizer results in more proximity to MILD condition. Indeed, syngas is more sensitive to hydrogen addition than methane, which makes hydrogen as an additive to syngas better to reach MILD condition.

As seen, NO_x emission depends on operating conditions and flame configuration. It has been demonstrated that in MILD combustion regimes, thermal NO is implicitly reduced by lowering flame peak temperature. The other pathways may also have a crucial role in the formation of NO, namely: Fenimore-NO, also called prompt NO which is activated at temperatures below 1800 K, the N_2O-intermediate, NNH, and NO-reburning route. Several studies have been conducted to analyze NO_x formation mechanisms and pathways in MILD combustion using CH_4/H_2 mixtures. Galletti et al. [57] studied numerically and experimentally the NO formation in a lab-scale burner fed by hydrogen-enriched fuels under MILD conditions. Several chemical combustion kinetics were considered for instance KEE 58, DRM 19, and Gri 3. The authors found that NNH and N_2O-intermediate pathways are the dominant sources of NO production for MILD combustion of CH_4/H_2 mixtures. In a numerical/experimental study, Sepman et al. [58] considered transition to the MILD combustion of a co-flow diffusion flame of CH_4/H_2 mixture. Mechanisms Gri 2.11 and Gri 3 were used in computations, the results showed that prompt route is dominant in laminar co-flow diffusion flames in transition to MILD combustion regime. In a laboratory-scale furnace, Li et al. [59] investigated experimentally and numerically the NO formation in MILD combustion of CH_4/H_2 mixture. The combustion mechanism Gri 2.11 was used to describe kinetics. The authors reported that for a lean CH_4/H_2 mixture, $\phi \leq 0.8$, N_2O-intermediate followed by NO-reburning are the dominating routes in NO formation. Hydrogen addition

enhances NNH route and depresses prompt one keeping constant global NO_x emission. Increasing oxygen improves N_2O route and decreases prompt and NNH ones. Globally, at rich conditions, prompt route dominates NO production however N_2O-intermediate route controls under fuel-lean conditions. In a recent paper, Wang et al. [60] investigated numerically a jet flame of CH_4/H_2. Kinetics of MILD combustion was described by Gri 2.11 mechanism. It was found that under MILD conditions ($O_2 \leq 3\%$, T_{ox}=1300K and 12% H_2), the most important contribution ($\approx 50\%$) to the total NO emission results from the N_2O-intermediate route, followed by the prompt ($\approx 30\%$)and then the NNH route ($\approx 20\%$), while the contribution of the thermal route is negligible. However, when oxygen increases, the thermal route is enhanced. Furthermore, for high hydrogen contents, the contribution of the NNH route to the total NO emission increases while those of the N_2O-intermediate and prompt routes both decrease. In a more recent paper on jet flames in MILD mode, Shu et al. [61] conducted a numerical study on the effect of diluent on NO formation. The Gri 2.11 was considered three diluents were studied, namely: N_2, H_2O and CO_2. It is found that dilution by H_2O and CO_2 reduced NO significantly, which is due to their high thermal capacities. The N_2O-intermediate route is found to prevail in cases of dilution by H_2O and CO_2; whereas, thermal and prompt contribute mostly in case of N_2 dilution. In counter-flow diffusion flames, Cheong et al. [62] studied numerically the effect of oxidizer dilution by CO_2 and H_2O on MILD combustion of CH_4. Many combustion mechanisms were compared, namely Gri 2.11, Gri 3, GDF and San Diego. The authors observed that NO emission is ultralow and dominated by N_2O-intermediate mechanism when dilution is practiced by CO_2. Moreover, prompt and thermal paths predominate MILD-N_2. A numerical study of the effects of H_2 addition and O_2 mass fraction on NO_x formation mechanism was conducted by Ghufran et al. [63]. Detailed chemical kinetics scheme (Gri 2.11) was considered in MILD combustion of hybrid fuel (CH_4/H_2) blends. It was further shown that H_2 addition enhanced NNH route while decreasing prompt route and N_2O intermediate pathway whereas thermal NOx route was insignificant for lower O_2 mass fraction of 3% and 6%.

Chapter II

Mechanisms of NO_x formation

II.1. Introduction

The role of nitrogen oxides in air pollution, because of their toxicity and their contribution to the formation of photochemical smog, having been demonstrated in recent years, concerns were expressed about a reduction in chemical emissions (industries using HNO_3) and specifically of thermal origin, by far the most important. Indeed, it was not until that Haagen-Smit [64] discovered the key mechanism responsible for the formation of photochemical smog, as found for example in Los Angeles, Tokyo, and others: atmospheric reaction between unburnt hydrocarbons and nitrogen dioxide in presence of ultraviolet light.

The mechanisms of nitrogen monoxide (NO) formation in combustion has been studied in 1966 when imposition of regulations was a stimulus for research. The unpopularity of NO is due to its influence on the mechanisms of formation of fog and acid rain.

The research on the formation of nitrous oxide (N_2O) is due to the ozone hole. In 1985, a report from NASA (National Aeronautics and Space Administration of the United States) mentioned a sudden and significant decrease in stratospheric ozone concentration, over the South Pole. Since 1986, the mechanisms responsible for the formation of N_2O during combustion have been studied.

Studies on nitrogen oxides (NO_X) are therefore relatively recent on the timeline of scientific discoveries, and most of them result from more or less constrained desire to reduce the harmful aspects of the industrial age. However, some researchers [65] now think that plants can be survived or adapted in the future despite increasing NO_X levels and decreasing ozone concentrations.

Pollutant emissions control is important in the design of new combustion systems. The MILD combustion is capable of emitting very low quantities of pollutants, in particular nitrogen oxides (NO_x), carbon monoxide (CO) and unburnt hydrocarbons (HC). This applies for configurations that operate with non-premixed [31] and premixed [66] injection.

II.2. Effects of nitrogen oxides on human's environment

II.2.1. Designation of NOx

From a chemical point of view, nitrogen oxides (NO_X) include all compounds of empirical formula N_XO_Y with an oxidation state varying from I a V; concerning industrialists, only nitrogen monoxide (NO), nitrogen dioxide (NO_2) and sometimes nitrous oxide (N_2O) are recognized under this name.

II.2.2. Human toxicity

II.2.2.1. Nitrogen monoxide (NO)

It is the principal component of nitrogen oxides, and its formation process has been the most studied. However, its toxicity is not well understood because it is naturally oxidized at ambient temperature to nitrogen dioxide in the atmosphere. It is therefore very difficult to estimate its effects on humans. However, it is causing mucous membrane irritation. The maximum permissible concentration of NO recommended in the industry is 30 mg/m^3 [67].

II.2.2.2. Nitrogen dioxide (NO_2)

Nitrogen dioxide is a reddish-brown gas at high concentration and yellow brown at a lower concentration. At 5ppm, it has a pungent odor. It is an irritant gas with a strong oxidizing character. Direct adverse effects on humans mainly concerned respiratory functions [68]. Exposure to NO_2 for 15 minutes at a concentration more than 5ppm can result in acute respiratory distress syndrome, cough, and irritation of the respiratory tract. Continuous exposure may result in an abnormal accumulation of gas in bronchi (pulmonary edema).

II.2.2.3. Nitrous oxide (N_2O)

Nitrous oxide is a narcotic (laughing gas) at high doses. It was used at the beginning of the century as an anesthetic. However, one of its main features is to be a greenhouse gas that causes global warming. Nitrous oxide also participated in the destruction of stratospheric ozone, which absorbs most of ultraviolet radiation that causes human immune system dysfunction, and may lead to cancer [69].

II.2.3. Environmental effects

Nitric oxide (NO) and nitrogen dioxide (NO_2) play a role in the formation of acid rain and this could have a significant impact on soil and groundwater. This acidification increases the solubility of heavy metals and thus constitute a danger to human health. Acid rainwater is held to be largely responsible for acidification of rivers and soils, leading to the disappearance of certain animal species and soil depletion [70]. In addition, these gases participate in the formation of ground-level ozone (it extends from the ground up to a variable height of approximately 14 kilometers above sea level) following the Chapman cycle [71].

$$NO_2 \rightarrow NO + O \quad \text{(II.1)}$$

$$O + O_2 + M \rightarrow O_3 + M \quad \text{(II.2)}$$

$$O_3 + NO \rightarrow NO_2 + O_2 \quad \text{(II.3)}$$

Where M is a third body, which carries off excess energy.

The concentration of ozone (O_3) in the atmosphere, which is irrititing to respiratory tracts, has increased from 30µg.m^{-3} to 50µg.m^{-3} in twenty years.

Nitrous oxide (N_2O) is the third most influential greenhouse gas responsible for global warming. The greenhouse effect is necessary for all life on the Earth. It keeps the average surface temperature of Earth at 15 degrees Celsius [72, 73]. Without this greenhouse effect, the average surface temperature would be –18 degree Celsius if all radiation emitted by earth would back into space. According to EPA [74], the contribution of N_2O to global warming is around 7% of total emissions. Carbon dioxide 80%, Methane contributed 10%, and others emissions (HFCs, CFCs, SF_6), 3%.

In addition, nitrous oxide absorbs radiation and traps heat in the atmosphere, where it can live for an average of 114 years, according to the EPA [75]. N_2O can float through the troposphere (15 km altitude) and can therefore reach the stratosphere (altitude between 15 and 50 km) where it contributes to the destruction of stratospheric ozone (the ozone layer). The latter is important to live on earth because it absorbs harmful ultraviolet radiation coming from the sun, which can cause cancer and immune system malfunctions.

II.3. Kinetics of nitric oxide formation

Reaction Mechanisms responsible for the formation of nitrogen oxides, which are produced by combustion, involve various stable and radical species and hundreds of elemental reactions. To reduce NO_X emissions it is necessary to understand these mechanisms.

II.3.1. Overview of NO_X formation process

During the combustion process, nitrogen monoxide (NO) is formed from molecular nitrogen (N_2) present in the air or from nitrogen atoms present in fuel.

Several mechanisms are available to describe the formation of NO:

- The thermal NO formation mechanism (or thermal-NO), Zeldovich (1946) [76],
- The Fenimore NO formation mechanism (or Prompt-NO), Fenimore (1971) [77],
- The N_2O route, Malte and Pratt (1974) [78],
- The NNH route, Bozzelli and Dean (1995) [79],
- Finally the NO mechanism obtained directly from fuel (Fuel-NO), Fenimore and Jones (1961) [80].

In our study, we focused specifically on biogas-syngas mixture flame, without the fuel-N additives. Therefore, the fuel-NO mechanism is not more detailed in this work.

II.3.1.1. The thermal NO formation mechanism

The thermal NO mechanism is given by Zeldovich in 1946 [76]. This is the simplest mechanism that accounts for the nitrogen monoxide formation of molecular nitrogen of air (via N≡N bond breaking and formation of nitrogen atoms). It is based on the following three reactions:

$$O + N_2 \leftrightarrow NO + N \quad \text{(II.4)}$$

$$N + O_2 \leftrightarrow NO + O \quad \text{(II.5)}$$

$$N + OH \leftrightarrow NO + H \quad \text{(II.6)}$$

As its name suggests, thermal NO formation is highly temperature-dependent, so the hotter the combustion, the more NOx is formed (T >1800K). This is due to the high activation energy (315 kJ/mole) of the limiting reaction, the reaction (II.4), which

results in high dependence of NO production rate on temperature. Therefore, the kinetic data for high temperature are required to account for this mechanism. Furthermore, the importance of this mechanism may also be correlated O atoms and OH radical concentrations in flame. This is shown by several authors [81, 82, 83] who observed that concentrations of O atoms and OH radicals were abnormally higher than the equilibrium value in flame. To reduce thermal NO, the flame temperature should therefore be decreased, residence time, and/or reduce the oxygen concentration in the flame front area.

II.3.1.2. The prompt NO formation mechanism

Prompt NO formation was introduced by Fenimore in 1971 [77].This formation begins in flame fronts where concentrations of hydrocarbon radicals CH_i (i = 0, 1, 2) are the highest. The formation of NO is dominated by the initiation reaction between the methylidyne radical CH and the molecular nitrogen of air N_2:

$$CH + N_2 \leftrightarrow HCN + N \quad \text{(II.7)}$$

The energy barrier of this reaction is lower than that the reaction (II.4), the NO resulting from the prompt route is formed more rapidly at a given temperature. This route is sensitive to the equivalence ratio of the mixture. Indeed, the excess of CH_i radicals in the case of rich flame favors the formation of NO-prompt compared to the case of stoichiometric mixture where the Zeldovich mechanism is more active.

Although the link between the methylidyne radical present in flame front and NO has been established experimentally by several authors [84, 85]. The NO-prompt mechanism has been the subject of widespread controversy when it was first proposed, as the initiation reaction, corresponding to the reaction between $CH(X^2P)$ radical and N_2 molecule producing the HCN molecule and atomic nitrogen $N(^4S)$, is a spin-forbidden reaction. Nevertheless, numerous studies have conducted on experimental and theoretical determination of the reaction rate constant, assuming that the products were HCN and N [86, 87, 88]. Miller et al [18] proposed the first detailed mechanism of nitrogen chemistry including the Fenimore pathway, used more commonly by the combustion science community. In this mechanism, the initiation reaction produces hydrocyanic acid, HCN, which then reacts with atomic oxygen:

$$HCN + O \leftrightarrow H + NCO \quad \text{(II.8)}$$

Other products are formed from HCN in smaller quantities such as CN or NH:

$$HCN + O \leftrightarrow OH + CN \quad \text{(II.9)}$$

$$HCN + O \leftrightarrow NH + CO \quad \text{(II.10)}$$

CN radical produces NCO via:

$$CN + O_2 \leftrightarrow NCO + O \quad \text{(II.11)}$$

$$CN + OH \leftrightarrow NCO + H \quad \text{(II.12)}$$

In an oxidizing environment, NCO leads to NO and CO via reactions:

$$NCO + OH \leftrightarrow NO + CO + H \quad \text{(II.13)}$$

$$NCO + O \leftrightarrow NO + CO \quad \text{(II.14)}$$

This NO-prompt sub-mechanism has been integrated into the most detailed mechanism that exist: Lindstedt [89], Dagaut [90], Konnov [91], GRI-Mech [92] and GDF-kin® [93] with some adjustments of constants, especially that of initiation reaction: $CH + N_2 \leftrightarrow HCN + N$

In 2004, Miller et al. [94] highlighted the importance of the theoretical work of Moskaleva et al [95], which showed that the products of the reaction between CH and N_2 are NCN and H and not HCN and N.

In 2006, the new initiation reaction of NO-prompt $CH + N_2 \leftrightarrow HCN + N$ has been integrated for the first time into the detailed kinetic mechanism GDF-kin®3.0_NCN [93].

In 2007, Harding et al. [96] proposed a velocity constant based on ab initio calculations using a different theoretical approach from that Moskaleva et al work [95].

Theoretical calculations of Harding et al [96] help to explain the experimental results obtained in shock tubes by Vasudevan et al. [97]. The value obtained by Harding et al [96] for reaction velocity constant $CH + N_2 \leftrightarrow HCN + N$ is different from that of El Bakali et al. [93] at low temperature. Lin et al [98, 99] performed theoretical calculations of NCN oxidation reaction constants involving OH, O, O_2 and NO. Currently, these are the only theoretical data on these constants apart from current estimates proposed by Glarborg et al. [100].

Subsequently, several researchers worked on implementing the NCN pathway into existing reaction mechanisms to simulate different types of flames (premixed flat flames or diffusion flames).

Regarding the GRI-Mech3.0 mechanism, several studies have been carried out. (Sutton et al [101, 102, 103], Gersen et al [104], Naïk et al [105], Klein- Douwel et al [106], Sepman et al [107, 108, 109]). These authors suggest that the study of NCN sub-mechanism is necessary to improve the prediction of NO. However, pointed out that the lack of data on NCN chemistry does not allow concluding on initiation reaction and the value of reaction constant. However, the authors point out the importance of $CH + N_2 \leftrightarrow HCN + N$ reaction on NO formation.

In 2009, Konnov has revised the fifth version of his mechanism [91]. The new version of his mechanism (version 6) [110] showed good agreement between the predictions and different experimental data for NO and NCN profiles [101, 102, 110, 111, 112].

For the GDF-kin®3.0_NCN mechanism, Lamoureux et al. [113] adjusted the rate constant of initiation reaction $CH + N_2 \leftrightarrow HCN + N$ of El Bakali et al [93] by simulating NO and NCN profiles. In particular, rate constant for consumption reaction of NCN ($NCN + H \leftrightarrow HCN + N$, $NCN + O_2 \leftrightarrow NO + NCO$, $CN + NO \leftrightarrow CN + NO$ and $NCN + OH \leftrightarrow HCN + NO$) have been optimized relative to the NCN profiles and to the works of Zhu and Lin [98, 99, 114]. A good agreement was found between CH, NCN and NO measurements, and the new version of kinetic mechanism GDFkin ®3.0_NCN. In addition, the authors measured NCN at low pressure [113, 115, 116], NCO [117] and HCN [118] thereby optimizing NOx chemistry.

However, the reaction rate constants of prompt-NO sub-mechanism are always affected by a high degree of uncertainty; this is not only a rate constant of initiation reaction but also all those concerning NCN oxidation. Typically, the only species that are used in the confrontation of experience-modelling to validate the prompt-NO sub-mechanism in flames are CH and NO species. Certainly, a lack of quantitative data on other species such as NCN, NCO, HCN, CN, NH…and limited knowledge of rate constants of reaction involved are seen as impeding understanding the mechanism of the prompt-NO formation in flames. However, as was mentioned before, recent studies on direct measurement methods for NCN [103, 106, 113, 115, 116] were conducted at

low pressure or atmospheric pressure. These studies also permit to obtain fundamental, quantitative measurements for the validation of the reaction mechanism. However, to our knowledge, no measurements have yet been made at high pressure for nitrogen species other than NO.

II.3.1.3. NO formation via N_2O-intermediate mechanism

The mechanism of formation of NO via N_2O-intermediate pathway was evidenced by Malte and Pratt (1974) [78], following through on the work of Lavoie et al. (1970) [119]. This mechanism, relatively insignificant for stoichiometric and rich flames, played a significant role in the formation of NO in lean flames [78]. This mechanism includes the following 5 reactions:

$$N_2 + O + M \leftrightarrow N_2O + M \quad \text{(II.15)}$$

Where M is the collision partner

$$N_2O + O \leftrightarrow NO + NO \quad \text{(II.16)}$$

$$N_2O + O \leftrightarrow N_2 + O_2 \quad \text{(II.17)}$$

$$N_2O + H \leftrightarrow NO + NH \quad \text{(II.18)}$$

$$N_2O + H \leftrightarrow N_2 + OH \quad \text{(II.19)}$$

Other reactions involving N_2O may be considered in chemical kinetics calculations. As with the NO-thermal mechanism, this mechanism is sensitive to OH and O concentrations in flame front [120]. The collision partner (+M) present in the reaction (II.15) reflects its dependence on pressure. Thus, we can see the contribution of mechanism increasing at high pressure.

II.3.1.4. NO formation via NNH mechanism

Bozzelli and Dean (1995) [79] proposed a new mechanism of formation of NO via the NNH route. The NNH is first formed from the reaction between molecular nitrogen and the hydrogen atom. The product of this reaction is then attacked by an oxygen atom O:

$$N_2 + H \leftrightarrow NNH \quad \text{(II.20)}$$

$$NNH + O \leftrightarrow NH + NO \quad \text{(II.21)}$$

This work has been picked up by Hayhurst and Hutchinson (1998) [121] which measured NO_x concentration profiles in a flat flame of $H_2/O_2/N_2$ and $CH_4/O_2/N_2$. The results showed that this suggested route is responsible for NO formation especially in rich mixtures, with temperature below 2100 K. This reaction may be important in the flame front where the concentration of oxygen atoms is high.

When measuring the emissions of nitrogen oxides from the various combustion devices, it is useful to define an indicator allowing direct comparisons. This indicator, called $EINO_X$ (as the Emission Index of NO_X), is defined by the following formula:

$$EINO_X = \frac{mass\ of\ nitrogen\ oxides\ produced\ (g)}{mass\ of\ burnt\ fuel\ (kg)} \quad \text{(II.22)}$$

This index has the advantage of not taking into account the dilution of combustion products and thus allows an unbiased comparison of the emissions of the different installations. It is calculated from the composition of the fumes.

II.3.2. Kinetic mechanisms used in this thesis

II.3.2.1. Gas Research Institute mechanisms

II.3.2.1.1. GRI-Mech2.11

The Gas Research Institute mechanism GRI-Mech2.11 was developed in 1996 by Bowman et al. (1995) [122]. It is an improved version of 1.2, to which are added the nitrogen chemical processes and NO reburning (addition of 102 reactions for 17 species). The four NO formation mechanisms are included. For prompt-NO mechanism, proposed by Fenimore (1971). The initiation reaction is $CH + N_2 \leftrightarrow HCN + N$ and the reaction rate constant is: $k = 2.875 \times 10^8\ T^{1.1} \exp\left(-\frac{20400}{RT}\right) cm^3.mole^{-1}.s^{-1}$. The mechanism GRI-Mech2.11 thus contains 277 elementary chemical reactions of 49 species. It has been used for methane and has been validated with results obtained in flow reactors, in a perfectly stirred reactors and on low-pressure flames (< 1 atm).

II.3.2.1.2. GRI-Mech3.0

The Gas Research Institute mechanism GRI-Mech3.0 [92] was released in 1999 and replaces the GRI-Mech2.11 version. It contains 325 reversible reactions and 53 species. It includes the oxidation of C_1 and C_2 hydrocarbons, reduced kinetics of

propane oxidation and a sub-mechanism for NOx formation including Zeldovich mechanism (1946), Fenimore mechanism (1971) (the rate constant for initiation reaction is: $k = 3.12 \times 10^9 T^{0.88} \exp\left(-\frac{20130}{RT}\right) cm^3.mole^{-1}.s^{-1}$), [60, 63]. This mechanism was developed in the combustion of methane and natural gas. It is optimized for temperature conditions between 1000 and 2500 K, the pressure between 1.3 kPa and 1 MPa, and the equivalence ratio between 0.1 and 5. It has been validated under many experimental conditions: Shock tubes, flow reactors, and laminar flames. The GRI-Mech 3.0 mechanism is now a reference mechanism for simulation of methane combustion.

II.3.2.2. USC Mech II

The USC Mech II is composed of 111 species and 784 reactions, it was released in 2007 by Wang et al. [123]. This mechanism applies to a wide variety of combustion scenarios, incorporates the recent thermodynamic, kinetic, and species transport updates relevant to high-temperature oxidation of hydrogen, carbon monoxide, and C_1-C_4 hydrocarbons. This model was developed based on:

- An optimized reaction model of H_2/CO combustion
- GRI-Mech1.2 and 3.0
- A comprehensive reaction model of ethylene and acetylene combustion
- Reaction mechanism of C_3 fuel combustion
- 1,3-Butadiene oxidation at high temperatures.

Also, the rate parameters of CO+OH, OH+HO_2 and CO+HO_2 were updated from more recent studies. Rate parameters of several C_1 and C_2 reactions were reevaluated. The oxidation model of benzene and toluene was included. The reaction model was subject to validation tests against reliable H_2/CO/C_1-C_4 combustion data.

Chapter III

Flameless combustion

III.1 Introduction

To improve the energy efficiency of a burner, it is possible to transfer heat of burnt gases to fresh gases: this is the principle of regenerative burners. However, increasing the temperature of reactants has a direct impact on nitrogen oxides formation. New technologies have been developed to overcome this drawback with varying degrees of success. These technologies include Oxy-fuel combustion process, which has the major advantage of not emitting nitrogen oxides, since nitrogen from the air is absent. Another method, known as staged combustion, is used to reduce NOx emissions by limiting residence times at high temperatures or by promoting the recombination of nitrogen oxides with hydrocarbon radicals. Other methods exist, such as Selective Non-Catalytic Reduction (SNCR) and Selective Catalytic Reduction (SCR), which are based on injection of particular chemical species into combustion products to induce nitrogen oxide reduction reactions. Despite the range of technologies available to industry to reduce pollutant emissions, most of these methods cause significant operational and/or installation costs, but can also be done to detriment of overall efficiency of configurations.

In 1989, the flameless combustion is known under the acronym FLOX (FLameless OXydation) [31]. It is defined as a combustion regime for which no flame is visible, stable, with very low temperature gradients and emitting very few pollutants (CO and NO). It is then shown that the fundamental condition to obtain FLOX combustion regime is to dilute the fuel and/or oxidizer jets with a strong recirculation of flue gas before reaction. Following this work, this combustion regime was mainly developed in industry before becoming the subject of several studies by academic research laboratories [124]. Flameless combustion is now recognized as one of the most advanced combustion technologies to reduce the pollutants and fuel consumption. This regime is particularly interesting for industrial processes requiring homogeneous temperature field, mechanical stress monitoring, generation of low noise and low instabilities and being subject to evolution of strict NOx emission standards. There are many potential industrial applications of this type of combustion regime: glass furnaces, metallurgical furnaces, refineries, gas turbines...

Various terms have been used to describe combustion systems operating in the flameless combustion regime; which indicates that to date there is no rigorous common understanding of this regime. To clarify this, it is important to go over different definition proposed in the literature, and to establish the fundamental characteristics of combustion regime, which called in this manuscript "flameless" or "MILD".

III.2 Flameless combustion Phenomenology

Generally, in large-scale furnaces, high heat output is released and high temperatures are obtained in gases and walls. During such installation **(Fig.III.1),** when the conditions are suitable, there is a change in the flame regime, which can be observed directly. From a clearly identified luminous zone, corresponding to mixing zone for a conventional flame, to an invisible flame, as shown in **fig.III.2**. In such regime, the pressure fluctuations become negligible, the acoustic disturbances are reduced very significantly and the temperature becomes more homogeneous. The temperature peak disappears, its values in burner ranges from 1000°C to 1400°C. The walls of such installation, usually made of refractory bricks, under the effect of the high heat, begin to radiate intensely. As a result, by increasing the size and uniformity of hot zones, the radiative transfers are greatly improved. Finally, the formation of pollutants, particularly nitrogen oxides, is greatly reduced. At equal power, depending on the mode of operation (conventional or flameless), the literature reports variations in the production of nitrogen oxides ranging from 1 to 1/10th approximately, depending on whether one is in the conventional or flameless mode.

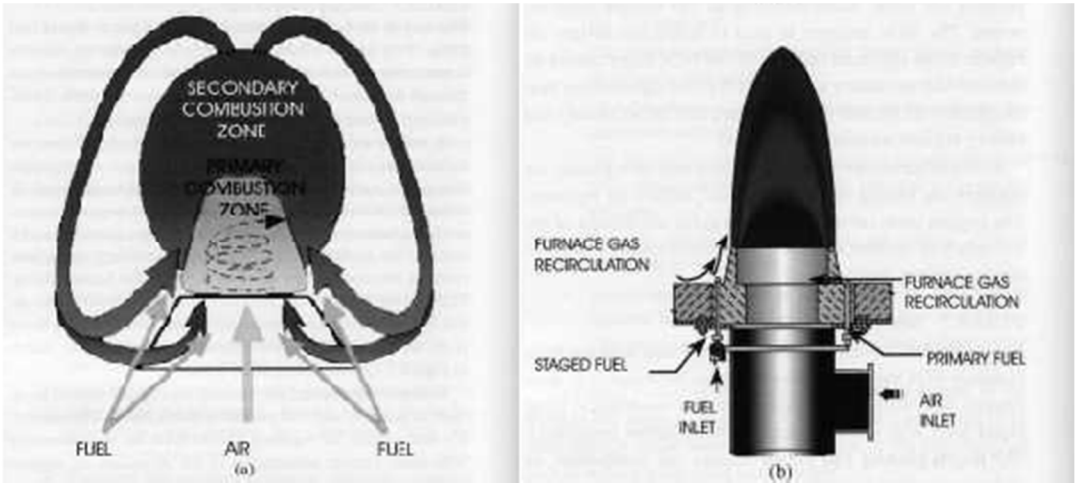

Fig. III 1: Schematic of furnace gas recirculation [125]

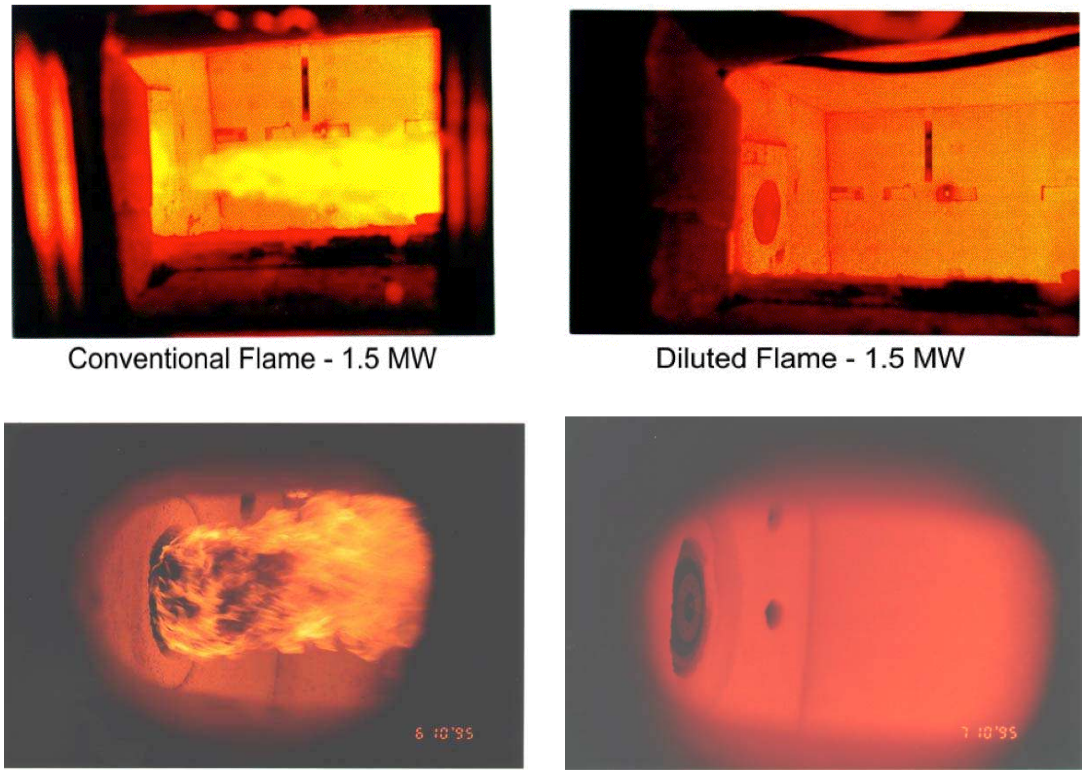

Fig.III.2: Comparison flame/flameless firing natural gas - CSM test furnace [126]

Research has followed several pathways to obtain low pollutant emissions furnaces. One of them was discovered at the beginning of the last decade of the 20th century, simultaneously and independently by several different teams. This innovation is "flameless combustion", a name consecrated by usage. Japanese and German researchers currently dominate this research theme, although other nations have also made serious efforts in this area. The various discoveries made are all going in the same direction, nevertheless bear different names.

- Flameless combustion or flameless oxidation, this nomenclature is prevalent in the Germanic world. It has given rise to the tabling of a series of patents and became a trade name [127]. The complete designation of "FLameless Oxidation", which is a trademark of the company WS Wärmetechnik, is "FLOX".
- Moderate or Intense Low oxygen Dilution (MILD) combustion. It uses low oxygen levels. This name is more widely used by Italian scientific community [128].

- High Temperature Air Combustion (HiTAC). This designation is used primarily in Japanese environments and is also a trade name.
- Highly Preheated Air Combustion (HPAC); it is also from the Japanese scientific community. It also resulted in the filing of a patent.

These last two names are the property of the Tokyo Gas Company.

The transition from conventional to flameless mode is not immediate. In particular, there is a period, during which operating conditions are established in furnace, during which a furnace is the site of conventional combustion. When conditions are right, the transition from one to the other is done by itself.

III. 3 Conditions for obtaining the flameless regime

There is abundant literature on the existence of this phenomena, and on its characteristics. However, there remains a lack of clarity concerning the conditions, which led to its appearance. All the observations were made in furnaces with thermally insulating walls, and relatively hot. Therefore, the containment of the enclosure seems to be an important characteristic. Furthermore, in all cases, the reactants are strongly preheated, suggesting that the temperature is also very important. The fact that a considerable heating time is necessary before obtaining said regime, suggests that the installation must be sufficiently close to thermal equilibrium before being able to switch to the flameless mode. Heat losses are therefore important.

The confinement used leads to the creation of a closed chamber, from which only part of fumes, is extracted. Therefore, a large proportion of burnt and hot gases are permanently located in the enclosure, which, by their movement, mix with fresh gases near their injection point. The movement of burnt gases is called recirculation: due to their temperature, the exhaust gases will pass in a reflux movement, near the walls and thus heat them by convection and radiation. After reaching the vicinity of the fresh gas injection zone, the fresh reactants will be simultaneously mixed and heated by the exhaust gas. This mixture leads to dilution of active species. Regarding this mixture, it is agreed upon that these movements decrease the intensity of the chemical reaction which would contribute to a thickening of the reaction zone. Therefore, Recirculation seems to have a crucial role.

III.4 Flameless Combustion Characteristics

MILD combustion permit to achieve very low levels of nitrogen oxide emissions, even with preheating combustion air, when the reactants are diluted by combustion products in in a high temperature environment. Many papers include both experimental and numerical studies; deal with combustion systems operating under this principle although referenced under different names. Generally, flameless combustion has one or more of these major characteristics:

- Invisible flame;
- High combustion efficiency;
- Low temperature gradients;
- Reductions in combustion noise;
- Zero or low NOx and CO emissions;

III.4.1 An overview of terms used in literature to describe flameless combustion

Different denominations of flameless combustion regime are mentioned in literature. **Table III.1** summarizes the main terms, and fundamental characteristics used to define the combustion regime.

Even though a general definition of flameless combustion is yet to establish, there is a fundamental relation between each of the definitions. Particularly, in flameless combustion, the recirculation of combustion products dilutes the reactants prior to combustion, resulting homogenization of temperature field and reduction of pollutant emissions. For ease of reference, the terms “flameless combustion” or “MILD combustion” will be used throughout this manuscript to characterize this process.

Table.III.1: Various names given to flameless combustion.

Acronym	Properties	Reference
MILD	No singular points on S-curve (T as a function of Damköhler).	[129]
	Reactants injection temperature higher than the auto-ignition temperature of mixture. The maximum temperature increase due to combustion should be lower than the auto ignition temperature of the mixture.	[37]
	Temperature fluctuations in flow under certain criteria.	[130]
Flameless/colorless	No flame is visible.	[31, 131]
HiTAC	Injection air temperature allows the self-ignition of mixture	[132]

III.4.2 Light emission

One of impressive properties of flameless combustion is able to manifest a particular light emitting mode. Indeed, under certain conditions of temperature and reactants dilution, the flame front is no longer visible (**fig.III.3**). Wunning et al [31] define flameless combustion based on this criterion: it is flameless oxidation (Flameless Oxidation or FLOX Combustion). More recently, Khalil et al. [133] and Arghode et al. [134] also described this regime as CDC, Colorless Distributed Combustion. However, the light emission is not zero. Instead, it becomes less intense than the light emitted

from the heated walls of the combustion chamber. This is due to species dilution, which implies a decrease in concentration of most light emitting species (especially CH* and C2* radicals) [32]. It also bears noting that some properties of flameless combustion regime (low temperature gradients, low nitrogen oxides emissions) can be achieved by distinguishing the reaction zone.

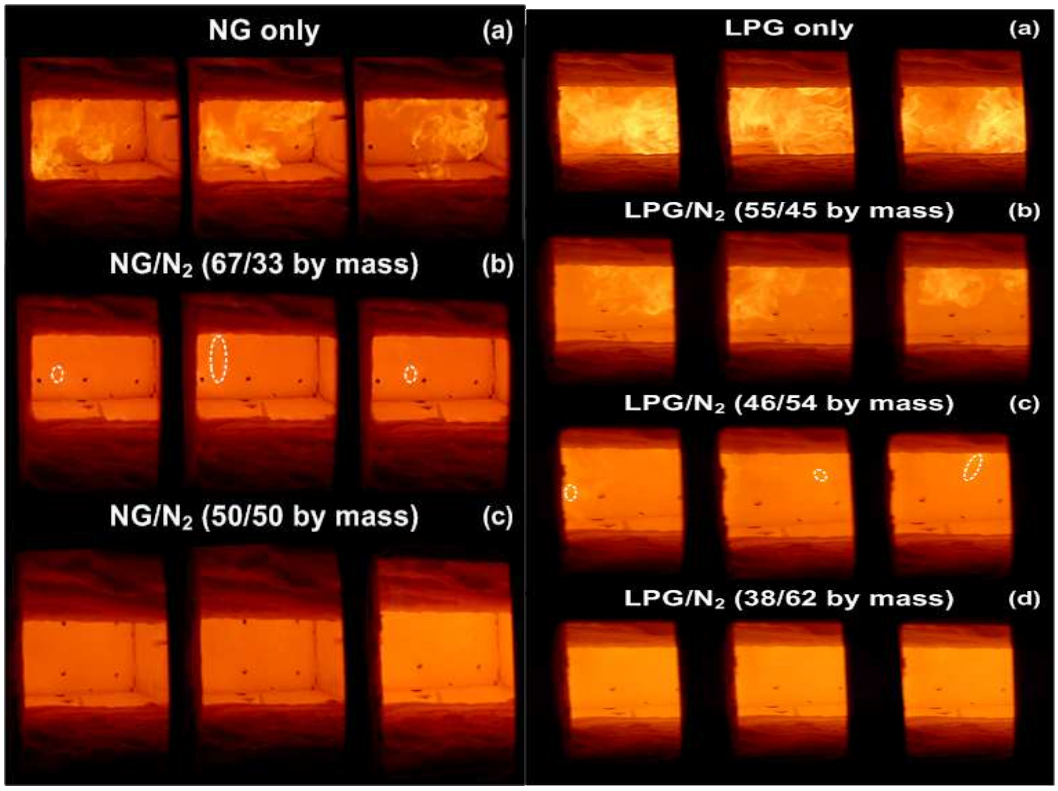

Fig.III.3: Sequence of instantaneous images of NG and LPG combustion with increasing N_2 dilution in a laboratory-scale combustion furnace (d = 3mm). The dashed circles represent reaction patches (Szegö et al, 2007).[135]

Therefore, in an overall context, the definition of the flameless combustion based on visual appearance of the combustion process altogether inadequate.

III.4.3 Reactants preheating

One of the major advantage of flameless combustion is reduction of nitrogen oxides emission, even by preheating the reactants. Preheating of reactants (usually oxidizer) allows fuel economy, increasing thermal efficiency and ensuring combustion process, in particular by promoting self-ignition. This has the effect of stabilizing combustion without any other means (pilot flame, swirl injection, etc.).

Reactants can be preheated externally, by heating reactants before they are injected into the combustion chamber, or internally, by recirculating hot exhaust gas to reactants. When air preheating is very important, Katsuki et al [136] define the Highly Preheated Air Combustion (HPAC). Similarly, when reactant dilution is significant, Cavaliere et al [37] identify HiTAC combustion for High Temperature Air Combustion. In this configuration, auto-ignition controls combustion in combustion chamber. The concept of air preheating is also intervened in the definition of MILD combustion, an acronym for Moderate or intense low oxygen dilution, as defined by Cavaliere et al [37].

It is important to note that this definition of MILD combustion assumed that air is preheated externally. However, in many configurations, the preheating temperature does not exceed the auto-ignition temperatures [137]: recirculation and reactant dilution of the reagents provide the heat required for combustion stabilization and ensuring flameless combustion process. In addition, it has been shown that flameless combustion could be achieved without preheating of reactants, although this case is not interesting for industrial applications [31, 135]. Finally, it should be noted that preheating of reactants is not exclusive to flameless combustion: large number of configurations operate with preheating to achieve a better efficiency without reaching flameless combustion regime. In fact, the preheating of reactants, whether internal or external, is a key component of MILD combustion in the sense that this combustion regime is operating at higher reactant temperature.

III.4.4 Recirculation of combustion products - Dilution of reactants

A fundamental aspect of flameless combustion is the low temperature gradient. This is achieved by diluting reactants and combustion products. The dilution can be carried out later via a pre combustion (the diluent is created by an additional combustion before entering the configuration) or directly in the combustion chamber, (the diluent is created in the combustion chamber). Obviously, sufficient internal dilution to obtain a flameless combustion regime will depend on the aerodynamics of the combustion chamber, its geometry and conditions of movement quantities at fuel and oxidizer injections, intended to ensure wide recirculation zones.

The dilution by combustion products allows to homogenize the temperature inside the furnace and to avoid hot spots in the combustion chamber. This directly

reduces formation of nitrogen oxides. From a technical point of view, the dilution of reactants is made by mixing fuel and oxidizer with combustion products before reaction zone. The main effect obtained is that temperature gradients are less important than in conventional combustion. Due to preheated air injection and the lower flame temperature, the temperature gradients are also decreased significantly. However, this technique requires precautions: dilution should be done before burning pure reactants. When dilution exceeds a certain threshold, the flameless combustion regime is reached [31]. Instead, if dilution is not favored or if it is too late, combustion can be conventional or unstable. This can be illustrated by plotting the locations of combustion zones as a function of furnace operating temperature and recirculation factor which is the ratio between the gas mass flow entrained by all jets ($\dot{m}_r$) , and the sum of air ($\dot{m}_a$) and fuel mass flows ($\dot{m}_f$) in the discharge $k_v = \dot{m}_r/(\dot{m}_f + \dot{m}_a)$. **Fig.III.4** Note that in this diagram, the flameless combustion regime must also be bound by straight line when the operating temperature becomes higher; in this case, the pollutant production explodes and the risk of getting off the flameless combustion mode is increased. **Fig.III.4** clearly shows the paramount importance of dilution, and therefore recirculation, on establishment of a MILD combustion regime.

Dilution requires large zone heat release and low temperature thermal fluctuations [138], is a key element to be considered in modelling flameless combustion.

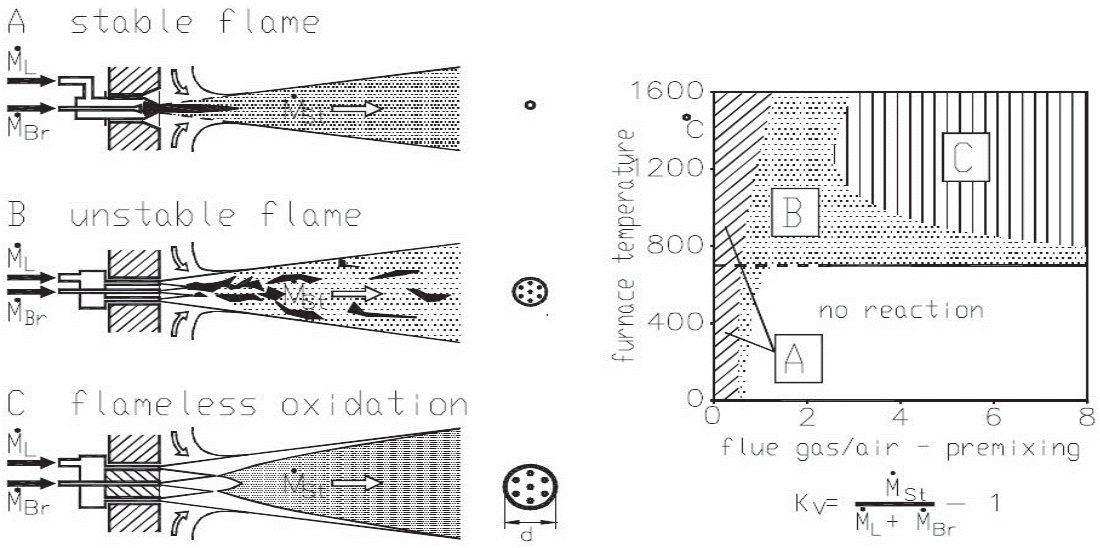

Fig.III.4: Schematic diagram of the stability limits for different combustion modes. (Wunning and Wunning, 1997) [31]

Finally, dilution providing heat to reactants by diluting them: the reactants are preheated before combustion. **Fig.III.5** shows the MILD combustion regime as a function of the recirculation rate k_v and temperature of the reactants. The flameless combustion regime can then be distinguished as a regime that operates at high temperatures of diluent and at relatively low oxygen contents (direct consequences of recirculation / dilution).

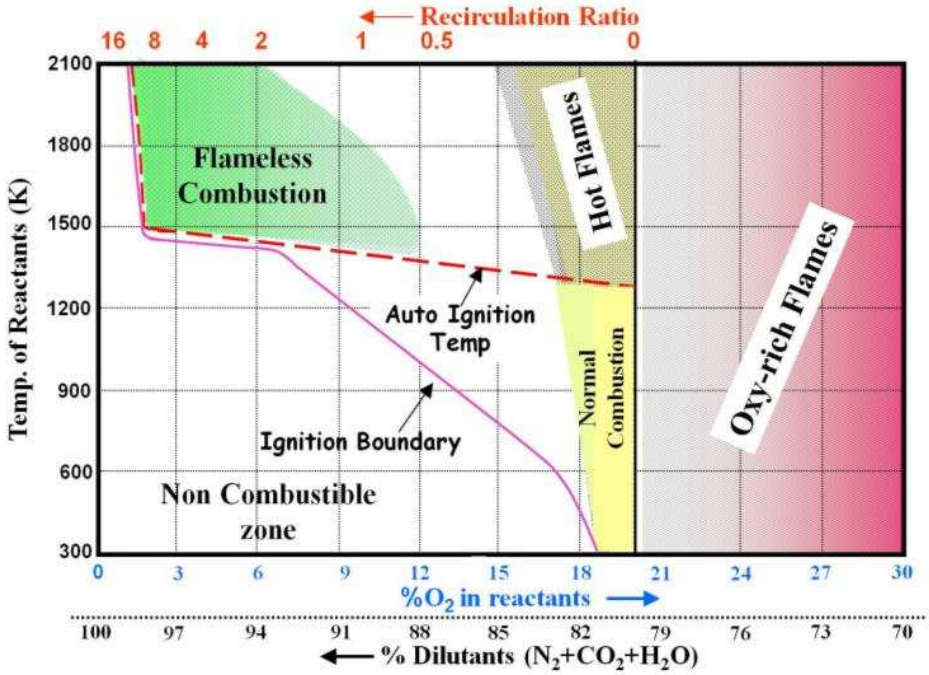

Fig.III.5: Schematic of different combustion regimes (Rao & Levy, 2010) [139]

III.5 Stability of flameless combustion regime

After outlining the characteristics of the flameless combustion regime, it is important to focus on current knowledge concerning stabilization mechanisms of MILD combustion before discussing modelling issues inherent to this regime. The parameters controlling the stability of flameless combustion are still under consideration. This is mainly due to fact that the extrapolation of conclusions obtained for a given configuration (operating conditions, geometry...) to a general case is difficult. In a conventional non-premixed combustion, combustion stabilization can be achieved by various means: flame trap, pilot flames, swirls or recirculation of hot gases close to the injection system [140]. In flameless combustion, the burners facilitate chemical reactions downstream of flow by slowing down the reactants mixing or by increasing the local strain rate. For this purpose, high reactant temperatures and high dilution rates

are necessary to stabilize the combustion (**Fig.III.4**). Mixture control inside MILD combustion chamber is therefore of paramount importance.

Studies dedicated to stability of the highly diluted combustion regime have been carried out at different scales, on various configurations. The chemical structure of laminar flames subjected to the different N_2 dilution level was analyzed by Payet [141], by calculating the one-dimensional opposed jet premixed flames with detailed chemistry. These calculations highlighted the importance of dilution on flame velocity, flue gas temperatures and flame thicknesses. In a more recent study, Min et al [142] examined the effect of air injection dilution by various diluents in laminar diffusion flames. They have isolated the effects of physicochemical properties of diluent, which they showed that it is responsible for flame extinction for a certain level of dilution, from pure dilution effects, which is responsible for flame length changes. Subsequently, this study was developed for various aerodynamic conditions. Min et al [143] and Mastorakos et al [144] analysed the extinction limits of opposed jet turbulent flames for injections of reactants diluted by combustion products. In this study, the authors show that combustion stabilization can only be achieved if the temperature of reactants increases with dilution. In addition, when the temperature of exhaust air exceeds a certain temperature, an auto-ignition phenomenon occurs and combustion is maintained, even for very strong flame stretch. The latter corroborates the findings of Darabiha et al [145], who observed similar behaviour on hydrogen-air flames for which the oxidizer temperature have been varied. Finally, Riechelmann et al [146] investigated the influence of dilution of air and fuel injections with different diluents (Ar, N_2 and CO_2) on extinction limits of methane-air diffusion flame. They were able to discriminate the effects of temperature increase of reactants from the effects of dilution and to demonstrate the importance of composition of diluent on flame structure.

Although, not all of the studies mentioned have been designed to simulate flameless combustion process, they help to highlight stabilization of combustion process when reactants are diluted and preheated.

The analysis of the MILD combustion stabilization in complex configurations (confinement, heat losses, high Reynolds number...) was mainly focused on the influence of recirculation rate K_v introduced by Wunning et al [31]. They estimate that flameless combustion is only stabilized at an operating temperature that is sufficiently

high (over 1100 K for methane-air combustion) and at recirculation rate higher than K_v = 0.3. Outside this zone, combustion is considered conventional and stable for recirculation rates below 0.5, whereas it is unstable (flame puffing, flame extinction, etc.) for intermediate K_v values. To characterize the transition from conventional combustion to the flameless combustion regime (based on the visual appearance of flame), Cavigiolo et al [147] conducted an experimental study on a confined cylindrical burner. They varied the recirculation rate by modifying the temperature of the injected air or by diluting the main air jet with nitrogen. Cavigiolo et al [147] investigated an experimental study on the enclosed cylindrical burner. They varied the recirculation rate by changing injected air temperature or by diluting the main air jet with nitrogen. For methane combustion, the authors showed that the MILD combustion regime was established for K_v values exceeding 4 for operating temperatures above 1100 K. Effuggi et al [148] extended this study on the use of different fuels. Finally, it should be noted that since the recirculation rate K_v is related to the ratio of fuel oxidizer injected into combustion chamber, some authors have discussed the stability of flameless combustion according to this ratio [135, 149].

In short, this section has provided a rapid review of current knowledge on stabilization mechanisms of the flameless combustion regime. While no final conclusions were reached, the studies available in the literature showed that certain parameters can play important role in simulation of this combustion regime:

- The dilution of reactants and the composition/temperature of diluent;
- The aerodynamics of jets and chamber.

III.6 Modeling issues

The MILD combustion regime is still poorly understood in complex configurations. Indeed, there is still much uncertainty regarding stabilization mechanisms or local flame structure in this regime. This poses major modelling issues, which we will describe in this section.

- Dilution of reactants by combustion products is the main key establishment and stabilization in MILD combustion and this poses major problems. First, reliable prediction recirculation zones and their interaction with fresh reactants is essential. Therefore, reliable modelling of combustion process and of mixing in the chamber is

utmost important. In the latter, it is interesting that simulations with RANS formalism (Reynolds Averaged Navier Stokes) have shown strong limitations on prediction of fuel jet dilution [150]. Studies have focused on this problem analytically [151] or experimentally [152]. Moreover, two parallel phenomena become apparent during recirculation of combustion products. Recirculation may cause a simple dilution, a change in composition and this without heat input. However, dilution of the reactants by exhaust gas can be done with energy input that will change the reactivity of mixture. This coupling is extremely problematic since it is unknown a priori in which order these processes are carried out. Moreover, this phenomenon is coupled with thermal losses, which will greatly influence the energy history of burnt gas pocket. Ultimately, dilution can have multiple effects depending on recirculation rate and heat loss. It is vitally important to characterize all possible chemical trajectories for different scenarios.

- Most the systems operating in a MILD combustion mode, excluding gas turbines, operate with separate injection of fuel and oxidizer. Fuel and oxidizer jets can be mixed only after being diluted. That represents an additional problem insofar, where the turbulent combustion model should take into account a mixture of three fluids (fuel, oxidizer, diluent).

- Then, combustion reactants takes place, the turbulent combustion model is supposed to reproduce the evolution of thermochemical variables of interest, such as temperature or pollutants.

- Combustion systems operating under flameless combustion conditions aim to transfer a maximum amount of heat from hot gases to a load. The heat losses by conduction-convection and radiation are very important. Therefore, a good prediction of temperature fields, pollutant, and stability of combustion regime depended on good prediction of heat losses through walls and by radiation.

- After combustion reactants, a portion of the exhaust gas, which may have been affected by different degrees of heat loss, recirculates upstream of the flow. The flow aerodynamics must be sufficiently well defined to capture the correct recirculation rate. The latter depends on the amount of injected reactants and on chamber geometry.

III.7 Applications

III.7.1 Furnaces

Industrial furnaces are the only current industrial application of flameless combustion, especially in Japan. The fuel used is natural gas or methane. Heat losses due to heating materials reduce the flue gas temperature and the uniform temperature obtained is a good advantage for these applications. The materials are heated in line, pairs of regenerative burners or self-regenerative burners are installed in parallel along the production line (**Fig.III.6** and **Fig.III.7**). Another way is to use radiant tubes: flameless combustion takes place inside and the tubes radiate towards the charge (**Figure III.8**). Their shape allows the recirculation of flue gas.

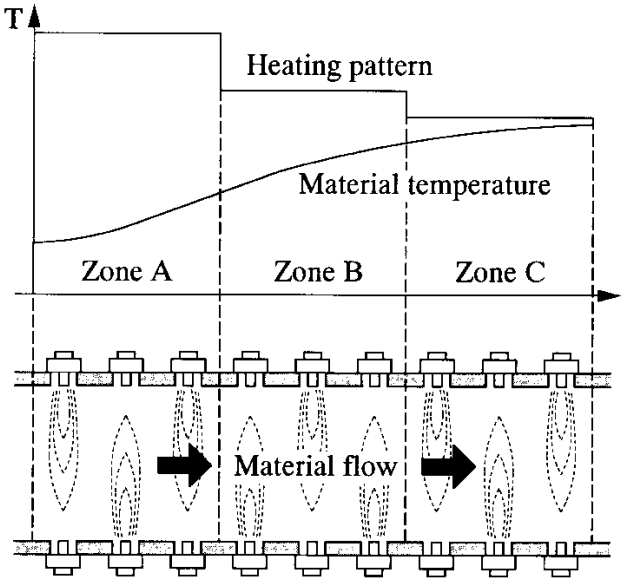

FigIII.6: Line heating with pairs of burners. [136]

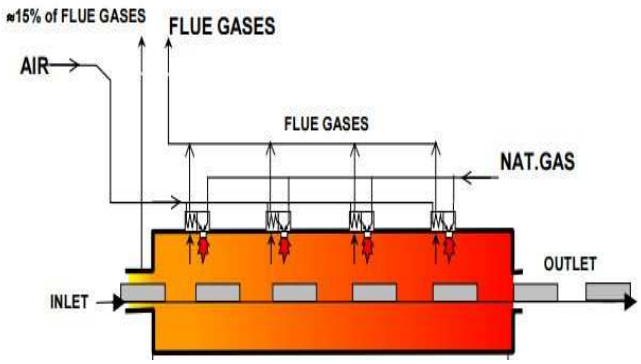

Fig III.7: Line heating with self-regenerative regenerating burner. [126]

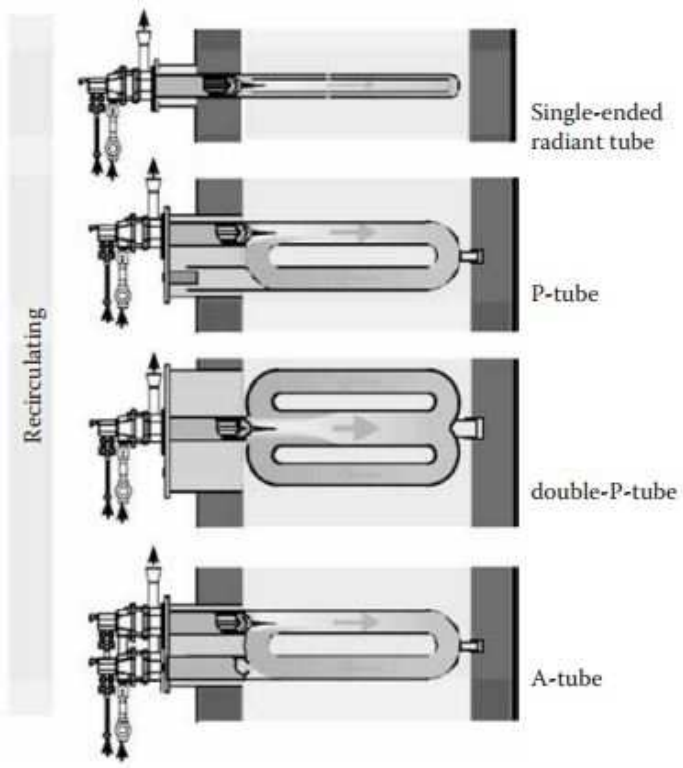

Fig.III.8: Different types of radiant tubes with flue gas recirculation. [153].

III.7.2 Future applications

There are many signs of hope for production of electricity from flameless gas turbine. Unlike a furnace, it is more difficult to lower the final temperature by heat losses significantly, which is why Guoqiang et al. [154] achieve premixed flameless combustion rather than with separate reactant injection. Therefore, the temperature is fixed by equivalence ratio. The flameless regime is obtained close to the extinction limit. The necessity of dilution of reactants change considerably the geometry of the combustion chamber. In the experience of Guoqiang et al. [154], the injectors encircle a central cavity that recirculates flue gas (**Fig.III.9**). This experiment takes place under nominal pressure of one bar, the phenomenon at higher pressures remains to be studied for application with real turbines. In addition, it should remember that the injection temperature of premixed combustion should not be too high due to the risk of self-ignition and flashback.

Fig.III.9: (a) Photograph of the fuel injectors and (b) Top view of the burner with the central cavity. [154]

Another application is directed to the vehicle industry, more specifically hybrid diesel engines. This is called a Homogeneous Charge Compression Ignition (HCCI). The main setting is self-ignition because it is necessary to ensure the combustion of the mixture in each cycle. In addition, it is possible to use low calorific value fuels. Therefore, these engines could work with biofuels, for example. The difficulty in producing these engines is due to the high dependence of the auto-ignition time on pressure, temperature and mixture [37]. An on-board computer is required to adjust these different setting according to engine speed.

Chapter IV

Geometry, equations, and strategy of numerical calculation

IV.1 Introduction

This chapter will be organized into three parts:

In the first part of this chapter, the definition and Characteristics of opposed-jet diffusion flame are presented.

In the second part, we will define some parameters used in combustion studies, including the strain rate which is necessary to study laminar flames.

In the third part, the equations describing the gas reactive flows are recalled. These equations can be divided into balance equations, Thermodynamic equations, chemical kinetics, transfer phenomena, thermal flux, and transport proprieties.

IV.2 Geometry

The diffusion flame involves many physical phenomena, which are mutually related. The opposed jet configurations are particularly well suited for the study of these flames, for both laminar and turbulent flows. Indeed, cylindrical symmetry or axial symmetry allows restricting the study to a plane phenomenon. On centerline, the radial flow of the mean stream is zero, which allows having a one-dimensional phenomenon, if the study is limited to this particular line. Finally, on this line, and in the vicinity of the stagnation point, the velocity field is particularly simple, since it is potential flow.

A picture and schematic of opposed jet flame are achieved by aligning two burners vertically opposite each other, as shown in **Figure IV.1**. In the reactive case, the fuel is injected at the first side while the oxidizer, which is usually air or pure oxygen, is injected at the second one. The jets can have different temperatures to promote mixing. The two burners are separated by distance d, which is generally proportional to the diameter of each jet. The flame takes place between the two burners in the zone between fuel and oxidizer.

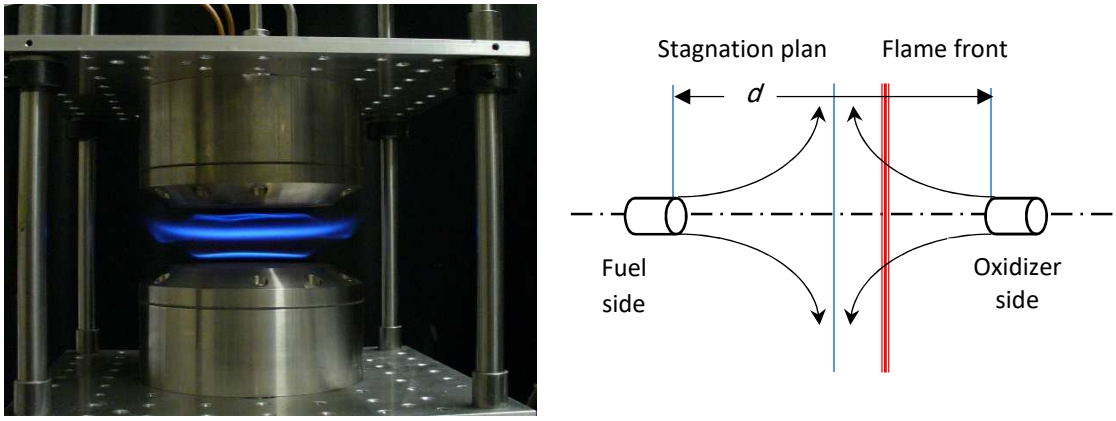

Fig IV.1: The counterflow non-premixed flame: (left) picture [155]; (right) schematic.

IV.2.1 Characteristics of opposed-jet diffusion flame

Opposite jets, have several interesting characteristics that facilitate their treatment:

- The velocities of two jets can be taken in a way that the stagnation plane, corresponding to flame, is in the middle between the two nozzles.
- It is possible to compare two different opposed jet systems if the global strain rate is the same, despite the difference in boundary conditions.
- The opposite-jet configuration is axisymmetric, which facilitates numerical simulation by decreasing the mesh size and minimizing computation time.
- The cylindrical coordinates can be chosen for calculation.
- In the stagnation plane, the axial velocity is close to 0 regardless of radial coordinates.
- This configuration permits examinations of all possible cases of variables such as composition, injection velocities, strain rates, pressures, chemical mechanisms,…

Most of these characteristics have been highlighted by Mastorakos (1993).

IV.3 Choice of primitive variables

Combustion involves multiple species reacting through multiple chemical reactions. The Navier-Stokes equations apply for such a multi-species multi-reaction gas but they require some additional terms.

First, the mass of species k is defined by:

$$m_k = n_k W_k \qquad \text{(IV.1)}$$

Where W_k and n_k are respectively the molar mass and the number of moles of species k.

As a result, the total mass of gas in a given volume V is:

$$m = \sum_{k=1}^{N} m_k \quad \text{(IV.2)}$$

Where N is the number of species in the reacting mixture. Similarly, the total number of moles n is equal to:

$$n = \sum_{k=1}^{N} n_k \quad \text{(IV.3)}$$

This latter definition leads to the expression of the mean molecular weight of the mixture:

$$W = \frac{1}{n}\sum_{k=1}^{N} n_k W_k \quad \text{(IV.4)}$$

Species are characterized through their mass fractions Y_k or their molar fractions X_k for k = 1 to N where N is the number of species in the reacting mixture:

$$Y_k = \frac{m_k}{m} \quad \text{(IV.5)}$$

$$X_k = \frac{n_k}{n} \quad \text{(IV.6)}$$

The two relations (IV.5) and (IV.6) automatically verify the expression (IV.7):

$$\sum_{k=1}^{N} Y_k = \sum_{k=1}^{N} X_k = 1 \quad \text{(IV.7)}$$

The passage from one parameter to another is via the following relation:

$$Y_k = \frac{W_k}{W} X_k \quad \text{(IV.8)}$$

The molar concentration C_k is the number of moles of species k per unit volume. It is the quantity used to evaluate kinetic rates of chemical reactions:

$$C_k = \frac{n_k}{V_T} \quad \text{(IV.9)}$$

The density of species k is defined by:

$$\rho_k = \frac{m_k}{V_T} \quad \text{(IV.10)}$$

Where V_T is the total volume of the mixture. The total molar concentration C and the density of the multi-species gas ρ are deduced from the two previous relations:

$$C = \sum_{k=1}^{N} C_k \quad \text{(IV.11)}$$

$$\rho = \sum_{k=1}^{N} \rho_k \quad \text{(IV.12)}$$

IV.3.1 Strain rate

Opposed-jet counterflow diffusion-flame is used to test the flammability limits of different fuel/oxidizer systems. It is one of the simplest configurations in which the extinction of diffusion flames can be measured or simulated. Extinction occurs when fuel oil and oxidant flows exceed a certain limit. An intuitive interpretation of this phenomenon is that the flame is blown out when chemical reactions cannot happen quickly to maintain a bath of reactive species to counteract the flow of injected reactants. The change in extinguishing condition with changing fuel composition is an indicator of the reactivity of each fuel mixture. The extinction condition may be characterized by fuel and oxidizer flows that cause flame extinction.

To quantify the extinction limit, a fundamental quantity is used, namely the velocity gradient upstream of the flame, or strain. This quantity allows different types of flames or compositions to be compared. Strain rate is in units of inverse time, for this flow in this configuration and under differential assumptions, the extinction strain rate is proportional to overall reaction rates. For counterflow flame, the strain rate is the maximum velocity gradient along the axis of a jet on the oxidizer side of the stagnation plane, which usually occurs upstream of flame.

Two expressions corresponding to different assumptions on output velocity are proposed to estimate the strain rate based on the composition and flows of two jets. If the strain rate calculated ignores chemical effects and temperature variation, it is called global strain rate it is defined by:

$$a = \frac{V}{2d} \quad \text{(IV.13)}$$

Where V is the velocity of the fuel and oxidizer jets, and d is the distance between the ducts.

Two cases for the flow geometry are typically encountered experimentally. If the two jets are formed from long straight tubes with no obstructions, the axial velocity profile at the tube exit as a function of radial position follows a parabolic profIle, which produces a radially diverging flow downstream of the tube exit. This configuration is often modeled by imposing a potential flow solution as the boundary condition. If on the other hand the axial velocity profIle is radially uniform across the tube exit (usually achieved experimentally by screens or by

converging nozzles), the flow does not diverge downstream of the tube exit, and is modeled as plug flow. In practice, flow fields have been found to be between these two idealizations for both converging nozzles and straight tubes [156 ,157].

The strain rate for the parabolic case is given by the formula (IV.14) which represents the solution of potential flow, in which the strain rate is uniformly distributed from tube outlet to stagnation plane, whose position is given by the relative momenta of the two jets:

$$a = \frac{2u_{Ox}}{d}\left[1 + \frac{u_{Fu}^2\,\rho_{Fu}}{u_{Ox}^2\,\rho_{Ox}}\right] \quad \text{(IV.14)}$$

where a is the strain, u the mean axial velocity at the tube exit (the centerline velocity is 2u), ρ the gas density, and d the tube separation. Subscripts Fu and Ox refer to fuel and oxidant, respectively. In the case of plug flow, Seshadri and Williams [158] have derived the following expression for the velocity gradient near the stagnation plane:

$$a = \frac{2(u_{Ox})}{d}\left[1 + \sqrt{\frac{u_{Fu}^2\rho_{Fu}}{u_{Ox}^2\rho_{Ox}}}\right] \quad \text{(IV.15)}$$

To characterize the strain rate in the absence of local velocity measurements, Puri and Seshadri [159] derived an expression given below as equation (IV.16), based on assuming a large Reynolds number and a thin mixing layer. However, laser-Doppler velocimetry (LDV) measurements showed that this expression could over-predict the strain rate by a factor of two [156].

$$a = \frac{2|u_{Ox}|}{d}\left[1 + \frac{|u_{Fu}|}{|u_{Ox}|}\sqrt{\frac{\rho_{Fu}}{\rho_{Ox}}}\right] \quad \text{(IV.16)}$$

IV.4 Balance equations

Balance equations for reacting flows translate the conservation of mass, species, momentum, and energy.

Total mass balance:

$$\frac{\partial \rho}{\partial t} + \nabla . (\rho V) = 0 \quad \text{(IV.17)}$$

It represents the continuity equation for reactive and inert flows. In expression (IV.17), ρ is the total density and V the velocity vector.

For 1D axisymmetric geometries and at steady state, we introduce a stream function in the form $\Psi(x,r) = r^2 U(x)$ was introduced [160], which satisfies the continuity equation:

$$\frac{\partial}{\partial x}(r\rho u) + \frac{\partial}{\partial r}(\rho v r) = 0 \qquad \text{(IV.18)}$$

Where x is the axial coordinate, r is the radial coordinate, u is the axial velocity depends on x, and v is the radial velocity varies linearly in r.

The stream function is described by

$$\frac{\partial \Psi}{\partial r} = r\rho u = 2rU \qquad \text{(IV.19)}$$

$$-\frac{\partial \Psi}{\partial x} = r\rho v = -r^2 \frac{dU}{dx} \qquad \text{(IV.20)}$$

The temperature *T* and species mass fractions Y_k are also functions of *x* alone. Using a small Mach number approximation, the thermodynamic pressure *p* is constant throughout the flow field, but pressure gradient terms still appear in the momentum equations.

Mass balance for the species k:

$$\rho \frac{dY_k}{dt} + \nabla . \left(\rho Y_k V_{D_k}\right) = \dot{\omega}_k \qquad \text{k=1,2,……,N} \qquad \text{(IV.21)}$$

Equation (IV.21) is the conservation equation for a chemical species. In this expression, Y_k, V_{D_k} and $\dot{\omega}_k$ are k^{th} species mass fraction, diffusion velocity, and reaction rate, respectively.

Momentum balance:

$$\rho \frac{\partial V}{\partial t} + \rho(V . \nabla)V = -\nabla \bar{P} + \sum_{k=1}^{N} \rho_k f_k, \qquad \text{(IV.22)}$$

$$\bar{P} = pI + \Pi \qquad \text{(IV.23)}$$

The variable f_k designates the external force per unit mass acting on k^{th} species and *I* is the unit matrix. $\bar{P}$ is the pressure tensor, it includes the internal stresses due to the pressure *p* and the viscous stress tensor *Π*. As a function of these variables, the conservation equation of (IV.22) becomes:

$$\rho \frac{\partial V}{\partial t} + \rho(V . \nabla)V = -\nabla_p - \nabla . \Pi + \sum_{k=1}^{N} \rho Y_k f_k \qquad \text{(IV.24)}$$

Von Karman [161], recognized that *v/r* and other variables should be functions of *x* only, we define

$$G(x) = -\frac{\rho v}{r} \qquad \text{and} \qquad U(x) = \frac{\rho u}{2}$$

For which continuity reduces to

$$G(x) = \frac{dU(x)}{dx} \tag{IV.25}$$

Under this hypothesis, the perpendicular (x-direction) momentum equation writes:

$$H - 2\,\frac{d}{dx}\left(\frac{UG}{\rho}\right) + \frac{3G^2}{\rho} + \frac{d}{dx}\left[\mu\,\frac{d}{dx}\left(\frac{G}{\rho}\right)\right] = 0 \tag{IV.26}$$

In equation (IV.26), the quantities are only a function of *x*, so from the equation of continuity, ρ and *u* must depend only on *x*.

Consequently, from energy and species equations, *T* and Y_k should also depend only on *x*. The constant *H* is an eigenvalue that satisfies the perpendicular momentum equation

$$H = \frac{1}{r}\frac{\partial P}{\sigma r} = \text{constant} \tag{IV.27}$$

Energy conservation equation

$$\rho\frac{\partial e}{\partial t} + \rho(V.\nabla)e = -\nabla_q - \bar{P} : \nabla V + \sum_{k=1}^{N} \rho Y_k V_{D_k} f_k \ , \tag{IV.28}$$

Where *e* is the specific internal energy, *q* is the heat flux, and (:) the tensor product. By introducing the specific enthalpy h of the mixture (IV.30), and using the momentum equation (IV.24), the energy equation is written then:

$$\rho\frac{\partial h}{\partial t} + \rho(V.\nabla)h = -\nabla_q - \Pi : \nabla V + \sum_{k=1}^{N} \rho Y_k V_{D_k} f_k + \frac{\partial p}{\partial t} + (V\,.\nabla)p\,, \tag{IV.29}$$

$$h = e + \frac{p}{\rho} \tag{IV.30}$$

Equation (IV.29) is a result of the principle of conservation of energy. This equation and the expression of enthalpy *h* as a function of absolute temperature *T* and mass fractions Y_k (T, Y_1, $Y_2, \ldots\ldots, Y_N$), allow obtaining a conservation equation of energy in terms of the temperature *T*.

If we take into consideration radiation losses and heat produced by combustion, the energy conservation equation is written:

$$\rho u\frac{dT}{dx} - \frac{1}{Cp}\frac{d}{dx}\left(\lambda\frac{dT}{dx}\right) + \frac{\rho}{Cp}\sum_k C_{p_k} V_{D_k} Y_k \frac{dT}{dx} + \frac{1}{Cp}\sum_k h_k \dot{\omega}_k + \frac{1}{Cp}\dot{Q}_{rad} = 0 \tag{IV.31}$$

Radiative losses are modeled by the “optically thin” media approximation. In this model, the radiation emitted from other parts of gas is not re-absorbed by the local gas; the latter limits the

heat loss only to the exchange between the gas and the surrounding environment. This model is adequate for framelet radiation since high temperature region in the framelet is rather thin. For relatively low computation coast, this model is mostly accepted for practical purposes. Optically thin model was used in conjunction with flamelet approach in opposed jet flames, it was validated for several fuels and mixtures of biofuels [47, 51, 162, 163, 164]. Heat losses in optically thin model are given by:

$$\dot{Q}_{rad} = 4\sigma p \sum_j X_j \, a_i \left({T_r}^4 - T_f^4 \right) \quad \text{(IV.32)}$$

With σ is the Stefan Boltzmann constant ($5.67 \cdot 10^{-8} \frac{\mathrm{W}}{\mathrm{m^2 K^2}}$), T_r is the temperature of the radiating substance, T_f is far-field temperature, P is the gas pressure, X_i is the species i mole fraction and a_i is the Planck mean absorption coefficient for species i. This coefficient is given in a polynomial form $a_i = \sum_i c_i T^i$ and c_i are numerical factors given for each species for a specified temperature interval. The Planck mean absorption coefficients adopted are those computed by RADCAL program and available in Sandia site [165]; these coefficients were validated in opposed jet flame [166, 167]. The radiating gaseous species considered in this study are CH_4, CO, CO_2 and H_2O.

The balance equations governing reactive gas mixtures did not form a closed system. It is necessary to add:

- The thermodynamic relations express different thermodynamic quantities such as p, h, ... as a function of state variables.
- The chemical kinetics relations that give the expression of production rate $\dot{\omega}$ as a function of state variables.
- The transport relations that express the diffusion velocity V_{D_k}, the heat flux q and the pressure tensor $\bar{P}$ as a function of velocity V, of state variables T, p, Y_k, and their gradient.

These relations will be detailed in the next section. After that, the system will be closed and the computed variables are the density ρ, the mean velocity V, the thermodynamic pressure p, the mass fractions of the chemical species Y_k, and the temperature T.

IV.5 Thermodynamic variables

A thermodynamic study of the system aims to find, at thermodynamic equilibrium, relations between state variables. In this study, the gas is considered ideal, the equation of state is written:

$$pV_T = nRT, \tag{IV.33}$$

Where *T* is the temperature, *R = 8.314 J/(mole K)* is the perfect gas constant.

The specific enthalpy of mixture *h* is expressed as a function of the specific enthalpy of species h_k by the relation:

$$h = \sum_{k=1}^{N} Y_k h_k \tag{IV.34}$$

Assuming that gas is perfect, the specific enthalpy h_k as a function of temperature is given by:

$$h_k(T) = h_k(T_0) + \int_{T_0}^{T} c_{p_k}(T')dT' \tag{IV.35}$$

To make practical use of eq (IV.34), it is necessary to define a standard reference state. We employ a standard state temperature, $T_0 = 25°C$ (298.15 K), and standard state pressure,$P_0 = 1atm$ (101.325 Pa), consistent with the Chemkin [168] and NASA [169] thermodynamic databases.

Heat capacity at constant pressure as well as heat capacity of species k at constant pressure c_{p_k} are written:

$$c_{p_k} = \left.\frac{\partial h_k}{\partial T}\right|_p \quad , \tag{IV.36}$$

$$c_p = \sum_{k=1}^{N} Y_k c_{p_k} \tag{IV.37}$$

From equations (IV.34) and (IV.35) and using expressions (IV.36) and (IV.37), the enthalpy of mixture h is given by the following relation:

$$h = \sum_{k=1}^{N} Y_k h_k(T_0) + \int_{T_0}^{T} c_p(T')dT' \tag{IV.38}$$

Similarly, specific entropy of mixture *s* is expressed as a function of specific entropy s_k of species *k*:

$$s = \sum_{k=1}^{N} Y_k s_k \tag{IV.39}$$

Temperature dependence of specific entropy involves standard entropy of formation $s_k(T_0, p_{atm})$ of species *k* at the temperature T_0 and at reference pressure p_{atm}. Generally, specific entropy s_k is written:

$$s_k = s_k(T_0, p_{atm}) + \int_{T_0}^{T} \frac{c_{p_k}(T')}{T'} dT' - \frac{R}{W_k} Log \frac{p_k}{p_{atm}}, \tag{IV.40}$$

p_k is the partial pressure of k^{th} species, it is calculated by Dalton's law. In particular, if we note $s_k^0 = s_k^0(T, p_{atm})$, the entropy of species *k* at atmospheric pressure p_{atm}, we then have the following relation:

$$s_k^0 = s_k(T_0, p_0) + \int_{T_0}^{T} \frac{c_{p_k}(T')}{T'} dT' . \quad \text{(IV.41)}$$

Finally, the specific thermodynamic properties s_k^0 , c_{p_k} et h_k that were used to establish these relations are deduced from the corresponding molar thermodynamic properties S_k^0 , C_{pk} et H_k by the relations:

$$c_{p_k} = \frac{C_{pk}}{W_k}, \qquad h_k = \frac{H_k}{W_k}, \qquad s_k^0 = \frac{S_k^0}{W_k} . \quad \text{(IV.42)}$$

Molar thermodynamic properties S_k^0 , c_{p_k} et H_k are evaluated by approximation polynomials. This method is less computationally expensive than interpolation from numerical tables.

Molar heat capacity at constant pressure is written in the form of polynomials of fourth-degree temperature and over two approximating intervals $[T_{min}, T_m]$ and $[T_m, T_{max}]$:

$$\frac{C_{p_k}}{R} = a_{1k} + a_{2k}T + a_{3k}T^2 + a_{4k}T^3 + a_{5k}T^4 , \quad \text{if } T_{min} \le T \le T_m , \quad \text{(IV.43)}$$

$$\frac{C_{p_k}}{R} = a_{8k} + a_{9k}T + a_{10k}T^2 + a_{11k}T^3 + a_{12k}T^4 , \quad \text{if } T_m \le T \le T_{max} , \quad \text{(IV.44)}$$

The corresponding molar enthalpies are:

$$\frac{H_k}{RT} = a_{1k} + \frac{a_{2k}}{2}T + \frac{a_{3k}}{3}T^2 + \frac{a_{4k}}{4}T^3 + \frac{a_{5k}}{5}T^4 + \frac{a_{6k}}{T}, \quad \text{if } T_{min} \le T \le T_m , \quad \text{(IV.45)}$$

$$\frac{H_k}{RT} = a_{8k} + \frac{a_{9k}}{2}T + \frac{a_{10k}}{3}T^2 + \frac{a_{11k}}{4}T^3 + \frac{a_{12k}}{5}T^4 + \frac{a_{13k}}{T}, \quad \text{if } T_m \le T \le T_{max} , \quad \text{(IV.46)}$$

The molar entropies at 1atm are:

$$\frac{S_k^0}{R} = a_{1k}logT + a_{2k}T + \frac{a_{3k}}{2}T^2 + \frac{a_{4k}}{3}T^3 + \frac{a_{5k}}{4}T^4 + a_{7k}, \quad \text{if } T_{min} \le T \le T_m , \quad \text{(IV.47)}$$

$$\frac{S_k^0}{R} = a_{8k}logT + a_{9k}T + \frac{a_{10k}}{2}T^2 + \frac{a_{11k}}{3}T^3 + \frac{a_{12k}}{4}T^4 + a_{14k}, \quad \text{if } T_m \le T \le T_{max} , \quad \text{(IV.48)}$$

The intermediate temperature may depend on the species:

$$T_m = T_{mk}. \quad \text{(IV.49)}$$

IV.5.1 Enthalpy of combustion and heating values

The calorific value of fuel (units of *kJ/kg* or *kJ/m*^{3}) is the amount of heat released by total combustion by a unit quantity of fuel. The quantity of heat generated from fuel combustion depends on the water phase in products. If the water in products is gas, the energy released by total combustion of *1kg* or *1m*^{3} of fuel is called the Lower Calorific Value (LCV). When water

vapor is condensed to liquid, additional energy (the latent heat of vaporization) can be extracted, the total energy release is called the Higher Calorific Value (HCV). The LCV can be calculated from the HCV by subtracting the amount of energy released during the phase change of water from vapor to liquid.

Generally, the calorific values are expressed as a function of heat (enthalpy) of reaction by:

$$LCV = \frac{-\Delta H_R}{W_{fuel}} \tag{IV.50}$$

ΔH_R is the heat released from the stoichiometric combustion (enthalpy of combustion) of *1 kmole* of the fuel, and w_{fuel} is the molar mass of the fuel.

In turn, the higher calorific value is written:

$$HCV = LCV + \frac{N_{H_2O(p)} W_{H_2O} h_{fg}}{N_{fuel} W_{fuel}} \tag{IV.51}$$

Where $N_{H_2O(p)}$ is the number of moles of water in products and h_{fg} is the latent heat of vaporization. Under standard conditions h_{fg} = 2.44 MJ / kg = 43.92 MJ / kmol.

To compute the LCV for a biogas-syngas mixture, the complete stoichiometric combustion equation of biogas-syngas mixture with oxidizer composed by oxygen and nitrogen at 25°C and 1 atm can be written as:

$$\delta[(\alpha CH_4) + (1-\alpha)CO_2] + \gamma[(\beta H_2) + (1-\beta)CO] + a_{st}\left(O_2 + \frac{1-z}{z}N_2\right) \rightarrow$$
$$(\delta + \gamma - \gamma\beta)CO_2 + (2\delta\alpha + \gamma\beta)H_2O + a_{st}\frac{1-z}{z}N_2 \tag{IV.52}$$

With α, β, δ, and γ are stoichiometric coefficients, z is the mole fraction of oxygen in oxidizer stream, it is varied from 0.04 to 0.21 and $a_{st} = \frac{\gamma}{2} + 2\alpha\delta$. (IV.53)

The enthalpy of combustion can be calculated by:

$$\Delta H_R = Q_{cv} = H_P - H_R \tag{IV.54}$$

$$\Delta H_R = (\delta + \gamma - \gamma\beta)\bar{h}^{\circ}_{f,CO_2} + (2\delta\alpha + \gamma\beta)\,\bar{h}^{\circ}_{f,H_2O} - (\delta + \gamma)\bar{h}^{\circ}_{f,fuel\,mél} \tag{IV.55}$$

With

$$\bar{h}^{\circ}_{f,fuel\,mél} = \frac{1}{\gamma+\delta}\left[\delta\alpha\left(\bar{h}^{\circ}_{f,CH_4} - \bar{h}^{\circ}_{f,CO_2}\right) + \delta\bar{h}^{\circ}_{f,CO_2} + \gamma\,(1-\beta)\bar{h}^{\circ}_{f,CO}\right] \tag{IV.56}$$

The molar mass of fuel is given by:

$$W_{fuel} = \sum_{k=1}^{N} X_k W_k = \frac{\delta(44-28\alpha)+\gamma(28-26\beta)}{\delta+\gamma} \quad \text{(IV.57)}$$

After rearrangement, the lower calorific value is calculated by the following relation:

$$LCV = \frac{-\Delta H_R}{W_{fuel}} \quad \text{(IV.58)}$$

IV.5.2 Adiabatic flame temperature

One of the most important characteristics of the combustion process is the maximum temperature that can be achieved for given reactants. The temperature of products will be maximum when no heat is lost in the environment and all energy released by combustion will be used to heat products. This highest temperature is known as the adiabatic flame temperature (T_{ad}). There are two types of adiabatic flame temperature depending on how the process is completed: constant volume and constant pressure.

Constant pressure process:

From the first law of thermodynamics –isobaric process:

$$\Delta U = Q_P - W_P = Q_P - p\Delta V \quad \text{(IV.59)}$$

$$H = U + pV \quad \text{(IV.60)}$$

At constant pressure, $$\Delta H = \Delta U + p\Delta V + V\Delta p = \Delta U + p\Delta V \quad \text{(IV.61)}$$

In adiabatic process. $$Q_P = 0 \ , \ \Delta H = 0 \quad \text{(IV.62)}$$

At equilibrium,

$$H_{react}(T_{init}, p) = H_{prod}(T_{ad}, p) \quad \text{(IV.63)}$$

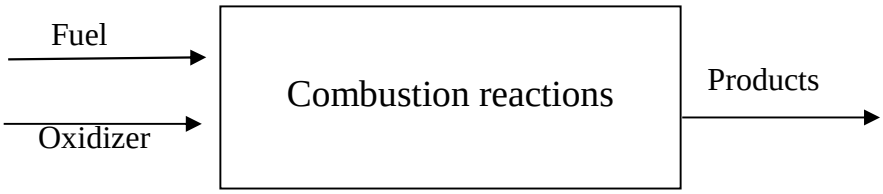

Fig.IV.2: Fuel combustion at constant pressure.

With

$H_{react}(T_{init}, p)$ is the enthalpy of reactants in the initial state (T_{init}=intial temperature, $P=1atm$)

$$H_{react}(T_{init}, p) = \sum_{kR=1}^{N} n_{kR}\left[\bar{h}^{\circ}_{f,kR} + (T_{init} - T_0)\bar{C}_{p,kR}\right] \quad \text{(IV.64)}$$

$H_{prod}(T_{ad}, p)$ is the enthalpy of products in the final state (T_{ad}=adiabatic temperature, P=*1atm*)

$$H_{prod}(T_{ad}, p) = \sum_{kP=1}^{N} n_{kP}\left[\ \bar{h}^{\circ}_{f,kP} + \int_{T_0}^{T_{ad}} \bar{C}_{p,kP} dT\ \right] \quad \text{(IV.65)}$$

Where, $\bar{C}_{p,kP}$ are the heat capacities expressed:

$$\bar{C}_{pk} = A_k + B_k T + C_k T^2 + D_k T^3 + E_k T^4 \quad \text{(IV.66)}$$

After rearrangement,

$$H_{prod}(T_{ad}, p) = \sum n_k \left[\begin{array}{c} \bar{h}^{\circ}_{f,kP} + RT_{ad}\left(A_k + \frac{B_k}{2}T_{ad} + \frac{C_k}{3}T_{ad}^2 + \frac{D_k}{4}T_{ad}^3 + \frac{E_k}{5}T_{ad}^4\right) \\ -RT_0\left(A_k + \frac{B_k}{2}T_0 + \frac{C_k}{3}T_0^2\ \frac{D_k}{4}T_0^3 + \frac{E_k}{5}T_0^4\right) \end{array}\right] \quad \text{(IV.67)}$$

Constant volume process:

The first law of thermodynamics requires:

$$Q_V = \Delta U\ , \quad \text{(IV.68)}$$

$$Q_V = Q_P - nRT = \Delta H_P - \Delta nRT \quad \text{(IV.69)}$$

In an adiabatic process,

$$Q_V = 0 = \Delta H_P - \Delta nRT \quad \text{(IV.70)}$$

$$U_{react}(T_{init,} P_{init}) = U_{prod}(T_{ad,} P_f) \quad \text{(IV.71)}$$

$$H_{react}(T_{init}, P_{init}) - H_{prod}(T_{ad}, P_f) - R(n_{react}T_{init} - n_{prod}T_{ad}) = 0 \quad \text{(IV.72)}$$

After rearrangement,

$$T_{ad} = \frac{LCVW_{fuel} + T_0(\sum_{kP=1}^{N} n_{kp}\bar{C}_{p,kP} - \sum_{kR=1}^{N} n_{kR}\bar{C}_{p,kR}) + T_i(\sum_{kR=1}^{N} n_{kR}\bar{C}_{p,kR} - Rn_R)}{\sum_{kP=1}^{N} n_{kP}\bar{C}_{p,kP} - Rn_P} \quad \text{(IV.73)}$$

IV.6 Chemical kinetics

Combustion is a complex chemical system that involves many elementary reactions and generates several molecular species and radicals during the process. In recent years, chemically reacting flows have been the subject of several studies. Thirty years ago, this type of flow was limited to combustion engineers and the theoretical schemes were simple.

Currently, chemical kinetics covers a vast and constantly growing field of chemistry. The most important phenomenon in the flame is the production of species formed from chemical reactions. Considerable efforts have been devoted to improving our knowledge in this field. The equations used were based on collision theory [170]. There are currently other theories that are more precise but more complex and more costly in terms of computing time. The combustion phenomenon is described by a sequence of hundreds or sometimes thousands (cases of complex hydrocarbons) of elementary reactions. The irreversible elementary reaction can be written in the form:

$$\sum_{k=1}^{N} \gamma'_{ki} A_k \rightarrow \sum_{k=1}^{N} \gamma''_{ki} A_k \ , \tag{IV.74}$$

With γ'_{ki} and γ''_{ki} are stoichiometric coefficients of the k^{th} species in the ith reaction. These coefficients are non-negative integers. A_k is the chemical symbol of species *k*. It can be included in both members of the reaction with different coefficients γ'_{ki} and γ''_{ki}.

Equation (IV.74) can be written as follows:

$$\sum_{k=1}^{N} (\gamma''_{ki} - \gamma'_{ki}) A_k = 0, \tag{IV.75}$$

The term a_k can be defined by the relation (IV.76), this term will be used later to define the degree of advancement:

$$a_k = \sum_{k=1}^{N} a_{ki} = \sum_{k=1}^{N} (\gamma''_{ki} - \gamma'_{ki}). \tag{IV.76}$$

A chemical reaction is a process that leads to provides additional information about the production of species that evolve in the system. Hirschfelder et al. [171] introduced a term called degree of advancement ξ, this term is defined by:

$$\xi = \frac{n_k - n_k^0}{a_k} \tag{IV.77}$$

$$m_{ki} - m_{ki}^0 = a_{ki} W_k \xi_i \ , \tag{IV.78}$$

m_{ki}^0 is the initial mass of species *k* in reaction *i*, n_k^0 represent the initial number of mole of species *k* and n_k the number of moles of the species *k* after the reaction *i* takes place. In the case of multiple reactions, the relation (IV.78) is written in the form:

$$m_k - m_k^0 = \sum_{i=1}^{J} a_{ki} W_k \xi_i \ , \tag{IV.79}$$

Where *J* is the number of chemical reactions in the reaction mixture.

Equation (IV.79) provides information on the mass of species *k* after reaction; it would be more useful to work with mass production rates. In the literature, it can be often found that some chemists preferred to use the word "specific velocity"; thus, the mass production rate of species *k* is $\dot{\omega}_k$, i.e. the mass of species produced per unit of time and unit of volume, is written for a reaction at rest:

$$\dot{\omega}_k = \frac{d\rho_k}{dt} = W_k \frac{dC_k}{dt}, \tag{IV.80}$$

ρ_k, W_k and C_k are the density, the molar mass, and the molar concentration of species *k* respectively. Moreover, for *J* reactions:

$$\dot{\omega}_k = \sum_{i=1}^{J} \dot{\omega}_{ki}. \tag{IV.81}$$

Where $\dot{\omega}_{ki}$ is the mass production rates of species k in reaction *i*.

The collision theory evaluates the mass production rate by using simpler models [172]. The mass production rate of k^{th} species in ith reaction is written:

$$\dot{\omega}_{ki} = W_k(\gamma''_{ki} - \gamma'_{ki}) k_B \prod_{k=1}^{N} C_k^{\gamma'_{ki}}, \tag{IV.82}$$

$$k_B = \beta T^{\alpha} exp\left(\frac{-E_i}{RT}\right). \tag{IV.83}$$

Where k_B is called the reaction rate constant. It depends on temperature and pressure. In equation (IV.83) βT^{α} is the pre-exponential factor, E_i is the activation energy for ith reaction and *R* is the universal gas constant.

We should then have the following equation:

$$exp\left(\frac{-E_i}{RT}\right) = exp\left(\frac{-T_i}{T}\right), \tag{IV.84}$$

Where T_i is the activation temperature for ith reaction. This equality defines the Maxell-Boltzmann distribution that gives a probability for a molecule to obtain energy E_i. The exponential plays a very important role in the evaluation of k_B as a function of temperature. Depending on activation energy values, the variation of k_B can be very slow or very fast. This variation strongly depends on the value of the activation temperature parameter T_i. It should be noted that the values α, β and E_i are determined experimentally over a wide range of temperatures and pressures.

Generally, the elementary reactions are reversible:

$$\sum_{k=1}^{N} \gamma'_{ki} A_k \underset{k_r}{\overset{k_f}{\longleftrightarrow}} \sum_{k=1}^{N} \gamma''_{ki} A_k \tag{85}$$

With γ'_{ki} and γ''_{ki} are stoichiometric coefficients of the kth species in the ith reaction. These coefficients are non-negative integers. In this case, the mass production rate of species *k* in reaction *i* and the rate constants for forward reactions are written:

$$\dot{\omega}_{ki} = W_k(\gamma''_{ki} - \gamma'_{ki}) \left(k_{f_i} \prod_{k=1}^{N} C_k^{\gamma'_{ki}} - k_{r_i} \prod_{k=1}^{N} C_k^{\gamma''_{ki}} \right), \tag{IV.86}$$

$$k_{f_i} = \beta_k T^{\alpha k} exp\left(\frac{-E_i}{RT}\right). \tag{IV.87}$$

The rate constants for reverse reactions k_r can be estimated using Arrhenius law:

$$k_{r_i} = \frac{k_{f_i}}{k_{e_i}} \tag{IV.88}$$

k_{e_i} is the equilibrium constant which is equal to the ratio of rate constants.

Thus, the equilibrium constant k_{e_i} of global reaction is given by thermodynamics:

$$k_{e_i} = (\frac{p_{atm}}{RT})^{\Delta\gamma_i} \exp(\Delta Z_k), \tag{IV.89}$$

$$\Delta\gamma_i = \sum_{k=1}^{N} a_{ki} \; ; \; \Delta Z_i = \sum_{k=1}^{N} \gamma_{ki} Z_k \; ; \; Z_k = \frac{S_k^0}{R} - \frac{H_k}{RT}. \tag{IV.90}$$

To estimate the rate constants for reverse reactions k_r are estimated accurately using the equilibrium constant k_{e_i} instead of Arrhenius law, because this constant is determined from thermodynamic variables, which are known with great precision while there is considerable uncertainty about the frequency factors α and β.

IV.7 Species transport phenomena

The diffusion velocity is obtained by a method based on molecular movement analysis, this method was developed by F.A Williams [173]. The diffusion velocity is obtained by considering the chemical species flow at the molecular scale and by analyzing their impact on macroscopic assemblies movement.

The diffusion velocity can be written in the form:

$$V_{D_k} = \mathrm{v_k} + \mathrm{w_k} + \mathrm{u} \qquad k = 1, \ldots\ldots\ldots, N, \tag{IV.91}$$

v_k is the ordinary diffusion vector due to the concentration gradient of species k, w_k is the thermal diffusion vector and u is a diffusion velocity.

The expression of v_k is given by Hirschfelder [171]:

$$v_k = -\left(\frac{1}{X_k}\right) D_k^H \nabla X_k \qquad k = 1, \dots \dots, N, \tag{IV.92}$$

X_k is the molar fraction of species k, D_k^H is the binary diffusion coefficient in the mixture. It is expressed as a function of another binary diffusion coefficient D_{kj} :

$$D_k^H = \frac{1-Y_k}{\sum_{\substack{j\neq k \\ k=1}}^{N} \frac{X_j}{D_{kj}}} \tag{IV.93}$$

The thermal diffusion vector is written:

$$w_k = \frac{D_k^H D_{T,k}}{X_k} \frac{1}{T} \nabla T. \tag{IV.94}$$

$D_{T,k}$ is the thermal diffusion factor. u is given by:

$$u = \sum_{j=1}^{N} \frac{D_j^H Y_j}{X_j} \left(\nabla X_j - D_{T,j} \frac{\nabla T}{T}\right) \tag{IV.95}$$

It should be noted that the effect caused by thermal gradients leads to diffusion known as the Soret effect. For a more complete discussion of the Soret effect, Dufour effect, and diffusion velocity as well as all the steps in this calculation, [172, 173]. It should be noted that the expression (IV.91) is an approximation for diffusion velocity, which will not necessarily satisfy the expression (IV.96). Therefore, a correction is necessary. A technique includes writing the diffusion velocity in the form (IV.97).

$$\sum_{k=1}^{N} Y_k V_{D_k} = 0, \tag{IV.96}$$

$$V_{D_k} = (v_k + w_k + u) + v_c. \tag{IV.97}$$

Taking into account the expression (IV.94), the correction velocity is expressed as:

$$v_c = -\sum_{k=1}^{N} Y_k \left(\left(\frac{-1}{X_k}\right) D_k^H \nabla X_k + \frac{D_k^H D_{T,k}}{X_k} \frac{1}{T} \nabla T + \sum_{k=1}^{N} \frac{D_k^H Y_k}{X_k} \left(\nabla X_k - D_{T,k} \frac{\nabla T}{T}\right) \right) \tag{IV.98}$$

The correction velocity v_c is independent of chemical species but, it can be varied spatially. It is introduced to ensure the condition (IV.96).

IV.8 Heat transfer flux

From Onsager reciprocal relations, the calculation of heat flux q shows a sum of four terms:

- Thermal conduction in gas:

$$-\lambda \nabla T. \tag{IV.99}$$

λ is the thermal conductivity of the mixture.

- Radiative heat flux:

$$\dot{Q}_{rad} \tag{IV.100}$$

- The energy provided by diffusion of molecular species k. This term is equal to the product of diffusion flux $\rho_k V_{D_k}$ and specific Enthalpy h_k. The term related to all molecules become:

$$\sum_{k=1}^{N} \rho_k V_{D_k} h_k. \tag{IV.101}$$

- The term corresponding to the Dufour effect, which is a coupling term due to concentration gradients, pressure, and temperature, is written:

$$RT \sum_{k=1}^{N} \sum_{j=1}^{N} \frac{X_k D_{T,k}}{W_k D_{kj}} (V_{D_k} - V_{D_j}). \tag{IV.102}$$

Total heat flux is written:

$$q = -\lambda \nabla T + \dot{Q}_{rad} + \sum_{k=1}^{N} \rho_k V_{D_k} h_k + RT \sum_{k=1}^{N} \sum_{j=1}^{N} \frac{X_k D_{T,k}}{W_k D_{kj}} \left(V_{D_k} - V_{D_j}\right). \tag{IV.103}$$

IV.9 Transport properties

The viscous stress tensor Π is cited in previous paragraphs **IV.3**, as well as the three transfer coefficients: two diffusion coefficients $D_{T,k}$ and D_{kj} and thermal conductivity coefficient λ which are used in balance equations. Therefore, it is necessary to express these transfer coefficients as a function of state variables.

By neglecting volume viscosity phenomena, the viscous stress tensor is written:

$$\Pi = -\nu \frac{2}{3} (\nabla . V) \mathrm{I} + \nu (\nabla V + (\nabla V + (\nabla V)^T), \tag{IV.104}$$

In a species-containing medium, the kinematic viscosity coefficient of mixture ν may be estimated from the following relation:

$$\nu = \frac{1}{2}\left(\sum_{k=1}^{N} X_k \nu_k + \frac{1}{\sum_{k=1}^{N} X_k (\nu_k)^{-1}}\right) \quad \text{(IV.105)}$$

To calculate the viscosity ν_k , a more rigorous relation is obtained from kinetic theory, as follows:

$$\nu_k = \frac{5\sqrt{\pi W_k k_B T}}{16\pi\sigma_k^2 \Omega^{(2,2)^*}} \quad \text{(IV.106)}$$

σ_k is the collision diameter of interaction potential of Lennard-Jones and $\Omega^{(2,2)^*}$ is a reduced collision integral.

For each species j, the thermal conductivity is expressed as:

$$\lambda_k = \frac{25\sqrt{\pi W_k k_B T}}{32\pi\sigma_k^2 \Omega^{(2,2)^*}} \frac{c_v}{W_k}, \quad \text{(IV.107)}$$

Where c_v is the specific heat at constant volume.

Different relations have been proposed to determine the thermal conductivity coefficient of mixture. The most common expression is:

$$\lambda = \frac{1}{2}\left(\sum_{k=1}^{N} X_k \lambda_k + \frac{1}{\sum_{k=1}^{N} X_k (\lambda_k)^{-1}}\right) \quad \text{(IV.108)}$$

To calculate the binary diffusion coefficientD_{kj}, a more rigorous relation is obtained from kinetic theory of gases, as follows:

$$D_{kj} = \frac{3\sqrt{\frac{2\pi k_B^3 T^3}{W_{kj}}}}{16\rho\pi\sigma_{kj}^2 \Omega_{k,j}^{(1,1)^*}} \quad \text{(IV.109)}$$

Where $\Omega_{k,j}^{(1,1)^*}$ is a reduced collision integral, σ_{kj} is the diameter of species pair (k, j), W_{kj} is the reduced mass of pair (k,j) which is given by:

$$W_{kj} = \frac{W_k W_j}{W_k + W_j} \quad \text{(IV.110)}$$

Finally, the thermal diffusion factors $D_{T,kj}$ and $D_{T,k}$ are estimated by following relations:

$$D_{T,kj} = \frac{15}{2} \frac{(2A_{kj}^* + 5)(6C_{kj}^* - 5)}{(16A_{kj}^* - 12B_{kj}^* + 55)} \frac{W_j - W_k}{W_j + W_k} X_k X_j, \quad \text{(IV.111)}$$

$$D_{T,k} = \sum_{\substack{j=1 \\ j\neq k}}^{N} D_{T,kj}, \tag{IV.112}$$

$$A_{kj}^{*} = \frac{\Omega^{(2,2)^{*}}}{\Omega_{k,j}^{(1,1)^{*}}}, \tag{IV.113}$$

$$B_{kj}^{*} = \frac{5\Omega_{k,j}^{(1,2)^{*}} - 4\Omega_{k,j}^{(1,3)^{*}}}{\Omega_{k,j}^{(1,1)^{*}}} \tag{IV.114}$$

$$C_{kj}^{*} = \frac{\Omega_{k,j}^{(1,2)^{*}}}{\Omega_{k,j}^{(1,1)^{*}}} \tag{IV.115}$$

The collision integrals A_{kj}^{*}, B_{kj}^{*} and C_{kj}^{*} are derived from the following collision integrals:

$$\Omega_{k,j}^{(l,s)^{*}} = \sqrt{\frac{2\pi k_B T}{W_{kj}}} \int_0^{\infty} \int_0^{\infty} e^{-\delta^2} \delta^{(2s+3)} [1 - cos^{l}\chi] \sigma d\sigma d\delta, \tag{IV.116}$$

k_B is Boltzmann constant, χ is deflection angle of two molecules *k* and *j* after collision, δ is a parameter given by the relation (IV.117). In equation (IV.117), g is the relative velocity equal to species velocity *k* minus that of *j* before collision:

$$\delta = \sqrt{\frac{W_{kj} g^2}{2k_B T}}. \tag{IV.117}$$

Thus, the reduced integrals are deduced by comparing collision integrals with those obtained by assuming elastic spheres for molecules *k* and *j*:

$$\Omega^{(l,s)^{*}} = \frac{\Omega^{(l,s)}}{\Omega_{elastic\ spheres}^{(l,s)^{*}}} = \frac{\Omega^{(l,s)} \sqrt{\frac{2\pi W_{kj}}{k_B T}}}{\frac{1}{2}(s+1)! \left(1 - \frac{1+(-1)^{l}}{2(1+l)}\right) \pi d^2} \tag{IV.118}$$

In this expression, represent integers that vary by calculation. For example:

- $s = l = 1$ for calculation of diffusion coefficients.
- $s = l = 2$ for calculation of the viscosity coefficients.

The previous formulas appear relatively complex, but in practice are presenting by polynomial temperature coefficients. For a more complete discussion of these relations and their validity limits [171].

IV.10 Sensitivity analysis

The sensitivity analysis helps to exploit the results obtained from a modeling calculation. Its main objective is to analyze and interpret quantitatively how the resulting solution depends on model parameters. From a kinetic point of view, the most important parameters are the postulated reaction diagram and the rate constants of the elementary reactions.

IV.10.1 First-order elementary sensitivity analysis

First-order elemental sensitivity analysis, Olsson and Andersson (1987) [174], is generally used to refine a chemical mechanism and reduce it to a smaller number of species and elemental reactions while maintaining its main characteristics. The coefficient of sensitivity S_i^k of the species k relative to the rate constant k_i of the reaction i is defined by the relation:

$$S_i^k = \frac{dlnX_k}{dlnk_i} \qquad \text{(IV. 119)}$$

where X_k represents the molar fraction of the species k and k_i is the rate constant of elementary reaction i.

IV.10.2 Raw sensitivity analysis

The raw sensitivity analysis includes varying each rate constant in its area of uncertainty one after the other and looking at their respective influence on the calculated molar fraction profiles. This method is quite easy to be implement but very long and very costly in terms of computing time. It allows, When the concentration profiles calculated can be compared with the corresponding experimental data, to adjust the rate constants of diffrent elementary reactions of the postulated chemical mechanism in their area of uncertainty.

IV.10.3 Reaction path analysis

The velocities of the different elemental reactions vary across the flame. It may therefore be interesting to specify their role in the different zones of the flame studied. The reaction path analysis method consists, once a postulated mechanism has been validated, for example by comparison between experimental and numerical modeling, in calculating the velocities of the diffrent chemical reactions and in studying their influence on the formation and / or disappearance of a given species. Elementary reactions, for which the contribution to the overall rate of evolution of a species is the most important, constitute the main reaction path of formation and / or disappearance of the species considered.

Chapter V

Results and Discussion

V. 1 Lower calorific value and adiabatic flame temperature

In a preliminary calculation, the effect of varying volume of methane in biogas and that of hydrogen in syngas on Lower Calorific Value (LCV) is studied. Then, another calculation of the adiabatic flame temperature of biogas-syngas mixture is carried out by varying the composition of the mixture. Fluent's Prepdf program is used to complete the calculation.

The compositions considered in this study are obtained by varying the fuel reactants molar coefficients in Eq. (IV.52), whereas the oxidizer is composed by a volume of 4% of oxygen and 96% of N_2. **Table V.1** presents some selected compositions. The biogas in the mixture is supposed to contain only CH_4 and CO_2 while syngas is composed by H_2 and CO. The notation BαSβ is used to identify the compositions of the blended fuels where B stands for biogas, S syngas, α is the percentage of methane in biogas (50 - α represents the percentage of CO_2) and β is the percentage of hydrogen in syngas (50 - β represents the percentage of CO). For example, B25S25 characterizes a mixture of biogas and syngas with 25% CH_4 (50 – 25 = 25% of CO2) and 25% H_2 (50 – 25 = 25% of CO).

Table. V.1: Examples of compositions considered.

Mixture	Biogas (B) (%)		Syngas (S) (%)	
BαSβ	CH_4 α%	CO_2 (50-α)%	H_2 β%	CO (50-β)%
B00S25	0	50	25	25
B25S25	25	25	25	25
B50S25	50	0	25	25
B25S00	25	25	0	50
B25S50	25	25	50	00

V. 1.1 Lower calorific value

Fig.V.1 shows the variation of lower calorific value as a function of H_2 and CH_4 percentage in the fuel mixture. The increase of H_2 and CH_4 volumes in fuel mixture induces an increase in LCV. However, the increase caused by methane addition (**Fig.V.1 (a)**) is greater than that caused by hydrogen (**Fig.V. 1 (b)**). This is due to the large per volume calorific value of methane compared to hydrogen. Quantitatively, for

0% hydrogen in mixture, if the methane varies from 0% to 50%, the LCV increases from 3930 Kj/Kg to 24668 Kj/Kg. Whereas, for 0% of methane in mixture, if the hydrogen varies from 0% to 50%, the LCV will increase slightly from 3930 Kj/Kg to 5258 Kj/Kg.

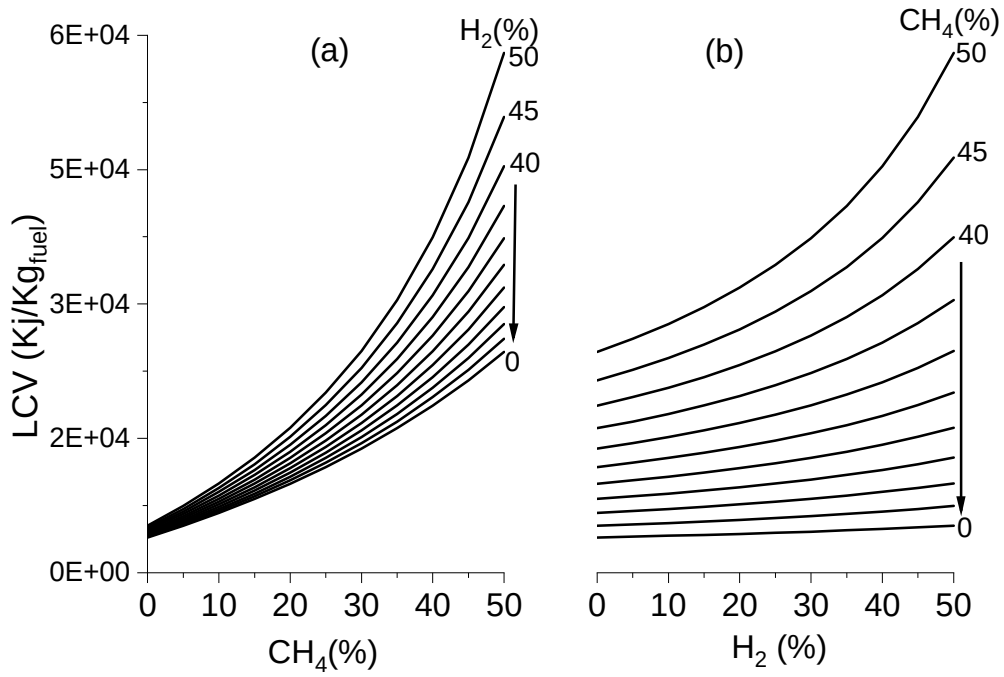

Fig.V.1: Effect of hydrogen and methane on the lower calorific value.

V. 1.2 Adiabatic flame temperature

Practically, the combustion can be uncontrolled, in fires and explosions, or controlled in burners, rocket engines and internal combustion engines [175]. The most important effect of combustion is the temperature increase, for this, it is crucial to know the maximum flame temperature in any combustion system. This temperature is defined as a maximum temperature that the combustion products can reach without exchanging heat with the boundaries, that is to say adiabatically. Moreover, the pollutants emitted from the combustion system such as oxides of nitrogen (NO_x) and carbon monoxides (CO) are controlled by the flame temperature.

Fig.V.2 shows the calculated adiabatic flame temperature as a function of H_2 and CH_4 percentage in the fuel mixture. The adiabatic flame temperature decreases with the increase in H_2 (**Fig.V.2 (a)**), due to the large per volume calorific value of CO compared to hydrogen. Quantitatively, for 0% of methane in the mixture, if the hydrogen varies

from 0% to 50%, the adiabatic flame temperature decreases from 1575K to 1532K. Whereas, the adiabatic temperature increases with the increase of CH_4 (**Fig.V.2 (b)),** this is because the methane substitutes the CO_2, which is a combustion product. Indeed, for 40% of hydrogen in the mixture, if the methane varies from 0% to 50%, the adiabatic flame will increase from 1542K to 1607K.

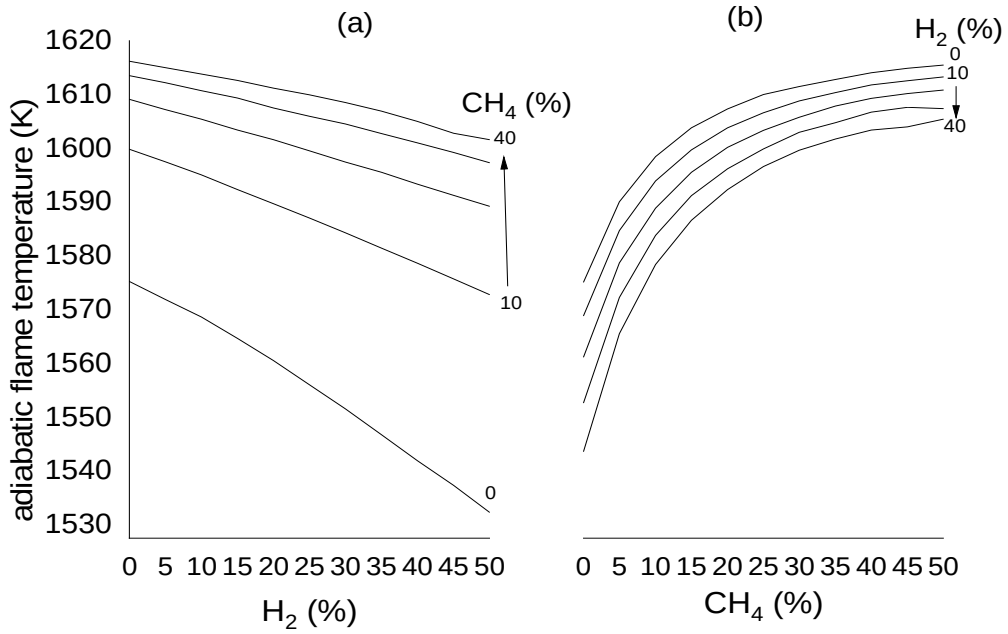

Fig.V.2: Effect of hydrogen and methane on the adiabatic flame temperature.

V. 2 Numerical procedure validation

No experimental measurements exist for biogas-syngas mixture in MILD combustion in opposed flow configuration. The simulation results of counterflow flame are validated with experiments of Jongmook Lim et al. [176] under the same conditions presented in **Table V.2**. Experiments were performed with methane (Airco Gas and Gear, 99% methane) introduced from bottom duct and preheated air introduced from the top duct. A nitrogen coflow was introduced from the top duct to stabilize the flames. The nitrogen coflow was also heated to reduce the heat loss from the air stream to negligible levels. The separation distance between ducts is 15 mm and inner diameter of both ducts is 20.1 mm, ambient pressure is 1 atm. Three air preheat temperatures, T_{AIR} = 300 K, 440 K, and 560 K, were considered. The exit temperature of the fuel stream was maintained at 300 K. The nominal exit velocities of methane and air were fixed at 70 cm/s for the three experimental conditions. A sufficient volumetric rate of nitrogen coflow was used to stabilize the flat flames. The rate of coflow was constant

for the three flames with the coflow velocity maintained at 60 cm/s. Major and minor species distributions are given in function of distance between ducts. Results of numerical calculations using GRI-Mech 2.11, GRI-Mech 3.0 and USC-GRI-Mech 2.11 were compared with measurements.

Table.V.2: Cases considered in validation.

Cases	T_{AIR} (K)	T_{FUEL} (K)	V_{AIR} (cm/s)	V_{FUEL} (cm/s)	a (s^{-1})
1	300	300	70	70	162
2	440	300	72.6	70	182
3	560	300	72.6	70	193

Fig.V.3 (a), (b) and **(c)** presents a comparison between predicted results and experimental data of gas species (H_2, CO, CO_2, N_2, O_2, CH_4, C_2H_2 and C_2H_4) for case 1, using Chemkin and USC-GRI-Mech 2.11 mechanism. It was found that the mechanism gives close results, it can be seen that all mole fractions of species (H_2, CO, CO_2, N_2, O_2, CH_4) match well with the experimental results. However, the C_2H_4 and C_2H_2 profiles shows a poor agreement between the data and the calculations **Fig.V.3(c).**

Comparisons between measurements and simulations of NO mole fraction for the three mechanisms (GRI-Mech 2.11, GRI-Mech 3.0 and USC-GRI-Mech 2.11) are shown in **Figs.V.3 (d), (e)** and **(f).** Three levels of air preheat temperatures are considered T_{AIR} = 300 K, 440 K, and 560 K. As found in precedent works [62, 177, 178], the major discrepancy between the data and the predictions occurs on the fuel-rich side for three preheat temperatures. Although, the composed mechanism USC-GRI-Mech 2.11 shows best approximation in terms of maximum NO values for all preheating levels.

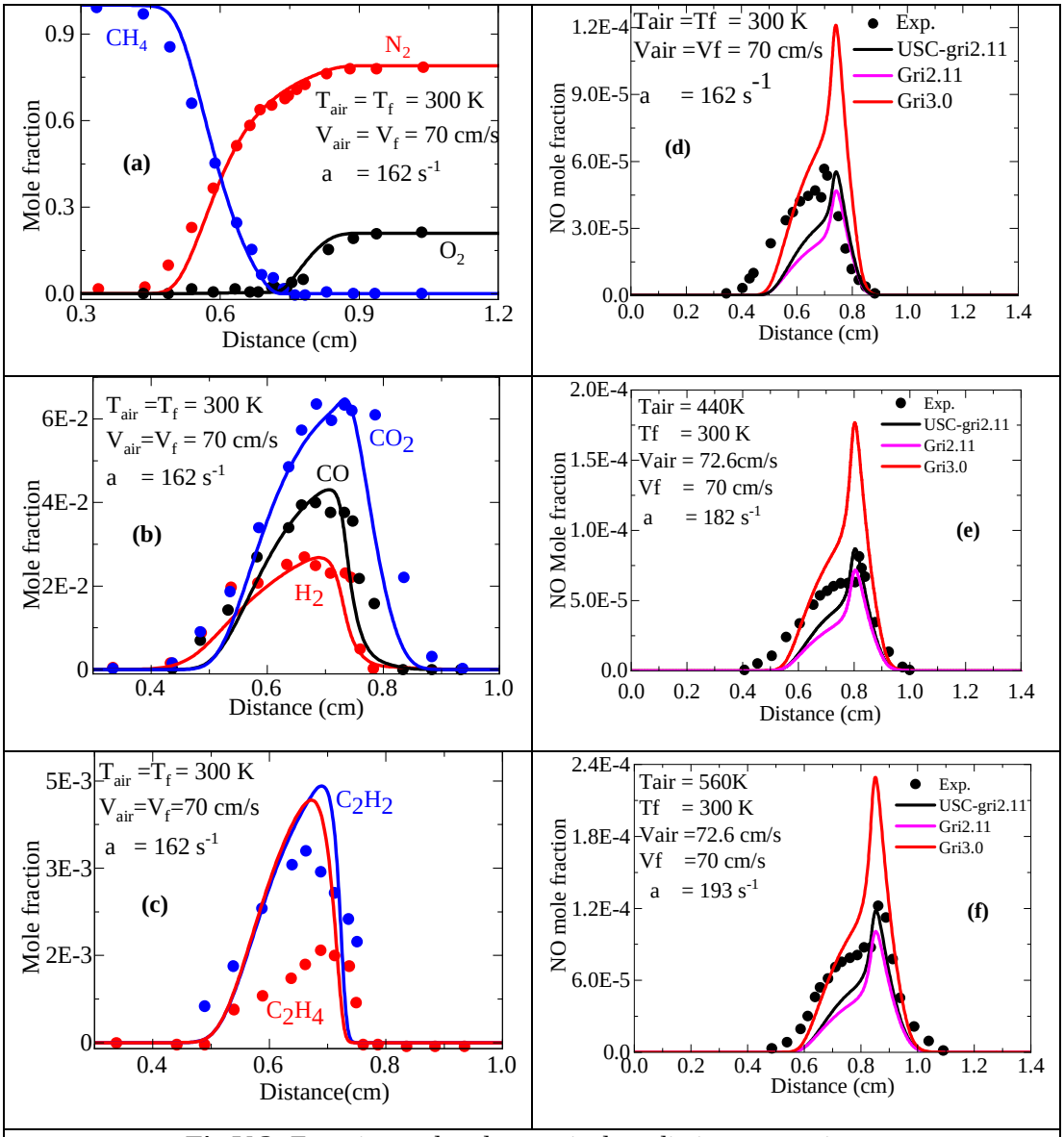

Fig.V.3: Experimental and numerical prediction comparison.

V. 3 Boundary conditions and computation strategy

Boundary conditions for fuel and oxidizer are:

- Injection temperature of fuel T_{Fu}=300 K.
- Composition of fuel at injection is:

$$\boldsymbol{Fuel\ mixture} = \boldsymbol{Biogas} + \boldsymbol{syngas} = [\alpha CH_4 + (0.5-\alpha)CO_2] + [\beta H_2 + (0.5-\beta)CO] \quad (V.1)$$

With α and β are stoichiometric coefficients which are varied from 0 to 0.5. Here notation BαSβ is used referring respectively to Biogas with α mole fraction of methane and Syngas with β mole fraction of hydrogen. So that B25S25 represents mean mixture composed from 0.25 of each compound.

- The composition of the oxidizer at injection is:

$$\boldsymbol{Oxidizer} = \mathrm{z}O_2 + (1 - \mathrm{z})N_2 \quad \text{(V.2)}$$

With z is the mole fraction of oxygen in the oxidizer stream, it is varied from 0.04 to 0.21.

- Injection velocities are equal for both fuel and oxidizer, the strain rate is computed in the function of injection velocities, the distance between injectors and reactants densities by [156]:

$$a = \frac{2(-u_{Ox})}{d} + \frac{2u_{Fu}}{d}\sqrt{\frac{\rho_{Fu}}{\rho_{Ox}}} = \frac{2(-u_{Ox})}{d}\left[1 + \frac{u_{Fu}}{(-u_{Ox})}\sqrt{\frac{T_{ox}W_{Fu}}{T_{Fu}W_{ox}}}\right] \quad \text{(V.3)}$$

For mean mixture B25S25, injection strain rate ranges from 10 to 10000 1/sec.

Chemkin Oppdif software is used for solving partial differential equations with their appropriated boundary conditions. For the chemical kinetics, a composed mechanism from the USC C_1-C_4 and the Gri 2.11 N-sub mechanism has been adopted for effects of all parameter except for pressure effect; the combustion kinetics is described by the composed mechanism USC-GRI-Mech 2.11 and compared with the GRI-Mech 3.0 mechanism, which handles 53 species in 325 elementary reactions [92]. The latter has been used for pressures up to 20 atm [179].

Computation of MILD combustion of the mixture biogas-syngas ((CH_4+CO_2)-(H_2+CO)) is organized in five sections. In each one, the effect of parameters variation on combustion structure, NO species reactions, production routes and NO emission index are considered. In addition, to discuss the effective mechanisms in the formation of NO, it is necessary to categorize these mechanisms. The five mechanisms of NO formation, including thermal, prompt, N_2O-intermediate, NNH, and NO-reburning [59-63] are listed in **Table V.3**. Since many reactions are shared by different routes, computing of NO from a specific route is operated by disabling its initiation reactions and making difference with the full NO mechanism. For instance, the thermal route is disactivated by disabling the reaction N+NO<=>N_2+O and the prompt one by suppressing reactions CH+N_2<=>HCN+N and CN+N<=>C+N_2. The accuracy of this procedure can be verified by summing different routes which should be close to the full mechanism results.

Table V.3: Main reactions of different mechanisms in NO production and consumption.

Mechanism	Reactions		
Thermal	R178 $N + NO \leftrightarrow N_2 + O$	R179 $N + O_2 \leftrightarrow NO + O$	R180 $N + OH \leftrightarrow NO + H$
Prompt	R180 $N + OH \leftrightarrow NO + H$	R191 $NH + H \leftrightarrow N + H_2$	R220 $CN + O_2 \leftrightarrow NCO + O$
	R222 $NCO + O \leftrightarrow NO + CO$	R223 $NCO + H \leftrightarrow NH + CO$	R230 $HCN + (M) \leftrightarrow CN + H + (M)$
	R231 $HCN + O \leftrightarrow NCO + H$	R233 $HCN + O \leftrightarrow CN + OH$	R239 $C + N_2 \leftrightarrow CN + N$
	R240 $CH + N_2 \leftrightarrow HCN + N$	R242 $CH_2 + N_2 \leftrightarrow HCN + NH$	R243 $CH_2(S) + N_2 \leftrightarrow NH + HCN$
N_2O-intermediate	R181 $N_2O + O \leftrightarrow N_2 + O_2$	R182 $N_2O + O \leftrightarrow 2NO$	R183 $N_2O + H \leftrightarrow N_2 + OH$
	R184 $N_2O + OH \leftrightarrow N_2 + HO_2$	R185 $N_2O+ (M) \leftrightarrow N_2 + O+ (M)$	R190 $NH + O \leftrightarrow NO + H$
	R199 $NH + NO \leftrightarrow N_2O + H$	R222 $NCO + O \leftrightarrow NO + CO$	R224 $NCO + OH \leftrightarrow NO + H + CO$
	R226 $NCO + O_2 \leftrightarrow NO + CO_2$		
NNH	R190 $NH + O \leftrightarrow NO + H$	R191 $NH + H \leftrightarrow N + H_2$	R192 $NH + OH \leftrightarrow HNO + H$
	R193 $NH + OH \leftrightarrow N + H_2O$	R194 $NH + O_2 \leftrightarrow HNO + O$	R195 $NH + O_2 \leftrightarrow NO + OH$
	R196 $NH + N \leftrightarrow N_2 + H$	R197 $NH + H_2O \leftrightarrow HNO + H_2$	R198 $NH + NO \leftrightarrow N_2 + OH$
	R199 $NH + NO \leftrightarrow N_2O + H$	R204 $NNH \leftrightarrow N_2 + H$	R205 $NNH + (M) \leftrightarrow N_2 + H + (M)$
	R206 $NNH + O2 \leftrightarrow HO_2 + N_2$	R207 $NNH + O \leftrightarrow OH + N_2$	R208 $NNH + O \leftrightarrow NH + NO$
	R209 $NNH + H \leftrightarrow H_2 + N_2$	R210 $NNH + OH \leftrightarrow H2O + N_2$	R211 $NNH + CH3 \leftrightarrow CH_4 + N_2$
	R212 $H + NO + (M) \leftrightarrow HNO + (M)$	R213 $HNO + O \leftrightarrow NO + OH$	R214 $HNO + H \leftrightarrow H_2 + NO$
	R215 $HNO + OH \leftrightarrow NO + H_2O$	R216 $HNO + O_2 \leftrightarrow HO_2 + NO$	
NO-reburning	R183 $N_2O + H \leftrightarrow N_2 + OH$	R196 $NH + N \leftrightarrow N_2 + H$	R198 $NH + NO \leftrightarrow N_2 + OH$
	R199 $NH + NO \leftrightarrow N_2O + H$	R212 $H + NO + (M) \leftrightarrow HNO + (M)$	R218 $CN + OH \leftrightarrow NCO + H$
	R220 $CN + O_2 \leftrightarrow NCO + O$	R223 $NCO + H \leftrightarrow NH + CO$	R229 $NCO + NO \leftrightarrow N_2 + CO_2$
	R231 $HCN + O \leftrightarrow NCO + H$	R232 $HCN + O \leftrightarrow NH + CO$	R233 $HCN + O \leftrightarrow CN + OH$
	R234 $HCN + OH \leftrightarrow HOCN + H$	R235 $HCN + OH \leftrightarrow HNCO + H$	R236 $HCN + OH \leftrightarrow NH_2 + CO$
	R244 $C + NO \leftrightarrow CN + O$	R245 $C + NO \leftrightarrow CO + N$	R246 $CH + NO \leftrightarrow HCN + O$
	R247 $CH + NO \leftrightarrow H + NCO$	R248 $CH + NO \leftrightarrow N + HCO$	R249 $CH_2 + NO \leftrightarrow H + HNCO$
	R250 $CH_2 + NO \leftrightarrow OH + HCN$	R251 $CH_2 + NO \leftrightarrow H + HCNO$	R252 $CH_2(S) + NO \leftrightarrow H + HNCO$
	R253 $CH_2(S) + NO \leftrightarrow OH + HCN$	R254 $CH_2(S) + NO \leftrightarrow H + HCNO$	R255 $CH_3 + NO \leftrightarrow HCN + H_2O$
	R256 $CH_3 + NO \leftrightarrow H_2CN + OH$	R274 $HCCO + NO \leftrightarrow HCNO + CO$	

For each parameter effect, computations are executed five times by disabling one NO route each time. Then NO production is computed by taking the difference with the full mechanism which is computed once.

Table V.4 Reactions involved in interpretations (T. Thermal and P. Prompt)

Route	Reaction	Route	Reaction
Thermal	R179 $N+O_2<=>NO+O$	Reburn	R244 $C+NO<=>CN+O$
P./T.	R180 $N+NO<=>N_2+O$		R245 $C+NO<=>CO+N$
N_2O-intermediate	R185 $N_2O+ (M) \leftrightarrow N_2 + O+ (M)$		R246 $CH+NO<=>HCN+O$
NNH	R208 $NNH+O<=>NH+NO$		R249 $CH_2+NO<=>H+HNCO$
	R212 $H+NO+M<=>HNO+M$		R274 $HCCO+NO<=>HCNO+CO$
	R214 $HNO+H<=>H_2+NO$		
	R215 $HNO+OH<=> NO +H_2O$		
Prompt	R240 $CH+N_2<=>HCN+N$		

The results of NO release are presented by the NO emission index (EINO) suggested by Takeno and Nishioka [180], as defined below:

$$EINO = \frac{\int_0^d W_{NO}\dot{\omega}_{NO}dx}{-\int_0^d W_{Fuel}\dot{\omega}_{Fuel}dx} \quad (V.4)$$

Where W represents molecular weight and $\dot{\omega}$ is the net production or consumption rates of relevant species. EINO depends on the flow conditions, as well as the physical and chemical properties of the fuel and oxidizer flows, which can provide independent results from other parameters.

The integral over the fuel injection is operated by summing fuel compounds except CO_2 which is a diluent.

V. 4 Composition effect

V.4.1 Effect on combustion structure

To characterize the effect of fuel mixture composition on combustion structure, NO species reactions, production routes and NO emission index, several mixtures are considered. First, the composition of syngas is kept constant with a volume of 25% hydrogen and 25% CO. On the other hand, the composition of biogas is varied by changing the volume of methane from 0% to 50%. Then the reverse of operation is carried out by keeping a constant composition of the biogas and by varying that of the syngas**.** The oxidizer is composed of a volume of 4% of oxygen and 96% of N_2. The strain rate is constant and equal to 200 s^{-1} while injection temperatures of fuel and oxidizer are 300 K and 1200 K respectively.

Fig.V.4 shows methane and hydrogen volume increase effects on combustion temperature profile since the latter has important implication in NO formation. It can be noticed that fuel is fed by the left side at temperature 300 K, while oxidizer ($4\%O_2$+ $96\%N_2$) is injected from the right duct at a high temperature of 1200 K and low-density **Fig.V.4 (a).** Consequently, the stagnation plane and combustion region are located on the oxidizer side [47, 164]. It is noticed that stagnation plane position X_{stag} and maximum temperature position X_{Tmax}, which is assumed to correspond to flame front, are both shifted to the left side when hydrogen or methane are increased **Fig.V.4(b).** Augmentation in temperature by combustion varies between $\Delta T_{combB25S00}$ = 244K and $\Delta T_{combB25S50}$ = 418K, which correspond to differences between oxidizer injection

temperature and maximum temperature of combustion for mixtures B25S00 and B25S50 respectively **Fig.V.4(a).** It can be seen that these differences did not exceed mixtures auto ignition temperature, which is of the order of 800K, this warrants the MILD combustion conditions regime. For all compositions, the temperatures increase from 300 K at the injection sides and reach their maximum values at the flame front position. For the mixture B00S25, where biogas is only composed by carbon dioxide and syngas by equal volumes of hydrogen and carbon monoxide, the maximum flame temperature is 1522 K reached at x=1.52 cm from the fuel duct. If the mixture B25S00 is considered, the maximum flame temperature is 1444 K located at the same position x=1.52 cm. If the equimolar composition B25S25 is considered, the maximum temperature is 1571 K, located at x = 1.49 cm. When the volume of methane increases up to 50% in the biogas (i.e. mixture B50S25) or hydrogen rises to 50% in syngas (i.e. mixture B25S50), the maximum flame temperature increases to nearly 1578 K at the position x = 1.43 cm and 1618K at the position x = 1.45 cm respectively.

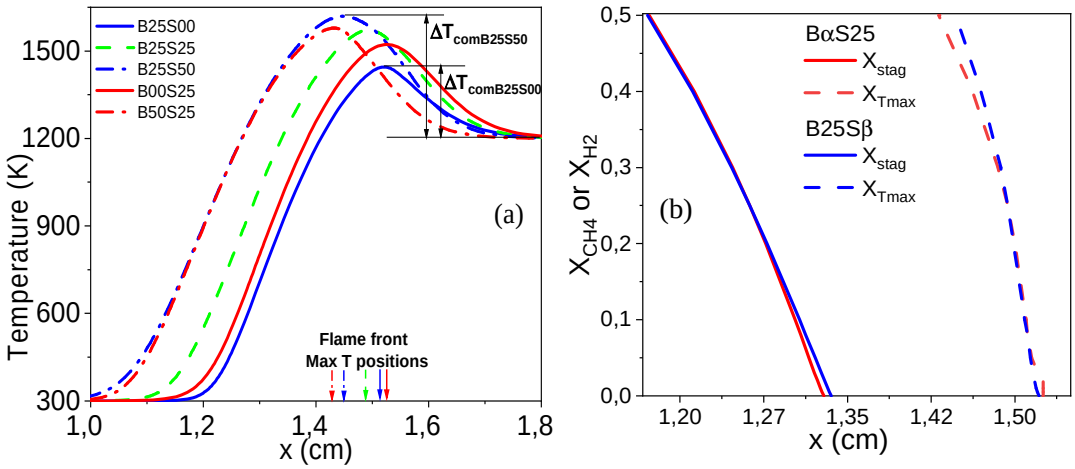

Fig.V.4: (a) Combustion temperature, (b) stagnation and flame positions.

Fig.V.5 (a) and **(b)** presents the H_2O and NO mole fraction variation along the x direction for different compositions; these species are produced on the whole reaction zone and its maximum corresponds to that of temperature. It can be noticed that for the set BαS25 with a constant composition of syngas (25% H_2 and 25% CO), when CH_4 increases from 0 to 25%, and then to 50%, the maximum H_2O decreases from 0.0645 (at x= 1.46 cm) to 0.0561 (at x= 1.49 cm) and then to 0.0538 (at x= 1.43 cm). In the same conditions, the maximum mole fraction of NO varies from 6 ppm (at x= 1.51 cm) to 7.97 ppm (at x= 1.52 cm) and then to 7.84 ppm (at x=1.46 cm). Now, if the set B25Sβ

is considered, biogas is kept constant (25% CH_4 and 25% CO_2) and hydrogen in syngas increases from 0% to 25%, and then to 50%. The maximum of H_2O raises from 0.0246 (at x = 1.51 cm) to 0.0561 (at x= 1.49 cm) and then to 0.0669 (at x = 1.46 cm). Similarly, in the same conditions, NO increases from 2.19 ppm (at x = 1.54 cm) to 7.97 ppm (at x= 1.52 cm) and then to 8.31 ppm (at x = 1.49 cm).

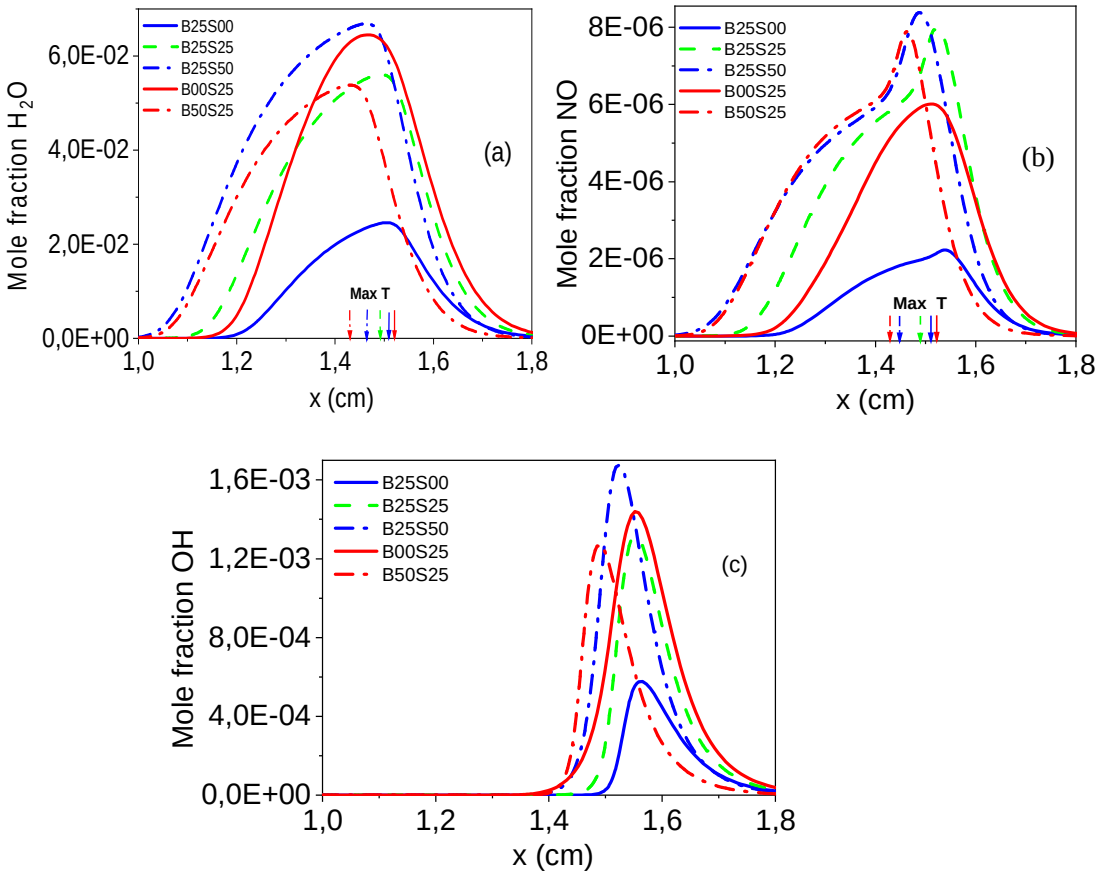

Fig.V.5: Molar fraction variations of (a) H_2O, (b) NO and (c) OH species.

In contrast with these properties, OH species, which indicates strength of combustion reaction, are produced in a thin region in fuel lean zone. From **fig.V.5 (c).** It can be observed that for the set of compositions BαS25 with constant syngas (25% H_2 and 25% CO), if CH_4 increases from 0 to 25% and then to 50%, the maximum mole fraction of OH varies from 0.0014 (at x = 1.55 cm) to 0.0013 (at x = 1.55 cm) and then to 0.00127 (at x = 1.49 cm). If the set of compositions B25Sβ is considered, biogas is kept constant (25% CH_4 and 25% CO_2) and hydrogen in syngas increases from 0% to 25% and then to 50%; the maximum mole fraction of OH increases from 5.77E-4 (at x = 1.56 cm) to 0.0013 (at x = 1.55 cm) and then to 0.0017 (at x= 1.52 cm).

On the whole, the increase of CH_4 or H_2 volumes make the mixture locally rich and lead to higher production of H_2O and OH with a shift of their profiles to the fuel side. Moreover, H_2O and OH productions are directly linked to hydrogen volume; their maximum values are reached for the mixture B25S50 whereas their minimum values are obtained for the mixture B25S00.

Fig.V.6 represents maximum temperatures variation in function of methane (curve BαS25) and hydrogen (curve B25Sβ) increase. It can be observed that when hydrogen volume rises in the fuel mixture, combustion maximum temperature rises from 1444K for X_{H2} = 0% to 1618K when X_{H2} = 50%, this gives an increase in maximum temperature of ΔT_{maxH2} = 174K. On the other hand, methane increase in fuel mixture varies temperature from 1522K for X_{CH4} = 0% to 1578K while X_{CH4} = 50%, which gives an augmentation of ΔT_{maxCH4} = 56K only. Growth in maximum temperature is much important when hydrogen is added compared to methane. This is because, in the case of methane addition (curve BαS25) and lake of oxygen environment (X_{O2}=0.04 to 0.06, which is the case of MILD combustion regime), important reactions that consume methane and hydrogen are CH_4+OH <=>CH_3+H_2O and OH+H_2 <=> H+H_2O respectively. These reactions involve oxygen through OH species. On the other hand, when hydrogen increases (curve B25Sβ), it is noticed that the main methane and hydrogen consumption reaction is CH_4+H<=>CH_3+H_2 which did not involve oxygenated species. This makes maximum temperature increase with hydrogen addition more important than methane.

The consequence of methane and hydrogen variation on NO production is shown by **Fig.V.5(b)** It can be noticed that maximum NO production is located after maximum temperature position on the oxidizer side (**Fig.V.5(b)**) since NO chemistry is relatively low. Levels of NO species are directly related to temperature maximums, low NO production is depicted for B00S25 composition, whereas high NO production is recorded for B25S50 composition, which has the maximum temperature. Before mixture B25S25, significant NO levels are obtained by methane addition (curve BαS25 on **Fig.V.6**); however, after B25S25, NO levels obtained by hydrogen increase are more significant (curve B25Sβ on **Fig.V.6** Production of NO species reaches a maximum and begins declining at a methane mole fraction of nearly 0.3. Whereas, when hydrogen is

added, NO mole increases monotonically to its maximum at X_{H2} = 0.4 and shows a slight reduction after **Fig.V.6**.

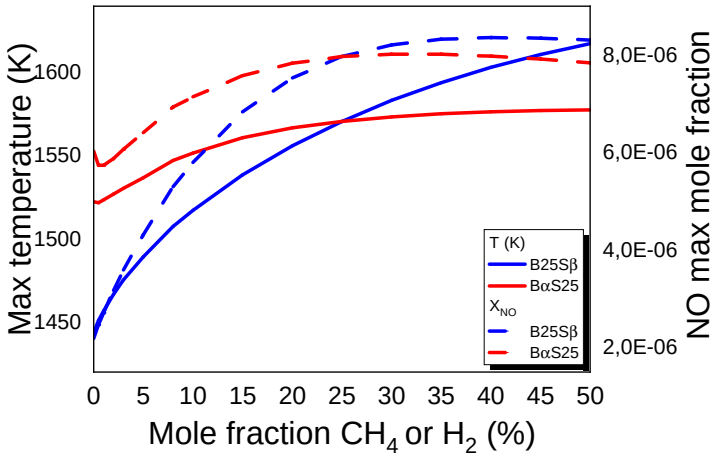

Fig.V.6: Maximum temperature and NO species.

V.4.2 Effect on NO species reactions and production routes

To have more insight in reactions responsible of NO production an absolute Rate Of Production (ROP) analysis is performed. Reaction ROP are plotted against distance between injection ducts, a description of reactions and involved routes are presented at flame front position which is assumed to coincide with maximum temperature.

Methane volume is varied in fuel mixture and important reactions producing NO are elucidated by **Figs.V.7 (a), (b)** and **(c).** It has been noticed that for low methane mole fraction, specifically $X_{CH4} \leq 0.07$ **Fig.V.7 (a)**, production of NO is fully governed by the NNH route through reactions R212 and R214, because hydrogen atom is abundant in the combustion pool. At the flame front (located at Tmax), the following most important reactions are R208 and R180, the former belongs to the NNH route and the latter to prompt one. Reaction R180 is assigned to the prompt path since the temperature is relatively low (Tmax<1550K) and N atom can't be formed by thermal mechanism. When methane increases in the mixture, it consumes H atoms for its depletion which depresses reaction R208 and then the NNH route. On the other hand, the prompt path is enhanced because ROP's of reactions R240 and R180 are increased by hydrocarbons radicals. For intermediate methane volumes, nearly $0.07 < X_{CH4} \leq 0.4$, **Fig.V.7(b)** shows that at the flame front, most important route is prompt one via

reaction R180 followed by NNH route through reactions R212, R215, R208 and finally reburn mechanism by reactions R246 and R249. When methane mole fraction exceeds 0.4, it is found that the most important reaction that produces NO at the flame front is R249 which belongs to reburn mechanism followed by R180 then R214 from prompt and NNH routes respectively **Fig.V.7(c).**

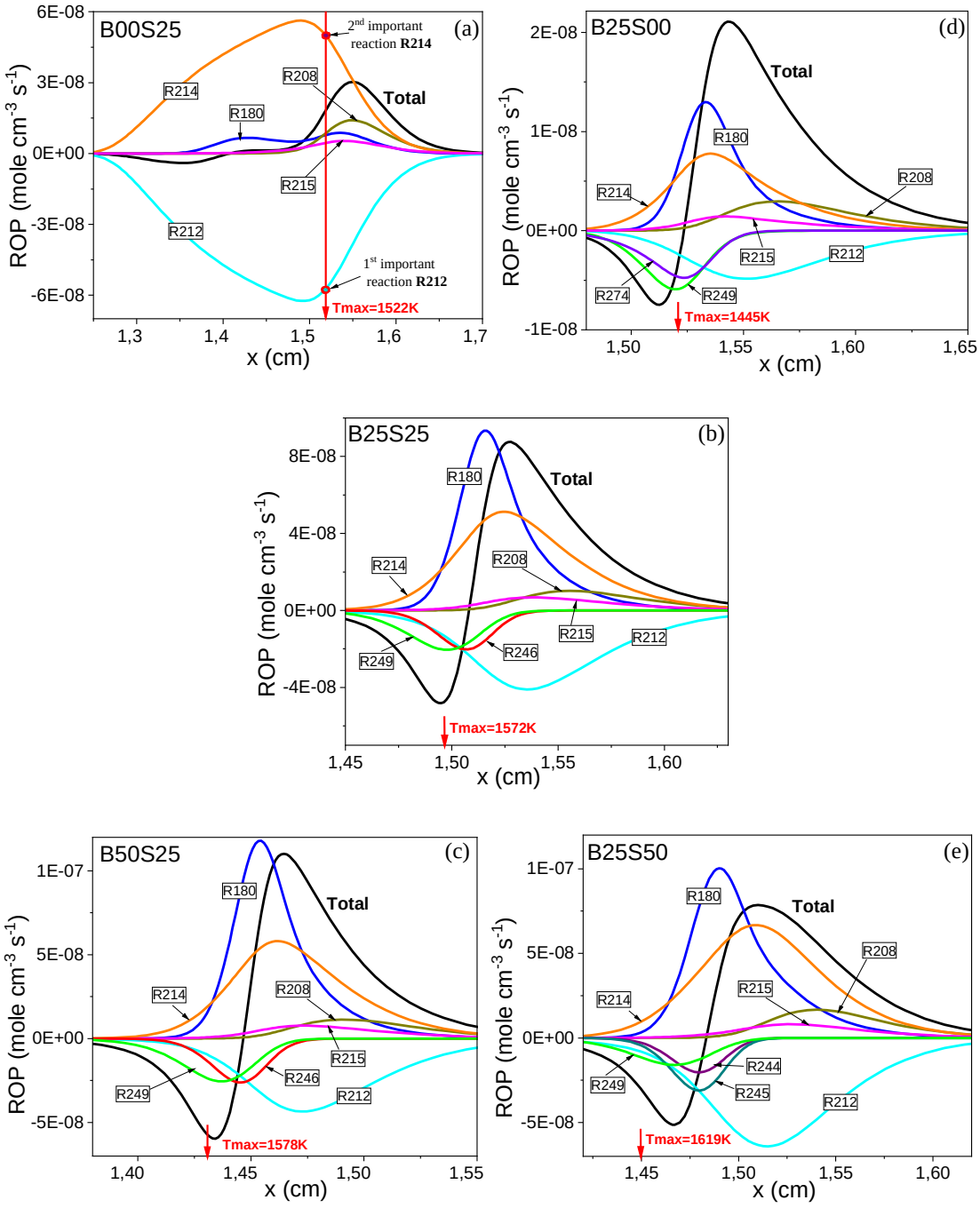

Fig.V.7: Main reactions involved in BαS25 and B25Sβ mixtures combustion (a)B00S25, (b)B25S25, (c)B50S25, (d)B25S00 and (e)B25S50.

Figs.V.7 (d), (b) and **(e)** show that at low and intermediate hydrogen volumes, NO production at the flame front is globally governed by the prompt route through reaction R180. Whereas, at high H_2 concentrations NNH route is activated via reaction R214, as said before this route seems to be linked to hydrogen availability. The second most important path is reburning one by reaction R249 which is favored for all hydrogen volumes. Last important reactions are reburn one R274 for low hydrogen content and NNH one R212 for other H_2 volumes.

V.4.3 Effect of CH_4 and H_2 addition on NO emission index

Fig.V.8 (a) shows NO production routes in the function of methane volume in the fuel mixture. It can be observed that three routes are important, namely: NNH, Prompt and reburn, this can be also seen on sensitivity analysis **Fig.V.9 (a).** At low CH_4 volume in the mixture, since mixture contains 25% of hydrogen, NO production is dominated by NNH route where the limiting step R208 is important at low methane volume and reduces when methane volume rises **Fig.V.9 (a).** It can be noticed from **Fig.V.8(a)** that when CH_4 volume rises, prompt NO increases and equalizes NNH NO at nearly CH_4=0.12 and EINO=0.44 g_{NO}/Kg_{Fuel}. The main reaction that produces prompt NO is R180 which is shared with the thermal route [59,60]; however, here it is fed by prompt reaction R240 **Fig.V.8 (a).** At high methane volume, CHn radicals are abundant, consequently, the prompt route is maximal whereas the NNH one is minimal. Reburn route is important at high methane volume in the mixture, it is activated through reactions R231, R246 and R249, this route is generally significant in the fuel-rich mixture [62]. **Fig.V.8 (a)** shows that computations by full mechanism does not differ a lot from the sum of routes which indicated that selected reactions represent fairly this route.

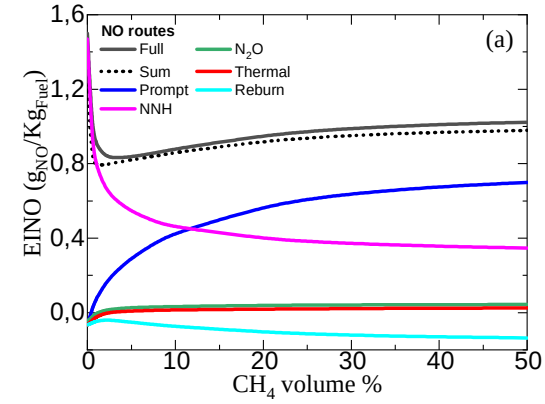

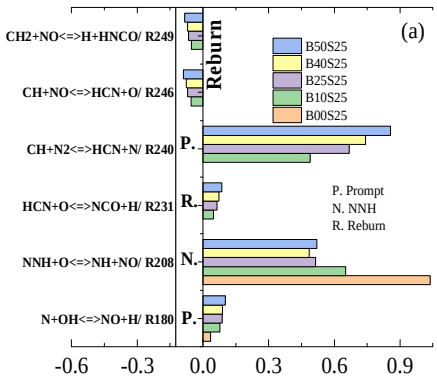

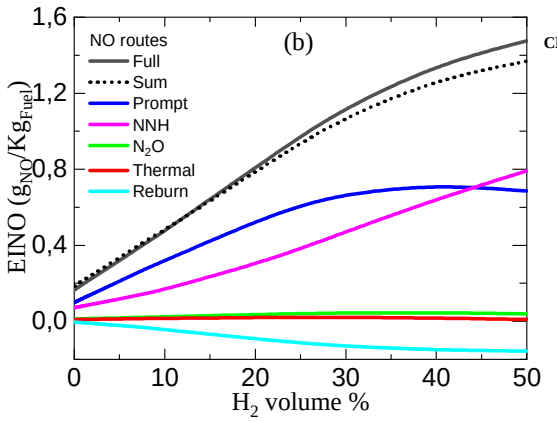

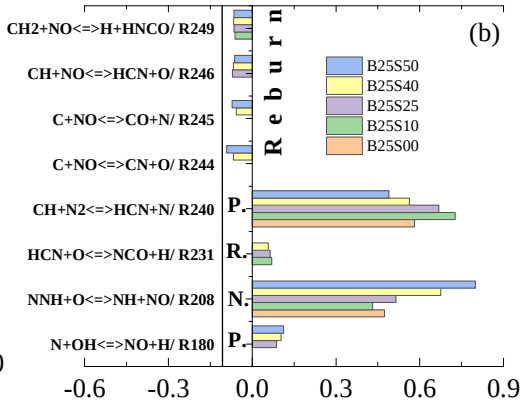

Fig.V.8: Emission by routes for (a)BαS25 and (b)B25Sβ mixtures

Fig.V.9: Sensitivity coefficients for NO production in (a)BαS25 and (b)B25Sβ mixtures.

The effect of hydrogen increase in fuel mixture on NO formation route is shown by **Figs.V.8(b)** and **V.9(b).** Minimum NO is produced at low hydrogen volumes. The most important mechanism is prompt, followed by NNH then reburn one. Hydrogen increase in the mixture enhances prompt route through reaction R240 which feds R180. Prompt production reaches a maximum at nearly H_2=40% and begins declining. On the other hand, the NNH production route exhibits an increasing behavior with hydrogen augmentation, it equalizes prompt route at nearly H_2=44% (EINO=0.75 g_{NO}/Kg_{Fuel}). The main limiting step for the NNH route is R208 which is enhanced by hydrogen increase as showed by **Fig.V.9(b)**. It can also be seen that, excepting at high hydrogen volumes, the difference between NO routes sum and full NO mechanism is negligible. It can be noticed that when methane or hydrogen volumes are varied in the fuel mixture, the production of NO by thermal or N_2O intermediate route are negligible.

V.5 Oxygen increase effect

In this part, the effect of oxygen is studied, the mole fraction of O_2 is increased from 0.04 to 0.21 replacing that of N_2. Mean composition B25S25 is used, however maximum variations of temperature and NO mole fraction are presented for other compositions in the function of oxygen volume. The strain rate is constant and equal to 200 s^{-1} while injection temperatures of fuel and oxidizer are 300 K and 1200 K respectively.

V.5.1 Effect on combustion structure

The volume of oxygen in the oxidizer is a key characteristic in the achievement of the MILD regime. The effect of oxygen concentration in oxidizer on combustion structure for the mixture B25S25 is shown in **Fig.V.10**. From **fig.V.10 (a),** it can be seen that when oxygen mole fraction increases from 4% to 8% and then to 21%, maximum temperature increases from 1571 K (located at x=1.49 cm) to 1836 K (located at x= 1.44 cm) and then to 2345 K (located at x=1.38 cm). When oxygen concentration increases inside the oxidizer, temperature profiles are shifted to the fuel side and the reaction zone thickness is increased. Since the temperature increase during combustion ΔT_{comb} is lower than mixture autoignition temperature, which is about 800K for these gases, the MILD combustion regime can be sustained by keeping oxygen volume near the limits of 2%-8%. Here it can be observed that at volume O_2=21% temperature increase $\Delta T_{combO2=21\%}$= 1145 K is greater than autoignition temperature of the mixture, which means that the MILD regime breaks down since conditions are not satisfied (conventional combustion). The H_2O and NO mole fractions are presented by **Fig.V.10 (b)** and **(d)** respectively; these species are increased and shifted to the fuel side with oxygen volume augmentation. Quantitatively, when oxygen volume increases from 4% to 8% and then to 21%, the maximum H_2O mole fraction is augmented from 0.0561 to 0.0977 and then to 0.1947; whereas the maximum NO mole fraction increases from 8ppm to 41ppm and then to 434 ppm respectively. OH species, which is an indicator of the strength of the global combustion reaction, is shown by **Fig.V.10 (c);** it is produced in the second half of the reaction zone near the oxidizer and is increased by oxygen increase in the oxidizer. When oxygen increases in oxidizer from 4% to 8% and then to 21%, the maximum OH mole fraction increases 0.0013 to 0.0038 and then to 0.0147 respectively.

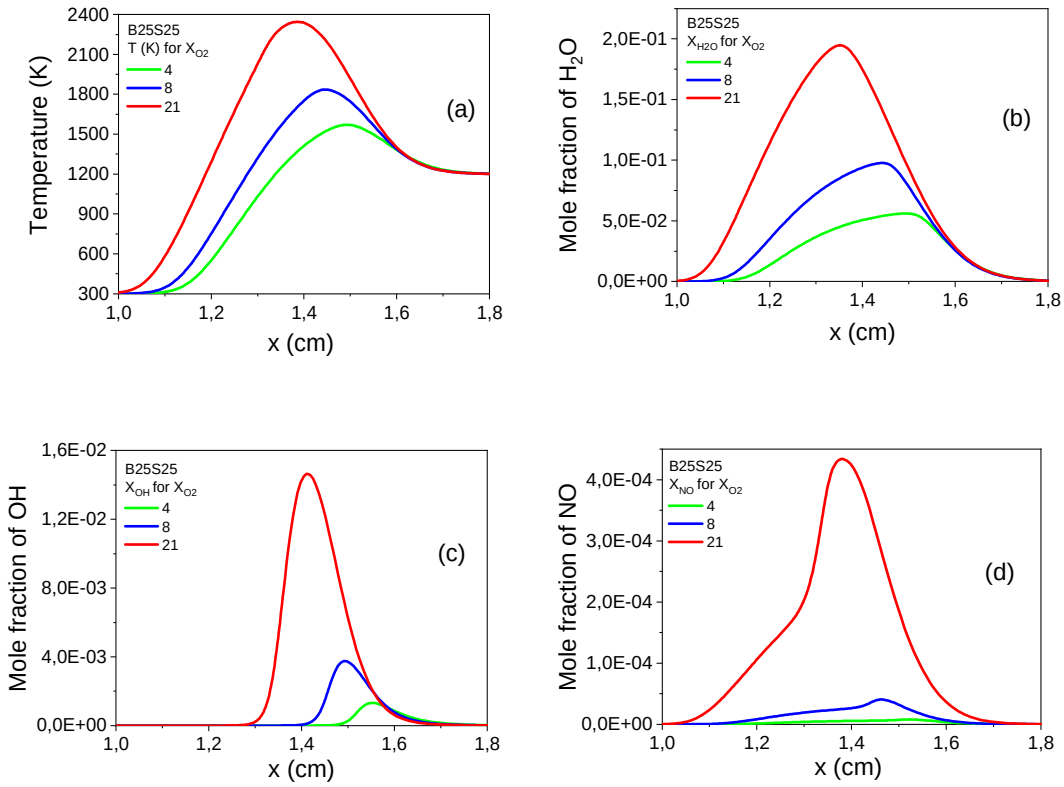

Fig.V.10: Temperature (a) and molar fraction variations of (b) H_2O, (c) OH and (d) NO species for different oxidizer concentration.

The oxygen effect on other mixtures is presented in **Fig.V.11**. From this figure, it can be noticed that maximum temperature and also NO mole fractions are obtained for composition B25S25 followed by B25S00 then B00S25. The exception is made for the interval O_2<0.064 in which the maximum temperature obtained by composition B00S25 is greater than that of B25S00, this behavior was already explained in section **V.4.1**. When oxygen is available for combustion and depending on Low Heat Value (LHV), most containing fuel (methane, hydrogen and CO) mixture will have a maximum temperature. **Fig.V.11** presents this trend for different oxygen volumes contained in the oxidizer. It is found that when oxygen is abundant, methane in mixture BαS25 is mainly consumed by reduction reaction $CH_4+H<=>CH_3+H_2$ whereas hydrogen is reacted through $OH+H_2<=>H+H_2O$ (except B50S25 in which hydrogen is mainly reacted via $CH_4+H<=>CH_3+H_2$). On the other hand, for the compositions B25Sβ, methane is mainly consumed by reaction $CH_4+OH<=>CH_3+H_2O$ and hydrogen through $OH+H_2<=>H+H_2O$.

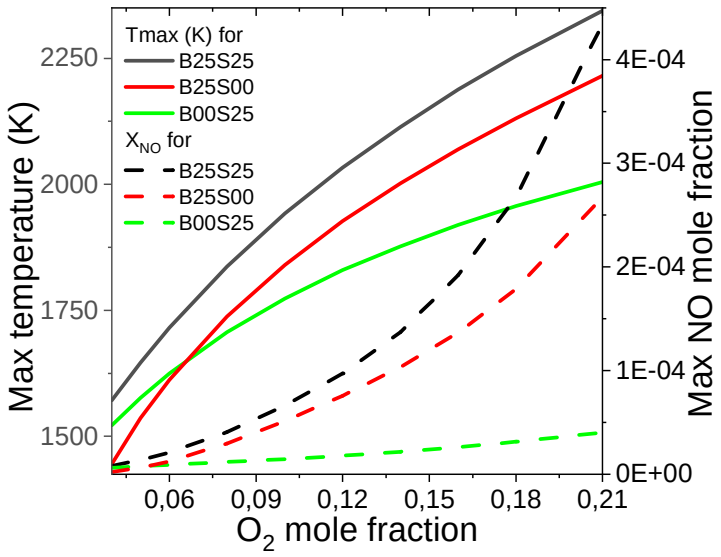

Fig.V.11: Maximum temperature and NO species for different compositions.

V.5.2 Oxygen effect on NO species reactions and production routes

Figs.V.12 (a), (b) and **(c)** show principal reactions involved in NO species production for mean composition B25S25, when oxygen increases in the oxidizer. Here, it is important to mention that at flame front presented by maximum temperature and for all oxygen volumes in oxidizer, NO species is produced principally by prompt mechanism via reactions R180. This reaction is shared by thermal and prompt mechanisms, it is fed by prompt reactions at low oxygen volumes. However, at high oxygen concentrations, thermal mechanism become important and R180 uses N produced from the two routes, this behavior is seen on the reaction R180 profile, **Fig.V.12(c).** The second most important route is NNH through reaction R214 for low and relatively high oxygen volumes **Figs.V.12(a)** and **(b)**, however for O_2=21% R212 is favored. The last important routes are reburn one through reactions R249 at O_2=8%, R245 at O_2=12% and thermal route for O_2=21% via R179 **Fig.V.12(b).**

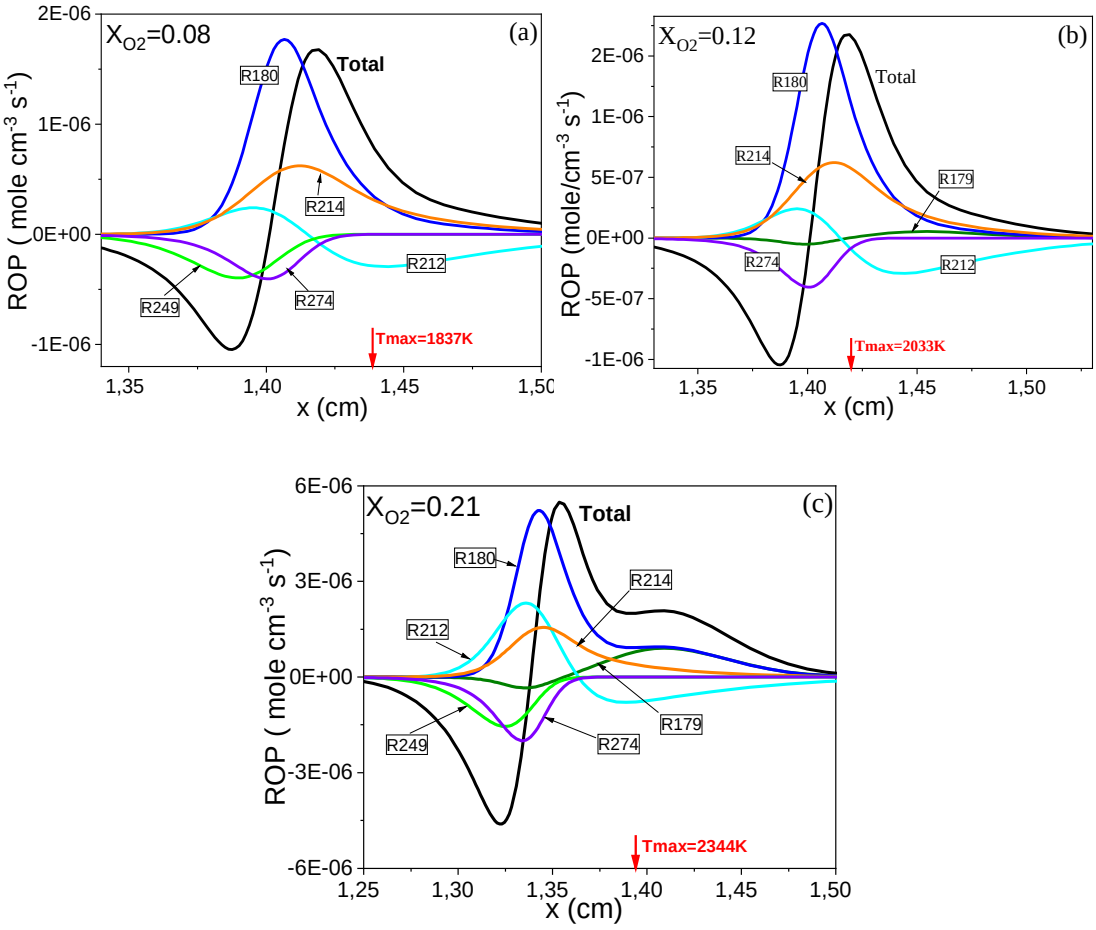

Fig.V.12: Main reactions involved with oxygen increase in the oxidizer (a) X_{O2} =0.08, (b) X_{O2} =0.12 and (c) X_{O2} =0.21.

V.5.3 Effect of O_2 increase in the oxidizer on NO emission index

Oxygen effect on NO production routes is showed by **Fig.V.13(a).** Mean mixture B25S25 is considered and oxygen volume is varied in oxidizer from 4 to 21%. It can be seen that at low oxygen volumes approximately O_2<12%, prompt route dominates NO production through reactions R239 and R240 which feeds R180 and produces NO **Fig.V.13(b).** The second most important route, in this case, is NNH one which is served by reaction R208, then reburn mechanism through reactions R246 and R249. When oxygen volume exceeds 12%, **Fig.V.13(a)** shows that the thermal route become more important than NNH one [59, 60]. Moreover, at nearly O_2=17%, the thermal mechanism surpasses the prompt route and produces important amounts of NO at high oxygen volumes in the oxidizer. **Fig.V.13(b)** shows that at high oxygen volumes, thermal reaction R179 is activated and reaction R180 produces NO by thermal route too. It is

important to mention the good concordance between NO produced by full mechanism and routes sum computations.

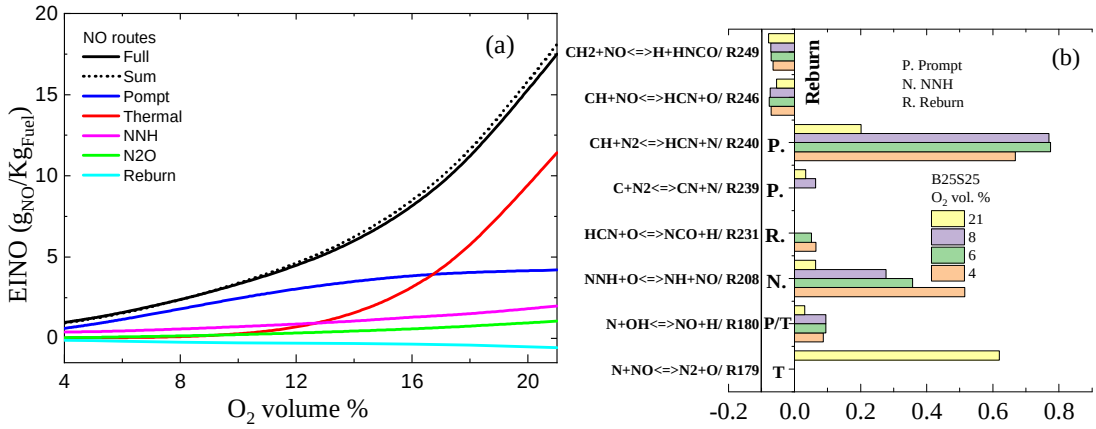

Fig.V.13: Emission NO routes (a) and sensitivity coefficients (b) in function of oxygen increase in oxidizer.

V.6. Strain increase effect

In this section, the effect of strain rate is considered, it is increased from near ignition to near extinction for the mean composition B25S25, nevertheless maximum variations of temperature and NO mole fraction are presented for other compositions in the function of strain rate. Mole fraction of O_2 is 0.04 while injection temperatures of fuel and oxidizer are 300 K and 1200 K respectively.

V.6.1. Effect on combustion structure

The flame structure is shown by **Fig.V.14** for the mixture B25S25 in the function of distance x from fuel duct for strain rates of 112 s^{-1}, 2788 s^{-1} and 8363 s^{-1} at ambient pressure of 1 atm and including radiation heat losses. The selected composition is the mean one that contains equal volumes of all mixture compounds. In **Fig.V.14**, it can be seen that when strain rate (or axial velocity) increases, the reaction zone is shifted to the fuel side flame thickness, the maximum flame temperature, H_2O, OH and NO species are depressed. Since the axial velocity is inversely proportional to the flow residence time at the flame front, the increase of axial velocity gradient (resultantly, the decrease of Damköhler number) makes chemical nonequilibrium effects be more pronounced [181]. It can be seen from **Fig.V.14 (a)** that temperature increases in the combustion zone and then decreases to injection values. Temperature reaches its maximum T=1587 K for a=112 s^{-1} (0.4 m/s) at x=1.58 cm, when strain rate increases

to 2788 s^{-1} (10 m/s), maximum temperature decreases to 1384 K at x=1.34 cm. Finally, at high strain rate value a=8363 s^{-1} (30 m/s), temperature is 1226 K at x=1.32 cm. It can be observed that the maximum temperature increase by combustion is 387K, which is far from autoignition temperature for considered mixtures, this guarantees the MILD combustion regime. It is shown in **Figure.V.14. (b)** that the maximum mole fractions of H_2O decrease monotonically with increasing axial velocity gradient. That is, it is consequently seen that flame strength is reduced by increasing axial velocity gradient. The radical OH and NO species are also reduced by increasing strain rate. The NO species production is generally governed by temperature variation which explains its reduction. **Fig.V.14 (d)** depicted that NO mole fraction follows the same behavior of temperature where a maximum of 10 ppm is recorded for a=112 s^{-1} located nearly at x=1.62 cm. NO mole fraction is highly reduced to 0.04 ppm at x=1.32 cm when strain rate increases to a high value of a =8363 s^{-1}.

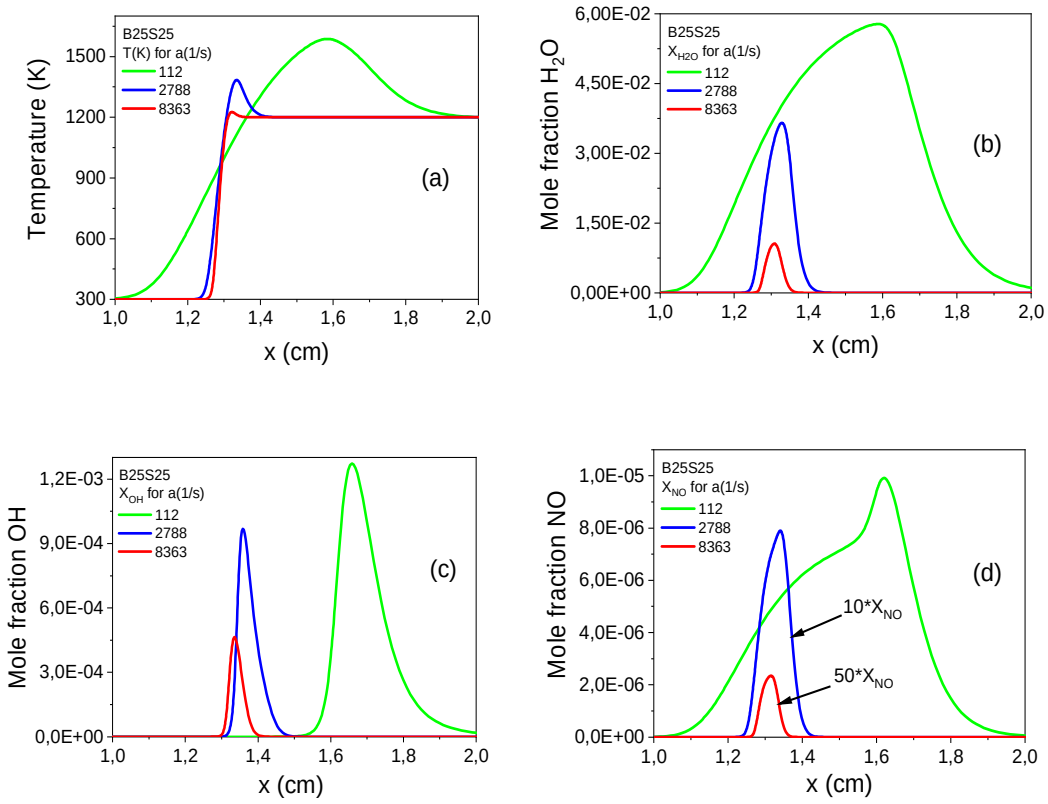

Fig.V.14: Temperature (a) and molar fraction variations of (b) H_2O, (c) OH and (d) NO species for different strain rates.

Variation of maximum temperature and NO mole fraction in the function of strain rate is showed by **Fig.V.15**. Non monotonic behavior with intermediate maximum located at nearly a=112 s^{-1} is noticed for both temperature and NO mole fraction. This

is the result of competition between radiation and reaction in the increasing region and non-equilibrium effect, reduction of residence time and formation of unburned products, in the decreasing zone [164]. It can be seen that in this regime, NO is drastically reduced by increasing the injection velocity of reactants (strain rate). **Fig.V.15 (b)** shows that MILD combustion of mixtures B25S25 and B00S25 prevails even at very high strain rate values, however, B00S25 produces less NO. Furthermore, composition B25S00 has a reduced working strain rate interval even it produces insignificant NO volumes **Fig.V.15(b).**

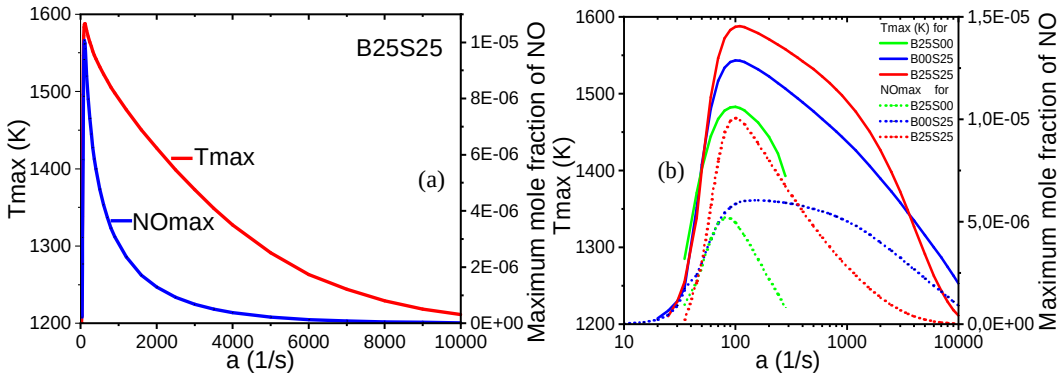

Fig.V.15: Maximum combustion temperature and NO species for different strain rates (a) B25S25 and (b) B25S00, B25S25 and B00S25.

V.6.2. Strain rate effect on NO species reactions and production routes

Reactions involved in NO formation are showed in **Figs.V.16 (a), (b)** and **(c)** for mixture B25S25 at considered strain rate values, namely a=112 s^{-1}, 2788 s^{-1} and 8363 s^{-1}. Globally strain rate increasing depresses all reactions. For low strain rate value at flame front **Fig.V.16 (a),** prompt mechanism dominates NO production by reaction R180 followed by R214 which belongs to NNH route then R249 which is a reburning reaction. For relatively high strain rates **Fig.V.16(b),** production is reduced for all NO mechanisms but routes order is preserved. However, for very high strain rates, NO formation is drastically reduced and the NO production mechanism is dominated by the NNH route through reaction R208 followed by the prompt route via reaction R214.

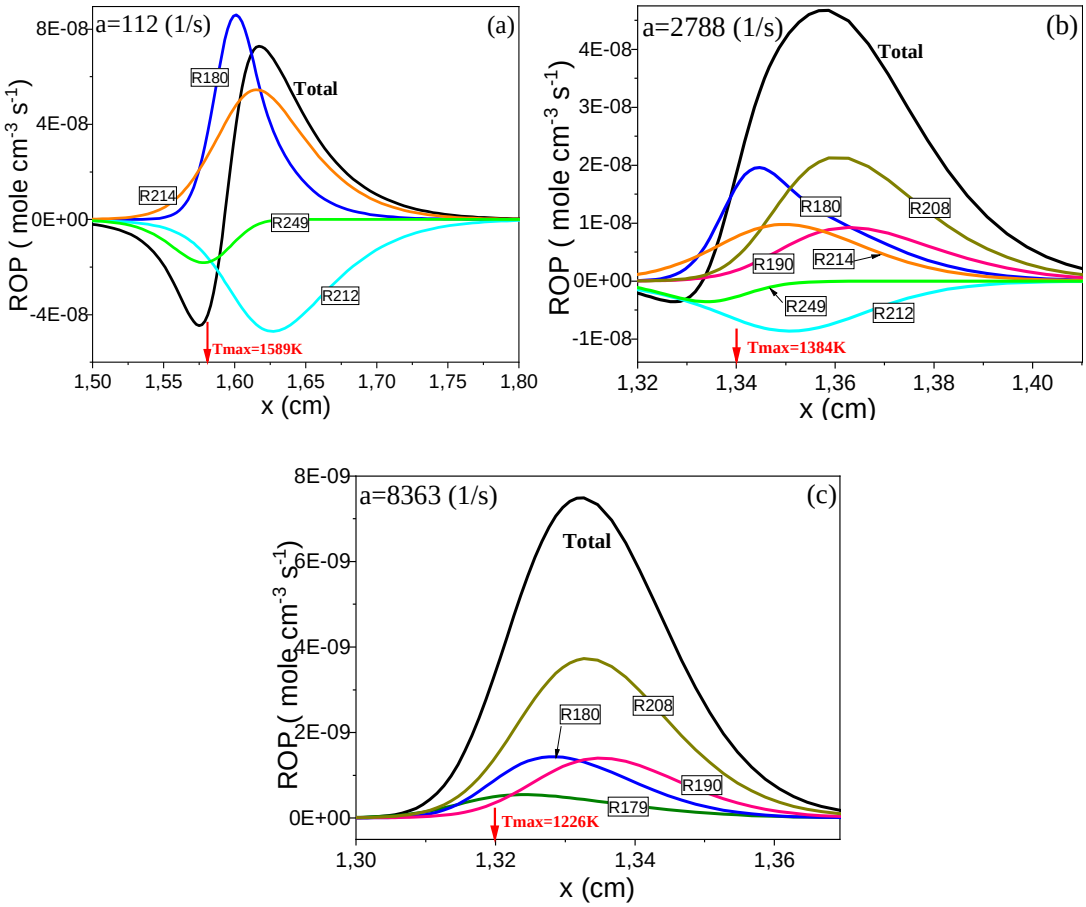

Fig.V.16: Main reactions involved with strain rate increase (a) a=112 s^{-1}, (b) a=2788 s^{-1} and (c) a=8363 s^{-1}.

V.6.3. Effect of strain rate increase on NO emission index

Emission index is computed for mean composition B25S25 and oxygen volume of 4%. The injection strain rate ranges from near "ignition" to near "extinction". From **Fig.V.17(a)** it can be observed that the emission index exhibits a maximum which corresponds to the trend of a radiative-reactive competing region [164], then it falls at a high strain rate in the nonequilibrium region. At low strain rates, the prompt route is dominant through reaction R240 which feeds R180 **Fig.V.17(b).** When strain rate increases at 311 s^{-1} (for EINO=0.39 g_{NO}/Kg_{Fuel}), prompt and NNH routes are equivalent, after that, NNH become more important. **Fig.V.17(b)** shows that the most significant reactions for the NNH mechanism are R195 and R208, the first is activated only at high strain rates. Also, reburn mechanism is maximal at low and relatively high strain rates but it is negligible at high ones, N_2O and thermal routes are insignificant. It is observed that at high strain rates, NO is only produced by NNH. Furthermore, the sum of routes and full mechanism computations are in good agreement.

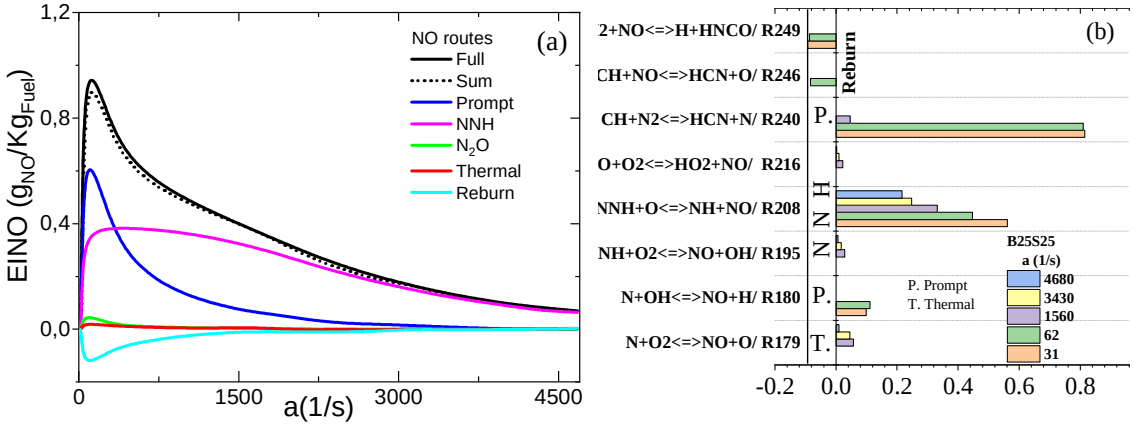

Fig.V.17: Emission NO routes (a) and sensitivity coefficients (b) in function of strain rate increase.

V.7. Oxidizer temperature effect

The oxidizer temperature is one of the critical parameters in the establishment of the MILD regime. In this section, the effect of inlet temperature is studied. Firstly, structure of the flame is shown in function of distance x from the fuel duct for injection temperature of 900K, 1200K and 1500K. Secondly, the ROP of the most important elementary reactions involved in the production of NO species is presented in the function of the distance x from the fuel duct for inlet temperatures 900K, 1200K and 1500K. Finally, emission index and sensitivity coefficients in the function of oxidizer temperature are discussed for different NO production routes. The mixture B25S25, which represents the mean composition, and strain rate of 200 s^{-1} are adopted.

V.7.1. Effect on combustion structure

Fig.V.18 highlights the effect of preheating temperature on flame structure. B25S25 composition is considered with a volume of oxygen in the oxidizer equal to 4%. In **fig.V.18 (a),** it can be seen that when oxidizer temperature increases from 900K to 1500K, the reaction zone is shifted to the oxidizer side, flame thickness is increased and the peak of temperature is increased from 1233K (located at x=1,38cm) to 1822K (located at x= 1,6cm). Maximum H_2O mole fraction (**Fig.V.18 (b)**) is increased from 0.045 to 0.058 and maximum NO mole fraction (**Fig.V.18(d)**) from 0.33 ppm to 35 ppm respectively. The OH species are produced in the second half of the reaction zone near the oxidizer (**Fig.V.18 (c)**). The maximum OH radical mole fraction values are

3.17E-4 reached at x= 1,44cm for T_{ox}=900 K and 2.48E-3 reached at x= 1,67cm for T_{ox}=1500K.

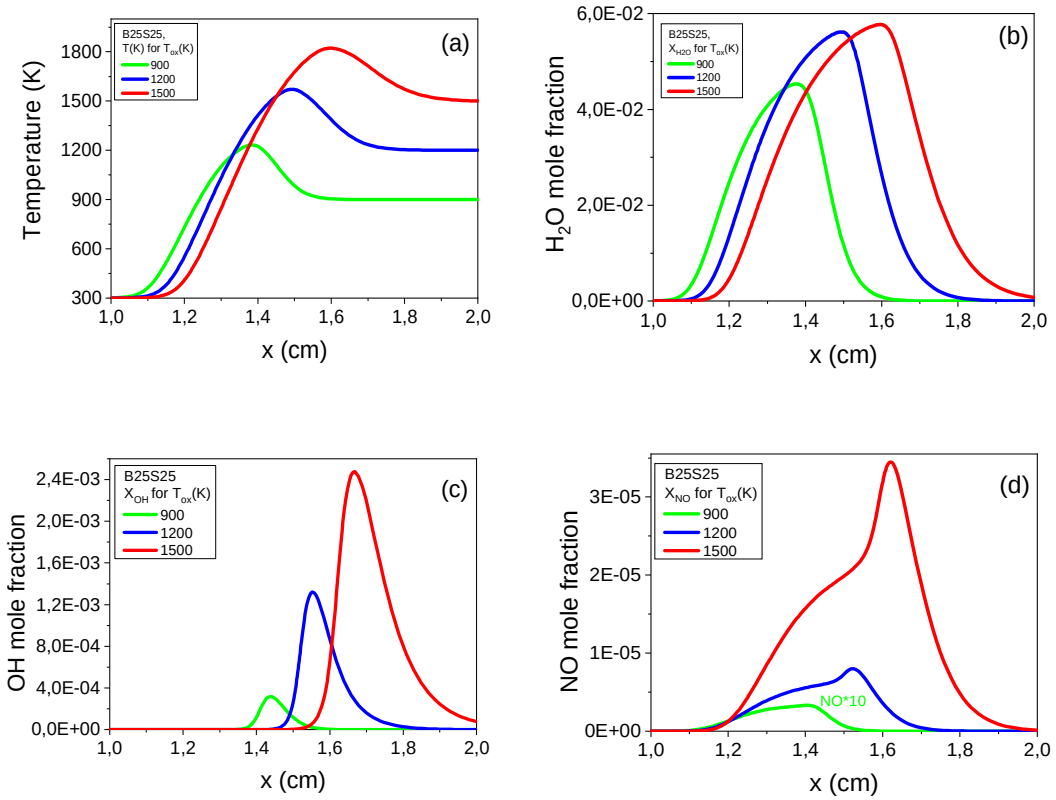

Fig.V.18: Temperature (a) and molar fraction variations of (b) H_2O, (c) OH and (d) NO species for different oxidizer temperature.

Fig.V.19 (a) displays the variations of maximum temperature and maximum NO mole fraction for the composition b25S25 at a constant strain rate of 200 s^{-1}. It can be noticed that oxidizer temperature increases the maximum flame temperature monotonically. The minimum temperature is 1233K recorded for Tox=900K, the maximum one is 1822K for Tox=1500K. The maximum NO mole fraction is substantially increased with temperature increment. For Tox=900K, maximum NO mole fraction is 0.33ppm; while oxidizer temperature increases to 1500K in oxidizer, the NO mole fraction maximum increases by 34.67ppm (to 35 ppm).

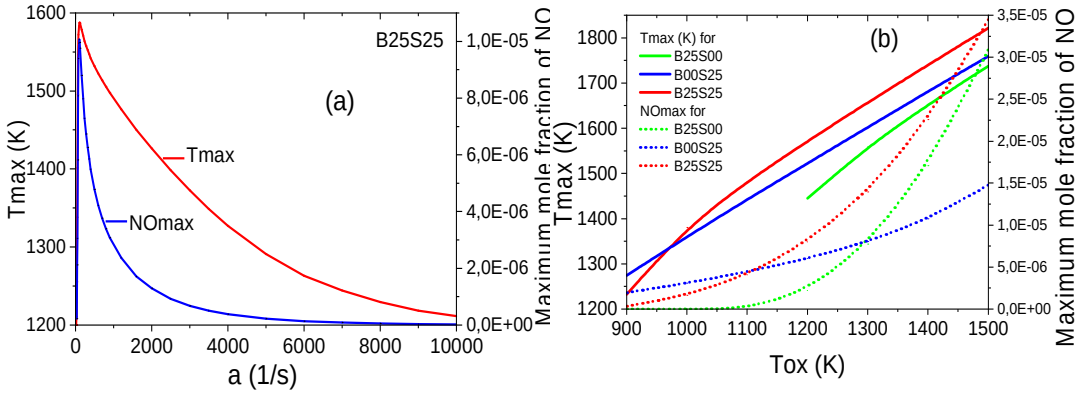

Fig.V.19: Maximum combustion temperature and NO species for different oxidizer temperature (a) B25S25 and (b) B25S00, B25S25 and B00S25

V.7.2. Oxidizer temperature effect on NO species reactions and production routes

The effect of oxidizer temperature on the ROP of the main elementary reactions involved in NO species production is shown in **Fig.V.20 (a)**, **(b)** and **(c).** Three values of inlet temperature are considered to elucidate this effect, namely; T_{ox}=900 K, T_{ox}=1200 K and T_{ox}=1500 K for mean composition B25S25. It can be observed that for low oxidizer temperature T_{ox}=900K **fig.V.20 (a)**, NO production at the flame front is globally governed by NNH route through reactions R212 and R214 followed by NO_2 route through reactions R189 (NO_2+H=NO+OH) and R186 (HO_2+NO=NO_2+OH) and finally prompt route by reactions R180 and R208. At T_{ox} = 1200 K and T_{ox} =1500K the prompt route become important by reaction R180 **fig.V.20 (b).** The second most important route is NNH through reaction R214 and R212. The reasons for the notable decrease of NO emission by the NNH route at the higher oxidizer temperatures is the reduction of the radical pool reactions: O + H_2=H + OH, H + O_2= OH + O, and 2H + M=H_2 + M that led to the decreasing H radical production and hence, decline the rates of reaction NNH=N_2 + H and NNH + (M)=N_2 + H + (M) [182]. The reduction of the NNH radical yields a decrease in the rate of reaction NNH + O=NH + NO, and NO emission drops by the NNH mechanism. The last important routes are reburn one through reactions R251 at T_{ox}=1200K and R245 at T_{ox}=1500K **Fig.V.20 (b)** and **(c).**

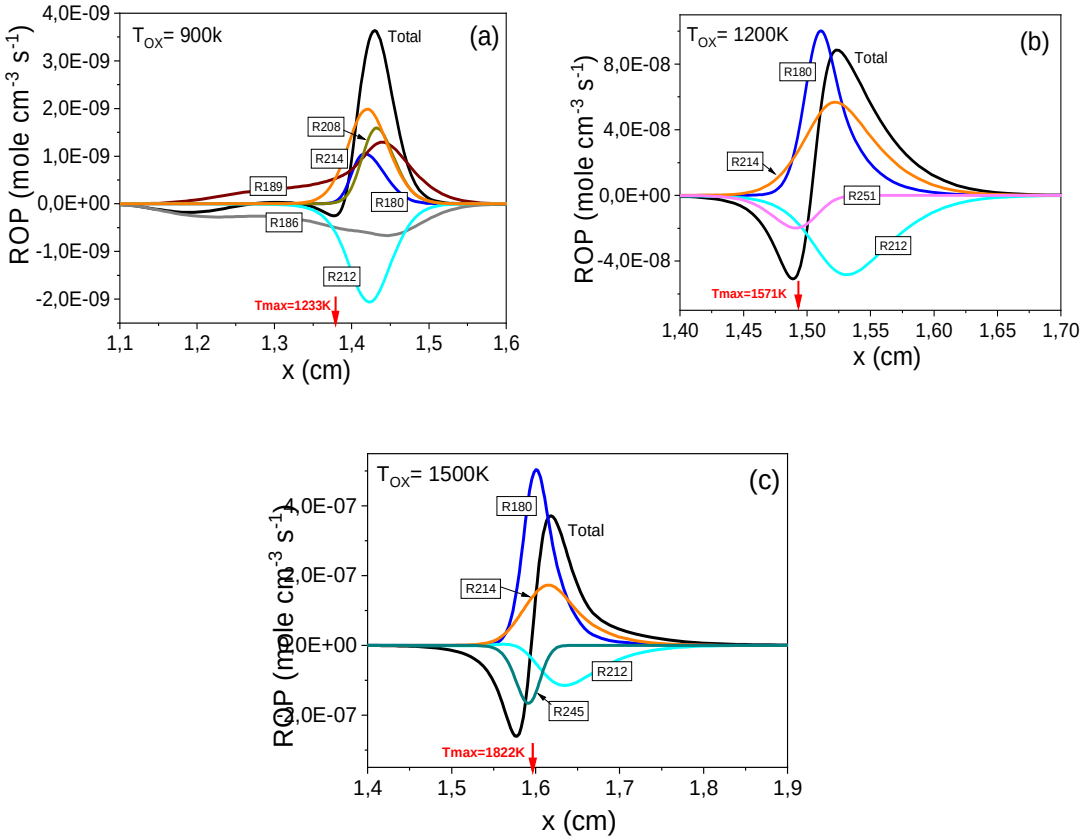

Fig.V. 20: Main reactions involved with oxidizer temperature increase (a) T_{OX}=900K, (b) T_{OX}=1200K and (c) T_{OX}=1500K.

V.7.3. Effect of oxidizer temperature increase on NO emission index

The effect of oxidizer temperature on NO production routes is analyzed by **Fig. V.21**. Mean mixture B25S25 is considered and oxidizer temperature T_{ox} is varied from 900K to 1500K. It can be observed for lower temperature T_{ox} <1075K, NO is produced mainly by NNH route and through reaction R208 **Fig.V.21(b)**. In this reaction, the produced NNH by the backward reactions of R204 and R205 reacts with the oxygen radicals, which results in the production of NO. The second most important route, in this case, is prompt one by reaction R240. By increasing the preheating temperature of the oxidizer, the main routes of NO emission change significantly. At T_{ox}=1200K, prompt/thermal reaction R180 is activated and reactions R240 and R231 produce NO by the Fenimore route, the latter becomes more important than the NNH route. The last important routes are reburn one through reactions R246 and R249. At T_{ox}= 1500K, N_2O reactions R182 and R185 are activated. NO production mechanism is dominated by the prompt route through reaction R240 followed by NNH route via reaction R208. The

thermal route is insignificant. Furthermore, the sum of routes and full mechanism computations are in good agreement.

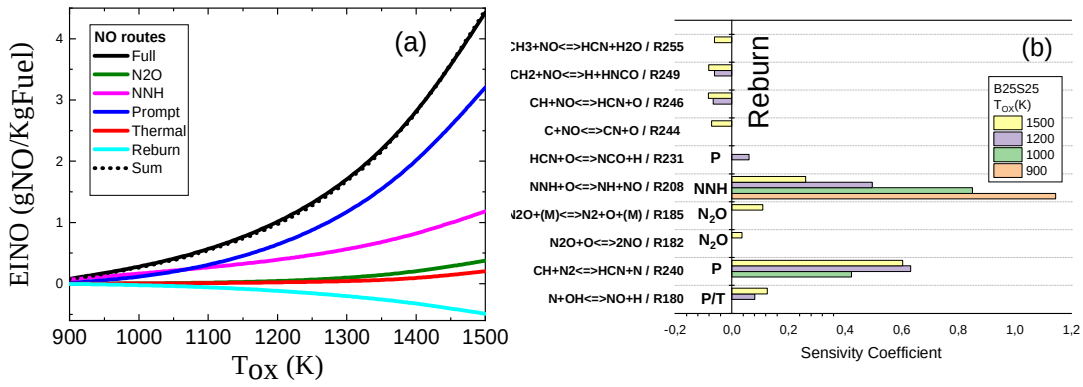

Fig.V.21: Emission NO routes (a) and sensitivity coefficients (b) in function of oxidizer temperature increase.

V.8 Pressure effect

In this section, the GRI-Mech 3.0 and the composed mechanism USC-GRI-Mech 2.11 are used to investigate numerically the effect of pressure on the flame structure and NO emissions characteristics. Firstly, structure of the flame is shown in function of distance x from fuel duct for ambient pressures of 1 atm, 5atm and 10 atm. Secondly, variation of maximum variables in function of pressure (from 1 to 10 atm) for different compositions are presented. Then, the ROP of the most important elementary reactions involved in production of NO species are presented in function of the distance x from fuel duct for pressures P=1atm, P=5atm and P=10 atm. Finally, emission index and sensitivity coefficients in function of ambient pressure are discussed for different NO production routes. The mixture B25S25, which represents the mean composition, and strain rate of 200 s^{-1} are adopted.

V.8.1. Effect on combustion structure

From **Fig.V.22,** it can be seen that the USC-GRI-Mech 2.11 mechanism gives results that are closer to those of the GRI-Mech 3.0 mechanism except the NO emission. **Fig.V.22 (a)** shows that the increase of the pressure from 1 atm to 5 atm and then to 10 atm increases the maximum temperature from 1567K (located at x=1.49cm) to 1625 K (located at x=1.38) and then to 1637K (located at x=1.35 cm) respectively, with USC-GRI-Mech 2.11. Whereas, with GRI-Mech 3.0, the maximum temperature increases from 1573K (located at x=1.49cm) to 1623 K (located at x=1.38) and then to 1631K

(located at x=1.35 cm) respectively. When pressure increases, thickness of reaction zone decreases and temperature profiles is shifted to the fuel side. The pressure augmentation produces the increase of the Damköhler number, it inhibits non-equilibrium effects and enhances recombination reactions [163, 183]. This reverses all phenomena seen when axial velocity is increased excepting the reaction zone thickness which is reduced by pressure increase. As observed before, the width of the combustion region is proportional to half power of diffusivity divided by strain rate ($\delta \propto (D/a)^{1/2}$). In addition, diffusivity is inversely proportional to ambient pressure ($D \propto P^{-1}$), this means that under a constant strain rate, increasing ambient pressure reduces reaction zone thickness.

The H_2O and NO mole fraction are shown by Figs. **V.22 (b)** and **(d)** respectively; these species exhibit the same behavior as temperature. They are produced on the whole reaction zone and they are shifted to fuel side with ambient pressure augmentation. Quantitatively, when pressure increases from 1 atm to 5 atm and then to 10 atm, the maximum H_2O mole fraction is augmented from 0.0559 to 0.0564 and then to 0.0565 respectively with USC-GRI-Mech 2.11; whereas with GRI-Mech 3.0, the maximum H_2O mole fraction is augmented from 0.0559 to 0.0561 and then to 0.056 respectively. The **fig. V22 (d)** indicates that the maximum NO species decrease with increasing pressure. However, it shows that the GRI-Mech 3.0 mechanism gives a higher prediction in NO formation (13ppm at P=1atm, 11ppm at P= 5atm and 8ppm at P=10atm) compared to USC-GRI-Mech 2.11 (8ppm at P=1atm, 7ppm at P= 5atm and 6ppm at P=10atm).

The OH species which indicates strength of combustion reaction is presented by **Fig.V.22 (c)**; it is produced in the second half of reaction zone near oxidizer and it is reduced by pressure. When pressure rises from 1 atm to 5 atm and then to 10 atm, the maximum OH mole fraction decreases from 1.2E-3 to 7.9E-4 and then to 5.8E-4 respectively, with USC-GRI-Mech 2.11; whereas with GRI-Mech 3.0, the maximum OH mole fraction is augmented from 1.15E-3 to 6.7E-4 and then to 4.4E-4 respectively.

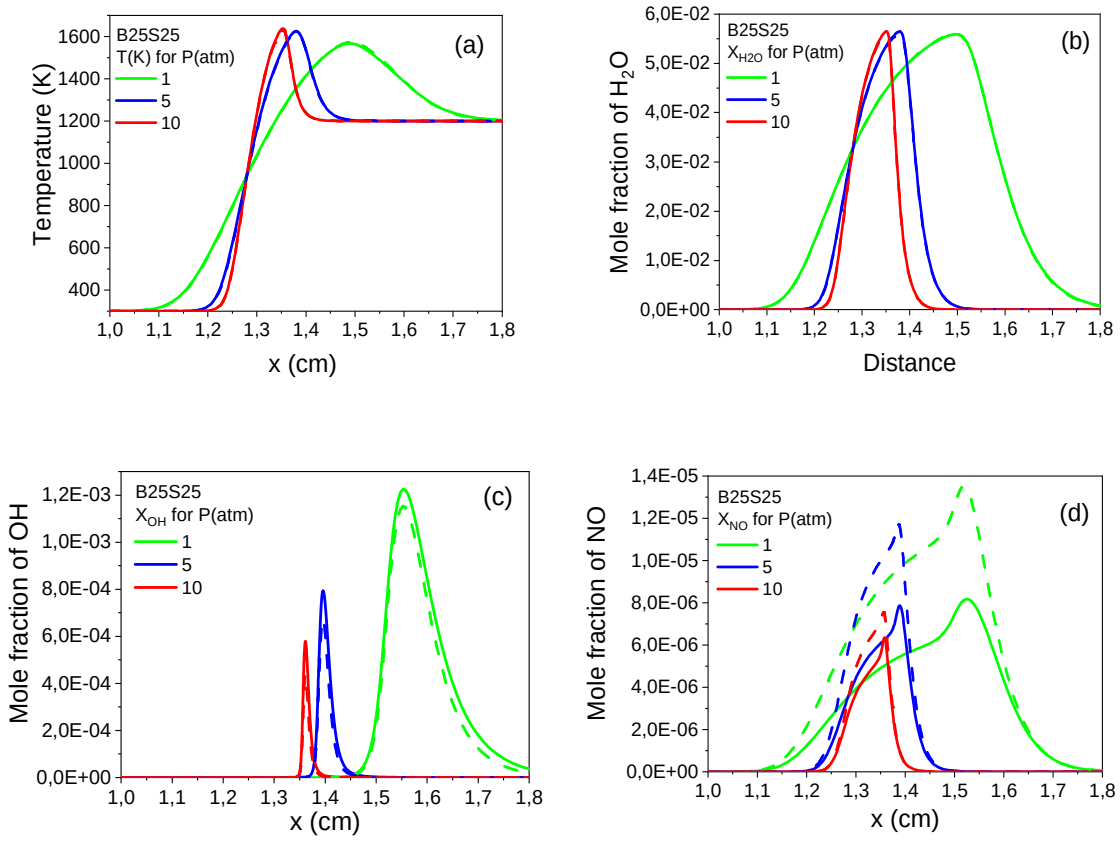

Fig.V.22: Temperature (a) and molar fraction variations of (b) H_2O, (c) OH and (d) NO species for different pressure for the two mechanisms USC-GRI-Mech 2.11 (solid line) and GRI-Mech 3.0 (dashed line).

The pressure effect on maximums temperature and NO emissions for different compositions (B00S25, B25S25, B25S00) for the two mechanisms USC-GRI-Mech 2.11 and GRI-Mech 3.0 is shown by **Fig.V.23** and **Fig. V.24**. It can be noticed in **Fig.V.23** and **Fig.V.24 (a)** that the maximum temperature increases monotonically with pressure for all composition except the composition B25S00. With USC-GRI-Mech 2.11, the maximum temperature decreases in the pressure range 5–10atm, whereas with GRI-Mech 3.0 the increase in pressure from 2 atm to 3 atm decreases the maximum temperature. Indeed, when methane volume increases in the mixture, the maximum temperature of the flame increases but the differences between their maximums $\Delta T_{B\alpha S25}$ are reduced with pressure increase. However, when hydrogen is added in the mixture the maximum temperature increases and the differences between their maximums $\Delta T_{B25S\beta}$ increase too for the two mechanisms.

Figure.V.24 (b) shows distribution of maximum NO mole fraction in function of pressure for different compositions. With the USC-GRI-Mech 2.11 and for B25S00 and B25S25 compositions, it is noticed that in the interval 1-2 atm the increase in pressure increases the NO. In the interval 2-10 atm a reduction in NO production is observed. For B00S25 composition, With increasing pressure, the maximum NO mole fraction decreases. The best composition that reduces NO species is B25S00 and the worst one is B00S25. The minimum value of NO mole fraction is 0.4 ppm recorded at P=8 atm for B25S00 and maximum one is 11 ppm recorded at P=1 atm for B00S25. It should be noticed that for considered properties variations are steeper when pressure varies between 1 atm and 5 atm [184]. With GRI-Mech 3.0, it is noticed that in the interval 1-2atm the increase in pressure increases the NO emission for the two composition B00S25 and B25S25. The most sensitive composition to pressure in terms of NO production is B25S25, the maximum value is 14ppm recorded at P = 2atm . Whereas, the least sensitive one is B25S00 which contains minimum of hydrogen volume. In the interval 2-10atm a reduction in NO production is observed with maximum under 15 ppm for all compositions. For B25S00, it can be noticed that from P=3atm NO is null.

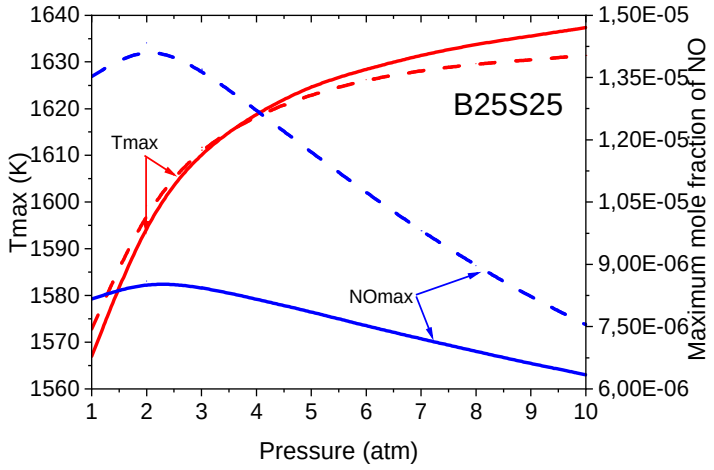

Fig.V.23: Maximum combustion temperature and NO species for different pressure for B25S25 mixture for the two mechanisms USC-GRI-Mech 2.11 (solid line) and GRI-Mech 3.0 (dashed line).

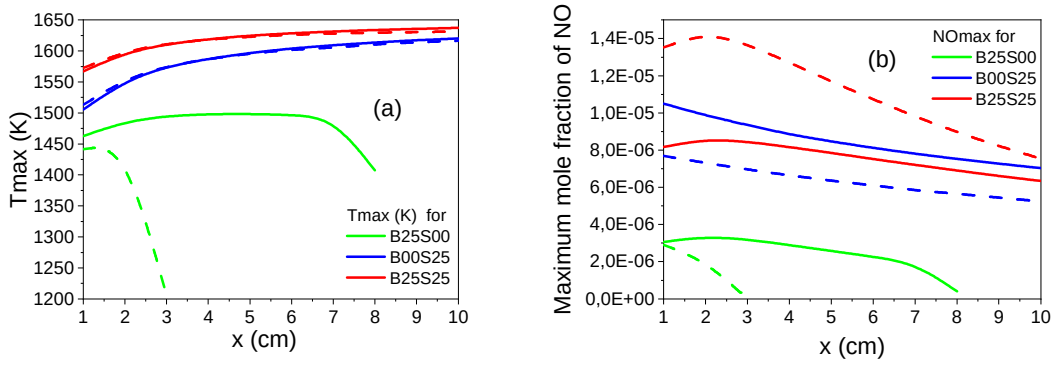

Fig.V.24: Maximum combustion temperature (a) and NO species (b) for different pressure for the two mechanisms USC-GRI-Mech 2.11 (solid line) and GRI-Mech 3.0 (dashed line).

V.8.2. Ambient pressure effect on NO species reactions and production routes

The effect of pressure on elementary reactions involved in NO production is shown by **Fig.V.25** and **Fig.V.26** for the two mechanisms USC-GRI-Mech 2.11 and GRI-Mech 3.0 respectively. Three values of pressure: 1atm, 5atm and 10atm were considered for the composition B25S25 at a strain rate a = 200 s^{-1}. At flame front, with USC-GRI-Mech 2.11, the **fig.V.25 (a)** shows that reactions R214 and R180, which belongs to the NNH and prompt pathways respectively are the most important in NO production. The second most important route is reburn one through reaction R249. From **fig.V.25(b)** and **(c),** the most important route is NNH one via reactions R214 and R212 followed by prompt route through reactions R180 and finally NO_2 route through reactions R189 (NO_2+H=NO+OH) and R187 (NO+O+M=NO_2+M).

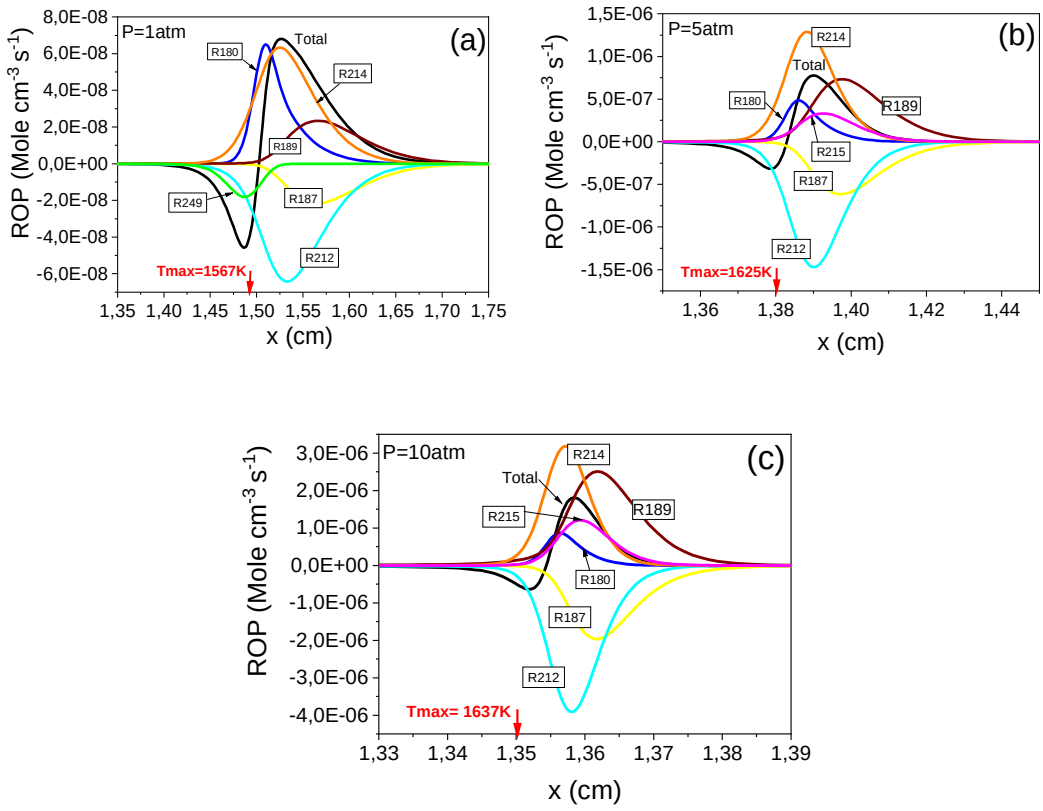

Fig. V.25: Main reactions involved with ambient pressure increase for USC-GRI-Mech 2.11 mechanism (a) P=1atm, (b) P=5atm, (c) P=10atm

The **Figs.V.26 (a), (b),** and **(c)** show principal reactions involved in NO species production for mean composition B25S25, With GRI-Mech 3.0. For P=1atm at flame front **Fig.V.26 (a)** shows that NO species production is principally due to the reactions R214 that belong to the NNH route, followed by prompt route by reaction R180. The last important route is reburn one through reactions R249 and R245. For P=5atm and P=10atm NO species is produced principally by NNH mechanism via reactions R214 and R212. The second most important route is NO_2 through reactions R189 (NO_2+H=NO+OH), R186 (HO_2+NO=NO_2+OH) and R187 (NO+O+M=NO_2+M) and finally prompt route via reaction R180.

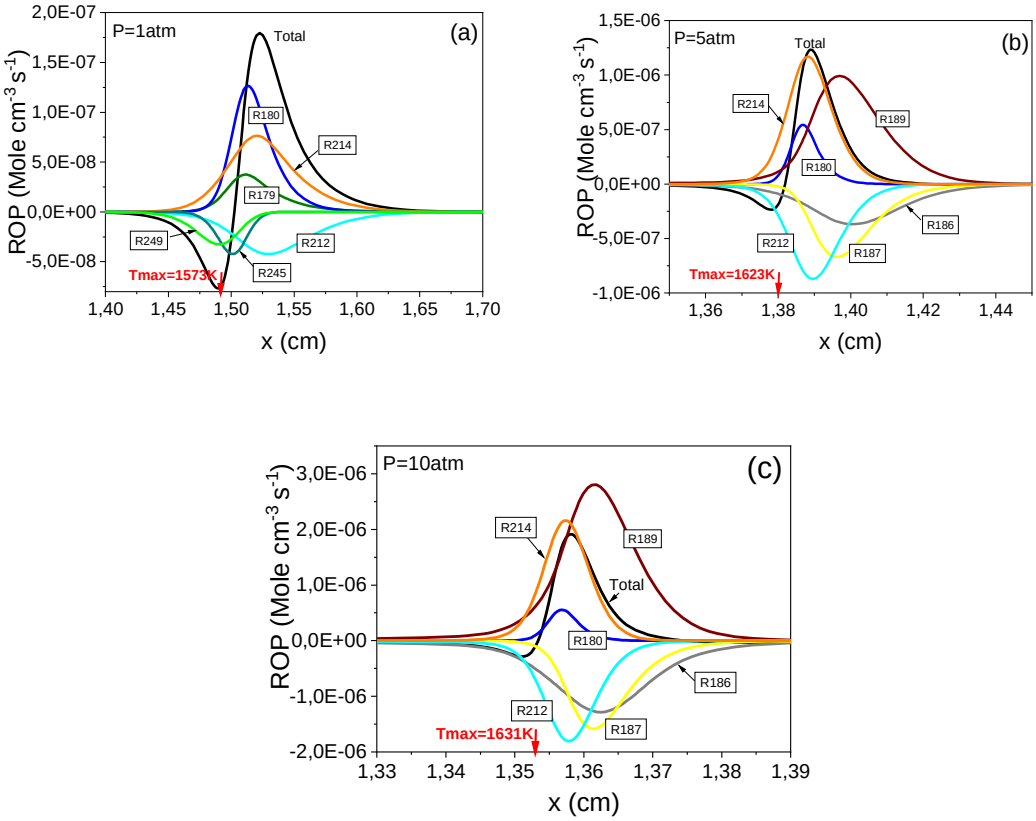

Fig. V.26: Main reactions involved with ambient pressure increase for GRI-Mech 3.0 mechanism (a) P=1atm, (b) P=5atm, (c) P=10atm.

V.8.3. Effect of ambient pressure increase on NO emission index

EINO profiles and sensitivity analysis and for different pressure are indicated in **Fig.V.27 and Fig.V.28** for the two mechanisms USC-GRI-Mech 2.11 and GRI-Mech 3.0 respectively. From **Fig.V.27**, it can be observed that at P=1atm, NNH route dominates NO production through reaction R208. The second most important route in this case is prompt one via R180 and R240, then reburn mechanism through reactions R249 and R246. At P= 3atm, thermal route is activated via reaction R179. However, with pressure augmentation, the contribution to NO production from N_2O-intermediate route exhibits a non-monotonic behavior. The production reaches a maximum at nearly P=8atm and begins declining. On the other hand, increasing pressure result in a decrease in the contribution of NNH and prompt mechanisms but a slight rise in the share of thermal and reburn mechanisms.

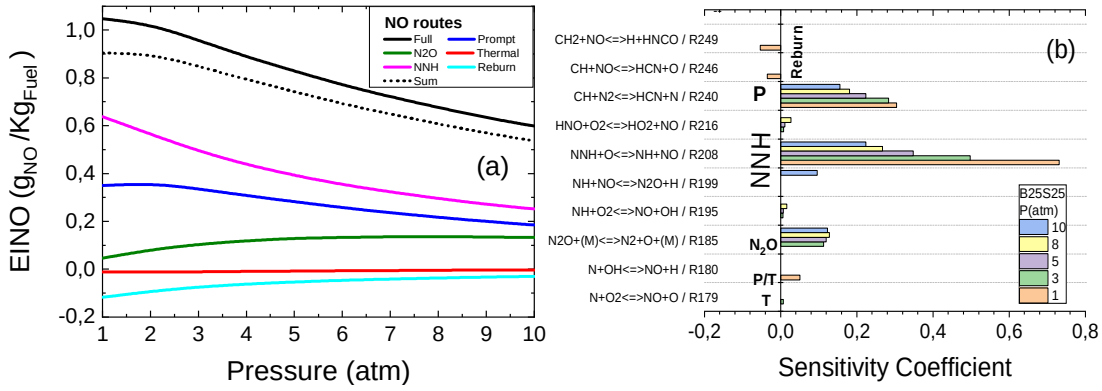

Fig.V.27: Emission NO routes (a) and sensitivity coefficients (b) in function of ambient pressure increase for USC-GRI-Mech 2.11 mechanism.

From **Fig.V.28**, the total EINO shows non-monotonic behavior with pressure. The prompt route is the most predominant NO formation mechanism via reaction R240, its contribution increases as a function of pressure until P=2atm. However, the contribution of the NNH pathway decreases monotonically with increasing pressure through reaction R208. **Fig.V.28(b)** shows that the NO_2 route is activated via reaction R186 and becomes important with pressure increase. Although the contribution of reburn pathway slightly increases with the increase of pressure, it is not significant. The NO emission via the thermal and the N_2O-intermediate pathways is negligible in the whole range of pressure.

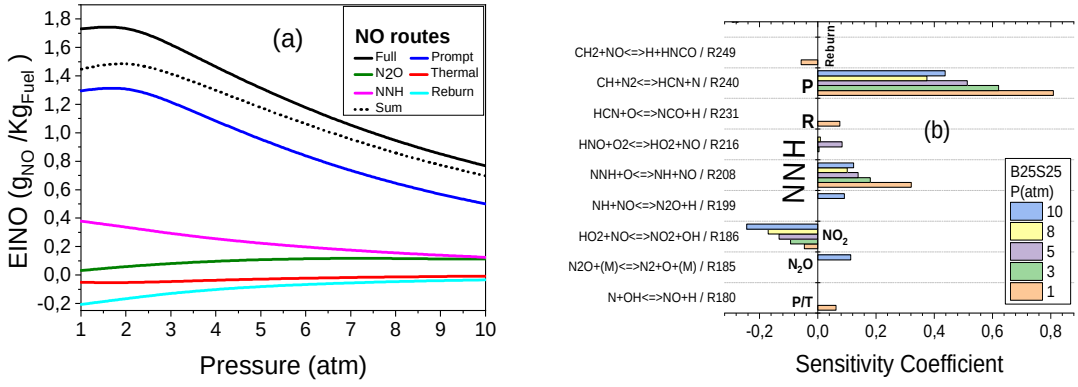

Fig.V.28: Emission NO routes (a) and sensitivity coefficients (b) in function of ambient pressure increase for GRI-Mech 3.0 mechanism.

Chapter VI

Conclusion

The present study is designed to prevent pollution and to improve emission control technologies, it aims to reduce combustion pollutants especially CO_2 and NOx. The CO_2 can be avoided by using a biofuel that is neutral in terms of CO_2 emission. Whereas, the NOx emissions can be reduced by decreasing the combustion temperature. This is can be granted by the flameless combustion regime.

The flameless combustion in MILD regime occurs when the reactants are locally preheated at a temperature higher than the mixture's self-ignition temperature. Moreover, it is characterized by low temperature increase in the combustion process.

The lower temperatures reduces the formation of nitrogen oxides through the thermal mechanism, which is the major formation route in most conventional combustion systems. NOx emissions in the MILD regime are mostly the result of alternative paths, such as the prompt NO, and/or N_2O intermediate. Furthermore, for hydrogen-enriched fuels, it is also necessary to consider the NNH route.

This study investigated numerically the influence of several operating conditions on the combustion structure and NO emissions characteristics of a biogas-syngas in counter-flow diffusion flame configuration. Several biogas-syngas are considered with a very wide range of injection velocities of reactant from ignition to extinction limit and under using different: oxygen mole fractions, oxidizer preheating temperatures and different pressures ranging from 1 to 10 atm.

Conclusions that can be drawn are:

- The adiabatic flame temperature of the biogas-syngas mixture is more affected by the increase of methane in biogas than the decrease of hydrogen in syngas.
- The lower calorific value of the biogas syngas mixture is more affected by the increase of methane in biogas than by the hydrogen in syngas.
- Temperature increase level and interval are more pronounced when hydrogen is added to fuel mixture compared to methane. However, MILD regime prevails since temperature increase didn’t exceed that of fuel mixture autoignition.

- Oxygen addition to oxidizer increases drastically temperature and breaks down MILD regime even for relatively low oxygen volumes. Since the temperature increase during combustion is lower than mixture self-ignition temperature $\Delta T_{comb} < T_{autign}$. The MILD combustion regime can be sustained by keeping oxygen volume near the limits of 2%-6%. MILD combustion mode breaks at O_2 = 21% (conventional combustion). Decreasing oxygen volume in oxidizer leads to lower values of NO mole fraction. Its maximum reaches a value of 8 ppm for O_2=4%, which is very low compared to conventional mode (435 ppm).
- Strain rate or injection velocity has a decisive impact on combustion structure and in minimizing pollutants. Indeed, when the velocity increases the residence time is reduced and therefore the combustion temperature and the different emissions. One can use high strain rates for high oxygen volume to maintain MILD regime.
- The oxidizer temperature is one of the critical parameters in the establishment of the MILD regime. Increasing the inlet temperature of oxidizer leads to a rise in maximum temperature and maximum NO mole fraction. For all cases, the temperature rise by combustion does not exceed 380 K, which sustain MILD regime.
- When pressure increases, the maximum temperature increases but the chemical reactions are inhibited which reduces the different species. For B25S00 and B25S25 compositions, the maximum NO mole fraction is increased by the increase of the pressure in the interval P = 1-3atm. Then it is reduced between P =3-10 atm. For B00S25 composition, with increasing pressure, the maximum NO mole fraction decreases. The best composition that reduces NO species is B25S00 and the worst one is B00S25 which is the least reactive and the least polluting too.
- Low methane volumes enhance NNH production route whereas prompt one is favored for high methane contents of fuel mixture.
- Low and relatively high hydrogen volumes in fuel mixture enhances prompt route however at high hydrogen volumes, prompt route dominates NO production.
- At high oxygen contents, NO production routes are governed by thermal mechanism despite contents of methane or hydrogen.

- For low and mean values of strain rate, prompt and NNH routes compete in NO formation, whereas, for high strain rate value only NNH route prevails.
- For low oxidizer temperature, the main source of NO formation is the NNH path followed by NO_2-intermediate and finally prompt route. By increasing the preheating temperature of oxidizer, the prompt route become important, whereas the NO emission by the NNH route is decreased. The last important routes are reburn one.
- For low pressure, the analysis of NO mechanism indicate that NNH route is the most prevalent mechanism for NO production The second most important route in this case is prompt one, then reburn mechanism. At P= 3atm, thermal route is activated via reaction R179. However, with pressure augmentation, the contribution to NO production from N_2O-intermediate route exhibits a non-monotonic behavior. The production reaches a maximum at nearly P=8atm and begins declining. On the other hand, increasing pressure result in a decrease in the contribution of NNH and prompt mechanisms but a slight rise in the share of thermal and reburn mechanisms.

References

[1] BP's 2020 Statistical Review of World Energy.

[2] IEA, World energy demand growth rate, 2011-2019, IEA, Paris https://www.iea.org/data-and-statistics/charts/world-energy-demand-growth-rate-2011-2019.

[3] IEA, Share of total primary energy demand by fuel, 2010-2019, IEA, Paris https://www.iea.org/data-and-statistics/charts/share-of-total-primary-energy-demand-by-fuel-2010-2019.

[4] IEA, Energy-related CO2 emissions, 1990-2019, IEA, Paris https://www.iea.org/data-and-statistics/charts/energy-related-co2-emissions-1990-2019-2.

[5] SOLAR

[6] Jalonsom, Functional schematic of the structure of a wind turbine, (2016), available from: https://commons.wikimedia.org/wiki/File:Wind_turbine_schematic.svg.

[7] https://archive.epa.gov/climatechange/kids/solutions/technologies/geothermal.html.

[8] K. Bonsor, How Hydropower Plants Work, (2001), available from: https://science.howstuffworks.com/environmental/energy/hydropower-plant.htm

[9] https://1800312ae2014.weebly.com/engineer.html.

[10] http://refuelingthefuture.yolasite.com/first-generation-biofuels.php.

[11] http://www.fabbiogas.eu/en/home/about-biogas/

[12] B. de la Farge, Le biogaz : procédés de fermentation méthanique, Elsevier Masson, (1995).

[13] A.M. Buswell and H.F. Mueller, Mechanism of fermentation, Industrial and Engineering Chemistry, 44(3) (1952) 550-552. https://doi.org/10.1021/ie50507a033.

[14] M. Beaudet, D.L, Les biogaz et les sites d'enfouissement, (2003), Available from: http://mendeleiev.cyberscol.qc.ca/chimisterie/2002-2003/MBeaudet.html.

[15] Biogaz : caractéristiques, incitations et ressources, Energie Plus, (1998) 213.

[16] L. Sasse, Biogas Plants, Deutsches Zentrum für Entwicklungstechnologien-GATE, Deutsche Gesellshaft für Technische, Zusammenarbeit (GTZ) GmbH, (1988).

[17] G. Foley and G. Barnard, Biomass Gasification in Developing Countries, (1985), Earthscan, London, UK.

[18] J.A. Miller and C.T. Bowman, Mechanism and modeling of nitrogen chemistry in combustion, Progress in Energy and Combustion Science, 15(4) (1989) 287-338. doi:10.1016/0360-1285(89)90017-8.

[19] S.E. Hosseini and M.A. Wahid, Feasibility study of biogas production and utilization as a source of renewable energy in Malaysia, Renew Sustain Energy Reviews, 19 (2013) 454–62. doi:10.1016/j.rser.2012.11.008.

[20] S.E. Hosseini and M.A. Wahid, Biogas utilization: experimental investigation on biogas flameless combustion in lab-scale furnace, Energy Conversion and Management, 74 (2013) 426– 432. doi:10.1016/j.enconman.2013.06.026.

[21] S. Jahangirian and A. Engeda, Biogas combustion and chemical kinetics for gas turbine applications, Volume 3: Combustion Science and Engineering, (2008) 13–22. doi:10.1115/imece2008-66667.

[22] N Hinton. and R. Stone, Laminar burning velocity measurements of methane and carbon dioxide mixtures (biogas) over wide ranging temperatures and pressures, Fuel, 116 (2014) 743-50. doi:10.1016/j.fuel.2013.08.069.

[23] T. Patterson, S. Esteves, R. Dinsdale, and A. Guwy, An evaluation of the policy and techno-economic factors affecting the potential for biogas upgrading for transport fuel use in the UK, Energy Policy, 39(3) (2011) 1806–1816. doi:10.1016/j.enpol.2011.01.017.

[24] S.E. Hosseini, M.A. Wahid, and A. A. A. Abuelnuor, Biogas flameless combustion: a review, Applied Mechanics and Materials, 388 (2013) 273–279. doi:10.4028/www.scientific.net/amm.388.273.

[25] S. Chen and C. Zheng, Counterflow diffusion flame of hydrogen-enriched biogas under MILD oxy-fuel condition, International Journal of Hydrogen Energy, 36(23) (2011) 15403-15413. doi:10.1016/j.ijhydene.2011.09.002.

[26] A.A.V. Perpignan, A. Gangoli Rao and D.J.E.M. Roekaerts, Flameless combustion and its potential towards gas turbines, Progress in Energy and Combustion Science, 69 (2018) 28-62. doi: 10.1016/j.pecs.2018.06.002.

[27] H. Tsuji, A. Gupta, T. Hasegawa, M. Katsuki, K. Kishimoto and M. Morita, High temperature air combustion, from energy conservation to pollution reduction, (2003), CRC Press, Boca Raton, Florida.

[28] S.E. Hosseini, M.A. Wahid and S. Salehirad, Environmental Protection and Fuel Consumption Reduction by Flameless Combustion Technology: A Review. Applied Mechanics and Materials, 388 (2013) 292–297. doi: 10.4028/www.scientific.net/amm.388.292.

[29] B.B. Dally, E. Riesmeier and N. Peters, Effect of fuel mixture on moderate and intense low oxygen dilution combustion, Combustion and Flame, 137(4) (2004) 418-431. doi: 10.1016/j.combustflame.2004.02.011.

[30] F.C. Christo and B.B. Dally, Modeling turbulent reacting jets issuing into a hot and diluted coflow, Combustion and Flame, 142(1–2) (2005) 117-129. doi: 10.1016/j.combustflame.2005.03.002.

[31] J.A. Wunning and J.G. Wunning, Flameless oxidation to reduce thermal NO-formation, Progress in Energy and Combustion Science, 23(1) (1997) 81-94. doi: 10.1016/S0360- 1285(97)00006-3.

[32] A.K. Gupta, S. Bolz and T. Hasegawa, Effect of Air Preheat Temperature and Oxygen Concentration on Flame Structure and Emission. Journal of Energy Resources Technology, 121(3) (1999) 209–216. doi: 10.1115/1.2795984.

[33] J. Wunning, Flammlose Oxidation Von Brennstoff Mit Hochvorgewarmter Luft, Chemie Ingenieur Technik, 63(12) (1991) 1243-1245. doi: 10.1002/cite.330631219.

[34] J.G. Wünning, Flammlose oxidation von brennstoff, (1996) Aachen: Mainz, Wiss-Verl.

[35] M.De. Joannon, A. Cavaliere, R. Donnarumma and R. Ragucci, Dependence of autoignition delay on oxygen concentration in mild combustion of high molecular weight paraffin, Proceedings of the Combustion Institute, 29(1) (2002) 139-46. doi: 10.1016/S1540-7489(02)80144-4.

[36] M. Torresi, S.M. Camporeale, B. Fortunato, S. Ranaldo, M. Mincuzzi, A. Saponaro, Diluted combustion in a arodynamically staged swirled burner fueled by diesel oil, Process and Technology for Sustainable Energy, (2010) 1-8.

[37] A. Cavalierea and M.De. Joannon, Mild Combustion, Progress in Energy and Combustion Science, 30(4) (2004) 329-366. doi: 10.1016/j.pecs.2004.02.003.

[38] F. Aguilé, Overview of the Gaz the France R&D activities on flameless oxidation applied to high temperature processes, 23rd World Gas Conference, (2006), Amsterdam.

[39] A. Touzet, P.J. Lhomme, A Quinqueneau, New Efficient technologies with very low NOx emissions available for the industry: two recent examples in the French metallurgy field, Proc. of the 4th International Symposium on HTACG (High Temperature Air Combustion and Gassification), (2001), Rome.

[40] S.E. Hosseini, G. Bagheri and M.A. Wahid, Numerical investigation of biogas flameless combustion, Energ. Convers. Manage, 81 (2014) 41-50. doi:10.1016/j.enconman.2014.02.006.

[41] Y. Liu, S. Chen, B. Yang, K. Liu and C. Zheng, First and second thermodynamic-law comparison of biogas MILD oxy-fuel combustion moderated by CO2 or H2O, Energy Conversion and Management, 106 (2015) 625-634. doi: 10.1016/j.enconman.2015.09.076.

[42] M. Mehregan and M. Moghiman, A numerical investigation of preheated diluted oxidizer influence on NOx emission of biogas flameless combustion using Taguchi approach, Fuel, 227 (2018) 1-5. doi: 10.1016/j.fuel.2018.04.049.

[43] M. Sahin, Combustion characteristics of various biogas flames under reduced oxygen concentration conditions, Energy Sources, Part A: Recovery, Utilization, and Environmental Effects, 41(19) (2019) 2415-2427. doi: 10.1080/15567036.2019.1601796.

[44] A. Mardani and S. Tabejamaat, Effect of hydrogen on hydrogen methane turbulent non-premixed flame under MILD condition, Int J Hydrog Energy, 35(20) (2010) 11324-31. doi:10.1016/j.ijhydene.2010.06.064.

[45] H.S. Zhen , C.W. Leung and C.S. Cheung, Effects of hydrogen addition on the characteristics of a biogas diffusion flame, Int J Hydrogen Energy, 38(16) (2013) 6874-81. doi:10.1016/j.ijhydene.2013.02.046.

[46] J. Li, H. Huang, Y. Huhetaoli, Y. Osaka, Y. Bai, N. Kobayashi and Y. Chen, Combustion and Heat Release Characteristics of Biogas under Hydrogen- and Oxygen-Enriched Condition, Energies, 10(8) (2017) 1200. doi:10.3390/en10081200.

[47] A. Mameri, F. Tabet, A. Hadef, MILD combustion of hydrogenated biogas under several operating conditions in an opposed jet configuration, International Journal of Hydrogen Energy, 43(6) (2018) 3566-3576. doi:10.1016/j.ijhydene.2017.04.273.

[48] M.C. Lee , S.B. Seo, J.H. Chung, S.M. Kim, Y.J. Joo, D.H. Ahn, Gas turbine combustion performance test of hydrogen and carbon monoxide synthetic gas, Fuel, 89(7) (2010) 1485–1491. doi:10.1016/j.fuel.2009.10.004.

[49] H. C. Lee, A. A. Mohamad and L. Y. Jiang, Comprehensive Comparison of Chemical Kinetics Mechanisms for Syngas/Biogas Mixtures, Energy & Fuels, 29(9) (2015) 6126-6145. doi:10.1021/acs.energyfuels.5b01136.

[50] S. Som, A. Ramırez, A. Hagerdorn, J. Saveliev, S. Aggarwal, A numerical and experimental study of counterflow syngas flames at different pressures, Fuel, 87(3) (2008) 319–334. doi:10.1016/j.fuel.2007.05.023.

[51] K. Safer, F. Tabet, A. Ouadha, M. Safer and I. Gokalp, Simulation of a syngas counter-flow diffusion flame structure and NO emissions in the pressure range 1-10 atm, Fuel Process Technol, 123 (2014) 149-58. doi:10.1016/j.fuproc.2013.10.019.

[52] M. Safer, F. Tabet, A. Ouadha and K. Safer, A numerical investigation of structure and emissions of oxygen-enriched syngas flame in counter-flow configuration, Int J Hydrogen Energy, 40 (6) (2015) 2890-8. doi:10.1016/j.ijhydene.2014.12.117.

[53] M. Huang, W. Shao, Y. Xiong, Y. Liu, Z. Zhang, F. Lei and Y. Xiao, Effect of fuel injection velocity on MILD combustion of syngas in axially-staged combustor, Appl Therm Eng, 66(1-2) (2014) 485-92. doi:10.1016/j.applthermaleng.2014.02.033.

[54] M. Huang, Z. Zhang, W. Shao, Y. Xiong, F. Lei and Y. Xiao, MILD combustion for hydrogen and syngas at elevated pressures, J Therm Sci, 23(1) (2014) 96-102. doi:10.1007/s11630-014-0682-x.

[55] M. Huang, Z. Zhang, W. Shao, Y. Xiong, Y. Liu and F. Lei and Y. Xiao, Effect of air preheat temperature on the MILD combustion of syngas, Energy Convers Manag, 86 (2014) 356-64. doi:10.1016/j.enconman.2014.05.038.

[56] A. Mardani and H. Karimi Motaalegh Mahalegi, Hydrogen enrichment of methane and syngas for MILD combustion, International journal of hydrogen energy, 44(18) (2019) 9423-37. doi:10.1016/j.ijhydene.2019.02.072.

[57] C. Galletti, A. Parente, M. Derudi, R. Rota and L. Tognotti, Numerical and experimental analysis of NO emissions from a lab-scale burner fed with hydrogen-enriched fuels and operating in MILD combustion, Int J Hydrogen Energy, 34(19) (2009) 8339-51. doi:10.1016/j.ijhydene.2009.07.095.

[58] A.V. Sepman, S.E. Abtahizadeh, A.V. Mokhov, J.A. van Oijen, H.B. Levinsky, and L.P.H. de Goey, Numerical and experimental studies of the no formation in laminar coflow diffusion flames on their transition to mild combustion regime. Combustion and Flame, 160(8) (2013) 1364–1372. doi:10.1016/j.combustflame.2013.02.027.

[59] P. Li, F. Wang, J. Mi, B.B. Dally, Z. Mei, J. Zhang and A. Parente, Mechanisms of no formation in mild combustion of CH4/H2 fuel blends, Int. J. Hyd. Energy, 39(33) (2014) 19187–19203. doi: 10.1016/j.ijhydene.2014.09.050.

[60] F. Wang, P. Li, J. Zhang, Z. Mei, J. Mi and J. Wang, Routes of formation and destruction of nitrogen oxides in CH4/H2 jet flames in a hot coflow, International Journal of Hydrogen Energy, 40(18) (2015) 6228-6242. doi:10.1016/j.ijhydene.2015.03.047.

[61] Z. Shu, C. Dai, P. Li and J. Mi, Nitric oxide of MILD combustion of a methane jet flame in hot oxidizer coflow: Its formations and emissions under H_2O, CO_2 and N_2 dilutions, Fuel, 234 (2018) 567-580. doi: 10.1016/j.fuel.2018.07.057.

[62] K.P. Cheong, P. Li, F. Wang and J. Mi, Emissions of NO and CO from counterflow combustion of CH_4 under MILD and oxyfuel conditions, Energy, 124 (2017) 652-664. doi: 10.1016/j.energy.2017.02.083.

[63] G. Ali, T. Zhang, W. Wu and Y. Zhou, Effect of hydrogen addition on NOx formation mechanism and pathways in MILD combustion of H2-rich low calorific value fuels, International Journal of Hydrogen Energy, 45(15) (2020) 9200-9210. doi: 10.1016/j.ijhydene.2020.01.027.

[64] A.J. Haagen-Smit, Chemistry and physiology of Los Angeles smog, Industrial & Engineering Chemistry, 44(6) (1952) 1342-6. doi:10.1021/ie50510a045.

[65] P.J. Lea, Oxides of Nitrogen and Ozone: Can Our Plants Survive? New Phytologist, 139(1) (1998) 25-26. doi:10.1046/j.1469-8137.1998.00169.x.

[66] R. Lckerath, W. Meier and M. Aigner, FLOX [sup ®] Combustion at High Pressure With Different Fuel Compositions, Journal of Engineering for Gas Turbines and Power, 130(1) (2008) 011505. doi:10.1115/1.2749280.

[67] Encyclopédie des gaz, Air liquide/Division scientifique, 1011-1017 and 1065-1072, ISBN 0-444-41492-4 – 1976.

[68] L.D. MacKenzie and D.A. Cornwell, Introduction to Environmental Engineering, McGraw-Hill International Editions, (1991).

[69] Solar and ultraviolet radiation, IARC (International Agency for Research on Cancer) monographs on the evaluation of carcinogenic risks to humans, Vol. 55 (1992), Lyon, France.

[70] S.H. Russell and J.E. Roberts, Oxides of nitrogen: Formation and control in resource recovery facilities, Journal of Energy Resources Technology, 107(2) (1985) 284. doi:10.1115/1.3231191.

[71] S. Chapman, A theory of upper atmospheric ozone, Mem. Roy. Meteor. Soc. 3, (1930) 103–125.

[72] J.T. Houghton, G.J. Jenkins and J.J. Ephraums, Climate change: The IPCC Scientific Assessment, (1990), Cambridge University Press, Cambridge, UK.

[73] J.T. Houghton, B.A. Callander, and S.K. Verney, Climate change: The supplementary Report to the IPCC Scientific Assessment, (1992), Cambridge University Press, Cambridge, UK.

[74] https://www.epa.gov/ghgemissions/inventory-us-greenhouse-gas-emissions-and-sinks.

[75] https://www.epa.gov/ghgemissions/overview-greenhouse-gases.

[76] Y.B. Zeldovich, The oxidation of nitrogen in combustion and explosions, Acta Physicochimica, USSR, 21 (1946) 577–628. doi:10.1515/9781400862979.404

[77] C.P. Fenimore, Formation of nitric oxide in premixed hydrocarbon flames, Symposium (International) on Combustion, 13(1) (1971) 373–380. doi:10.1016/s0082-0784(71)80040-1.

[78] P.C. Malte and D.T. Pratt, The role of energy-releasing kinetics in NOx formation: fuel-lean, jet-stirred CO-Air combustion, Combustion Science and Technology, 9(5-6) (1974) 221-231. doi:10.1080/00102207408960360.

[79] J.W. Bozzelli and A.M. Dean, O + NNH: A possible new route for NOx formation in flames, International Journal of Chemical Kinetics, 27(11) (1995) 1097-1109.XC. doi:10.1002/kin.550271107.

[80] C.P. Fenimore and G.W. Jones, Oxidation of ammonia in flames, The Journal of Physical Chemistry, 65(2) (1961) 298–303. doi:10.1021/j100820a027

[81] R.J. Cattolica, OH radical nonequilibrium in methane-air flat flames, Symposium (International) on Combustion, 18(1) (1981) 415–416. doi:10.1016/s0082-0784(81)80046-x.

[82] M.C. Drake and R.J. Blint, Calculations of NOx formation pathways in propagating laminar, high pressure premixed CH_4/air flames, Combustion

Science and Technology, 75(4-6) (1991) 261-285. doi:10.1080/00102209108924092.

[83] S. Narayan and S. Rajan, Superequilibrium O concentrations and prompt NO formation in laminar premixed methane-air flames, Combustion Science and Technology, 139(1) (1998) 159-171. doi:10.1080/00102209808952085.

[84] J. Blauwens, B. Smets and J. Peeters, Mechanism of "prompt" NO formation in hydrocarbon flames. Symposium (International) on Combustion, 16(1) (1977) 1055–1064. doi:10.1016/s0082-0784(77)80395-0.

[85] P.V. Heberling, "Prompt NO" measurements at high pressures. Symposium (International) on Combustion, 16(1) (1977) 159–168. doi:10.1016/s0082-0784(77)80321-4.

[86] A.J. Dean, R.K. Hanson and C.T. Bowman, High temperature shock tube study of reactions of CH and C-atoms with N_2, Symposium (International) on Combustion, 23(1) (1991) 259–265. doi:10.1016/s0082-0784(06)80268-7.

[87] D. Lindackers, M. Burmeister and P. Roth, Perturbation studies of high temperature C and CH reactions with N_2 and NO, In: Proceedings Combustion Institute, 23 (1991) 251-257.

[88] J.A. Miller and S.P. Walch, Prompt-NO: Theoretical prediction of the high-pressure rate coefficient for $CH+N_2 \rightarrow HCN+N$. International Journal of Chemical Kinetics, 29(4) (1997) 253-259. doi:10.1002/(SICI)1097-4601(1997)29:4<253::AID-KIN3>3.0.CO;2-T.

[89] R.P. Lindstedt, F.C. Lockwood and M.A. Selim, Detailed kinetics modelling of chemistry and temperature effects on ammonia oxidation, Combustion Science and Technology, 99(4-6) (1994) 253-276. doi:10.1080/00102209408935436.

[90] P. Dagaut, F. Lecomte, S. Chevailler and M. Cathonnet, Experimental and detailed kinetics modeling of nitric oxide reduction by a natural gas blend in simulated reburning conditions, Combustion Science and Technology, 139(1) (1998) 329-363. doi:10.1080/00102209808952093.

[91] A.A. Konnov, Detailed Reaction Mechanism for Small Hydrocarbons Combustion, Release 0.5, (2000), http://homepages.vub.ac.be/~akonnov/

[92] G.P. Smith, D.M. Golden, M. Frenklach, N.W. Moriarty, B. Eiteneer, M. Goldenberg, C.T. Bowman, R.K. Hanson, S. Song, W.C. Gardiner, Jr, V.V. Lissianski and Z. Qin, GRI-Mech3.0, (1999), http://www.me.berkeley.edu/gri_mech/.

[93] A. El Bakali, L. Pillier, P. Desgroux, B. Lefort, L. Gasnot, J.F. Pauwels and I. da Costa, NO prediction in natural gas flames using GDF-Kin®3.0 mechanism NCN and HCN contribution to prompt-NO formation, Fuel, 85(7-8) (2006) 896-909. doi:10.1016/j.fuel.2005.10.012.

[94] J.A. Miller, M.J. Pilling and J. Troe, Unravelling combustion mechanisms through a quantitative understanding of elementary reactions, Proceedings of the Combustion Institute, 30(1) (2005) 43-88. doi:10.1016/j.proci.2004.08.281.

[95] L.V. Moskaleva and M.C. Lin, The spin-conserved reaction CH+N2→H+NCN: A major pathway to prompt no studied by quantum/statistical theory calculations and kinetic modeling of rate constant, Proceedings of the Combustion Institute, 28(2) (2000) 2393-2401. doi:10.1016/s0082-0784(00)80652-9.

[96] L.B. Harding, S.J. Klippenstein and J.A. Miller, Kinetics of CH + N_2 Revisited with Multireference Methods, The Journal of Physical Chemistry A, 112(3) (2008) 522-532. doi:10.1021/jp077526r.

[97] V. Vasudevan, R.K. Hanson, C.T. Bowman, D.M. Golden and D.F. Davidson, Shock tube of the reaction of CH with N_2 : Overall rate and branching ratio, The Journal of Physical Chemistry A, 111(46) (2007) 11818-11830. doi: 10.1021/jp075638c.

[98] R.S. Zhu and M.C. Lin, Ab initio study of the oxidation of NCN by O_2, International Journal of Chemical Kinetics, 37(10) (2005) 593-598. doi:10.1002/kin.20066.

[99] R.S. Zhu and M.C. Lin, Ab initio study on the oxidations of NCN by $O(^3P)$: prediction of the total rate constant and product branching ratios, The Journal of Physical Chemistry A, 111(29) (2007) 6766-6771. doi:10.1021/jp068991b.

[100] P. Glarborg, M.U. Alzueta, K Dam-Johansen and J.A Miller, Kinetics modeling of hydrocarbon/nitric oxide interactions in a flow reactor, Combustion and Flame, 115(1-2) (1998) 1-27. doi:10.1016/S0010-2180(97)00359-3.

[101] J.A. Sutton and J.W Fleming, Towards accurate kinetic modeling of prompt NO formation in hydrocarbon flames via the NCN pathway, Combustion and Flame, 154(3) (2008) 630- 636. doi:10.1016/j.combustflame.2008.05.009.

[102] J.A. Sutton, B.A. Williams and J.W. Fleming, Laser-induced fluorescence measurements of NCN in low-pressure $CH_4/O_2/N_2$ flames and its role in prompt NO formation, Combustion and Flame, 153(3) (2008) 465-478. doi:10.1016/j.combustflame.2007.09.008.

[103] J.A. Sutton, B.A. Williams and J.W. Fleming, Investigation of NCN and prompt-NO formation in low-pressure C1-C4 alkanes flames, Combustion and Flame, 159(2) (2012) 562-576. doi:10.1016/j.combustflame.2011.08.023.

[104] S. Gersen, A.V. Mokhov and H.B. Levinsky, Diode laser absorption measurement and analysis of HCN in atmospheric-pressure, fuel-rich premixed methane/air flames, Combustion and Flame, 155(1-2) (2008) 267-276. doi:10.1016/j.combustflame.2008.04.006.

[105] S.V. Naïk and N.M. Laurendeau, Effects of CH-NO interactions on kinetics of prompt NO in high-pressure counterflow flames, Energy & Fuels, 22(1) (2008) 250-261. doi:10.1021/ef700327a.

[106] R.J.H. Klein-Douwel, A.A. Konnov, N.J. Dam and J.J. ter Meulen, NCN concentration and interfering absorption by CH_2O, NH and OH in low pressure methane/air flames with and without N_2O, Combustion and Flame, 158(11) (2011) 2090-2104. doi:10.1016/j.combustflame.2011.04.009.

[107] A.V. Sepman, A.V. Mokhov and H.B. Levinsky, The effects of hydrogen addition on NO formation in atmospheric-pressure, fuel-rich-premixed, burner-stabilized methane, ethane and propane flames, International Journal of Hydrogen Energy, 36(7) (2011) 4474-4481. doi:10.1016/j.ijhydene.2010.12.117.

[108] A.V. Sepman, A.V. Mokhov and H.B. Levinsky, The effects of the hydrogen addition on the HCN profiles in fuel-rich-premixed, burner-stabilzed C_1-C_3 alkane flames, International Journal of Hydrogen Energy, 36(21) (2011) 13831-13837. doi:10.1016/j.ijhydene.2011.07.090.

[109] A.V. Sepman, S.E. Abtahizadeh, A.V. Mokhov, J.A. van Oijen, H.B. Levinsky and L.P.H. de Goey, Numerical and experimental studies of the NO formation in laminar coflow diffusion flames on their transition to MILD combustion regime, Combustion and Flame, 160(8) (2013) 1364-1372. doi:10.1016/j.combustflame.2013.02.027.

[110] A.A. Konnov, Implementation of the NCN pathway of prompt-NO formation in the detailed reaction mechanism, Combustion and Flame, 156(11) (2009) 2093-2105. doi:10.1016/j.combustflame.2009.03.016.

[111] A.A. Konnov, I.V. Dyakov and J De. Ruyck, Probe sampling measurements and modeling of nitric oxide formation in methane-air flames, Combustion Science and Technology, 169(1) (2001) 127-153. doi:10.1080/00102200108907843

[112] I.V. Dyakov, A.A. Konnov and J De. Ruyck, Nitric oxide formation in laminar flames of methane-oxygen-nitrogen mixtures, in proceedings: 6th International Conference on Technologies and Combustion for a Clean Environment, Vol III (2001) 1441-1449.

[113] N. Lamoureux, P. Desgroux, A. El bakali and J.F. Pauwels, Experimental and numerical study of the role of NCN in prompt-NO formation in low pressure CH_4-O_2-N_2 and C_2H_2-O_2-N_2 flames, Combustion and Flame, 157(10) (2010) 1929-1941. doi:10.1016/j.combustflame.2010.03.013.

[114] R.S. Zhu, H.M.T. Nguyen and M.C. Lin, Ab initio study on the oxidation of NCN by OH: Prediction of the total rate constant and individual rate constants, The Journal of Physical Chemistry A, 113(1) (2009) 298-304. doi:10.1021/jp805821x.

[115] N. Lamoureux, X. Mercier, C. Western, J.F. Pauwels and P. Desgroux, NCN quantitative measurement in a laminar low pressure flame, Proceedings of the Combustion Institute, 32(1) (2009) 937-944. doi:10.1016/j.proci.2008.06.043.

[116] N. Lamoureux, C.M. Western, X. Mercier and P. Desgroux, Reinvestigation of the spectroscopy of the $\tilde{A}^3\Pi_u$-$\tilde{X}^3\Sigma_g^-$ transition of the NCN radical at high temperature: application to quantitative NCN measurement in flames, Combustion and Flame, 160(4) (2013) 755-765. doi:10.1016/j.combustflame.2012.12.009.

[117] N. Lamoureux, X. Mercier, J.F. Pauwels and P. Desgroux, NCO quantitative measurement in premixed low pressure flames by combining LIF and CRDS techniques, The Journal of Physical Chemistry A, 115(21) (2011) 5346-5353. doi:10.1021/jp201453k.

[118] N. Lamoureux, H. El Merhubi, X. Mercier, J.F. Pauwels and P. Desgroux, HCN quantitative measurement in a laminar low pressure flame at 1036nm using pulsed CRDS technique, Proceedings of the Combustion Institute, 34(2) (2013) 3557-3564. doi:10.1016/j.proci.2012.06.067.

[119] G.A. Lavoie, J.B. Heywood and J.C. Keck, Experimental and theoretical study of nitric oxide formation in internal combustion engines, Combustion Science and Technology, 1(4) (1970) 313-326. doi:10.1080/00102206908952211.

[120] M.C. Drake, J.W. Ratcliffe, R.J. Blint, C.D. Carter and N.M. Laurendeau, Measurements and modeling of flame front NO formation and superequilibrium

radical concentrations in laminar high-pressure premixed flames, Symposium (International) on Combustion, 23(1) (1991) 387-395. doi:10.1016/s0082-0784(06)80283-3.

[121] A.N. Hayhurst and E.M. Hutchinson, Evidence for a new way of producing NO via NNH in fuel-rich flames at atmospheric pressure, Combustion and Flame, 114(1-2) (1998) 274-279. doi:10.1016/s0010-2180(97)00328-3.

[122] C.T. Bowman, R.K. Hanson, D.F. Davidson, W.C. Gardiner, Jr, V. Lissanski, G.P. Smith, D.M. Golden, M. Frenklach and M. Goldenberg, GRI-Mech2.11, (1995), http://www.me.berkeley.edu/gri_mech/.

[123] H. Wang, X. You, A. V.Joshi, Scott G.Davis, A. Laskin, F. Egolfopoulos and C. K. Law, USC Mech Version II. High-Temperature Combustion Reaction Model of H2/CO/C1-C4 Compounds, (2007), http://ignis.usc.edu/USC_Mech_II.htm, May.

[124] P. Li, J. Mi, B.B. Dally, F. Wang, L. Wang, Z. Liu, S. Chen and C. Zheng, Progress and recent trend in mild combustion, SCIENCE CHINA Technological Sciences, 54(2) (2011) 255–269. doi:10.1007/s11431-010-4257-0.

[125] C.E. Baukal, Jr, The John Zink Combustion Handbook. Boca Raton, FL: CRC Press, (2001).

[126] A. Milani and B. Saponaro, Diluted combustion technologies, IFRF Combustion Journal, Article 200101, (2001), ISSN-1562-479X.

[127] J.A. Wünning and J.G. Wünning, Regenerative burner using flameless oxidation, IGRC, (1995), Cannes, France.

[128] A. Milani, G.V. Salamov, J.G. Wünning, Abatment of fuel consumption with compact regenerative burners in energy-intensive furnaces, EC TGERMIE Program, (1998).

[129] M. Oberlack, R. Arlitt and N. Peters, On stochastic Damköhler number variations in a homogeneous flow reactor, Combustion Theory and Modelling, 4(4) (2000) 495-509. doi: 10.1088/1364-7830/4/4/307.

[130] S. Kumar, P.J. Paul and H.S. Mukunda, Studies on a new high-intensity low-emission burner. Proc Combust Inst, 29(1) (2002) 1131–1137. doi:10.1016/s1540-7489(02)80143-2.

[131] V.K. Arghode and A.K. Gupta, Effect of flow field for colorless distributed combustion (CDC) for gas turbine combustion, Applied Energy, 87(5) (2010) 1631–40. doi: 10.1016/j.apenergy.2009.09.032.

[132] A.K. Gupta, Thermal characteristics of gaseous fuel flames using high temperature air, Journal of Engineering for Gas Turbines and Power, 126(1) (2004) 9. doi:10.1115/1.1610009.

[133] A. Khalil, V.K. Arghode and A.K. Gupta, Distributed Combustion With Swirl for Gas Turbine Application, 49th AIAA Aerospace Sciences Meeting Including New Horizons Forum and Aerospace Exposition, (2010), Orlando, Florida. doi:10.2514/6.2011-64.

[134] V.K. Arghode, A.K. Gupta, K.M. Bryden and K.H. Yu, High intensity colorless distributed combustion for ultra low emissions and enhanced performance, 47th AIAA/ASME/SAE/ASEE Joint Propulsion Conference & Exhibit, (2011), San Diago, California. doi:10.2514/6.2011-5532.

[135] G. Szegö, B Dally, G. Nathan, Scaling of NOx emissions from a laboratory-scale mild combustion furnace, Combustion and Flame, 154(1-2) (2008) 281–295. doi:10.1016/j.combustflame.2008.02.001.

[136] M. Katsuki and T. Hasegawa, The science and technology of combustion in highly preheated air, Symposium (International) on Combustion, 27(2) (1998) 3135–3146. doi:10.1016/s0082-0784(98)80176-8.

[137] M. Castela, A.S. Veríssimo, A.M.A. Rocha and M. Costa, Experimental Study of the Combustion Regimes Occurring in a Laboratory Combustor, Combustion Science and Technology, 184(2) (2012) 243-258. doi: 10.1080/00102202.2011.630592.

[138] G.M. Choi and M. Katsuki, Advanced low NO_x combustion using highly preheated air, Energy Conversion and Management, 42 (5) (2001) 639 – 652. doi: 10.1016/S0196-8904(00)00074-1.

[139] A.G. Rao and L. Yeshayahou, A new combustion methodology for low emission gas turbine engines, 8th International Symposium on HiTACG, (2010), Poznan, Poland.

[140] T. Poinsot and D. Veynante, Theorical and numerical combustion, R. T. Edwards Inc, 2nd edition, (2005).

[141] S. Payet, Analyse de l'oxy-combustion en régime dilué par simulation des grandes échelles de la turbulence. PhD thesis, (2007), INSA de Rouen.

[142] J. Min, F Baillot, H Guo, E Domingues, M Talbaut and B Patte-Rouland, Impact of CO_2, N_2 or AR diluted in air on the length and lifting behavior of a laminar

diffusion flame, Proceedings of the Combustion Institute, 33 (1) (2011) 1071 – 1078. doi:10.1016/j.proci.2010.06.100.

[143] J. Min and F. Baillot, Experimental investigation of the flame extinction processes of non premixed methane flames inside an air coflow diluted with CO_2, N_2, or AR, Combustion and Flame, 159(12) (2012) 3502-3517. doi: 10.1016/j.combustflame.2012.05.015.

[144] E. Mastorakos, A.M.K.P Taylor, and J.H. Whitelaw, Extinction of turbulent counterflow flames with reactants diluted by hot products, Combustion and Flame, 102(1-2) (1995) 101–114. doi:10.1016/0010-2180(94)00252-n.

[145] N. Darabiha and S. Candel, The influence of the temperature on extinction and ignition limits of strained hydrogen-air diffusion flames, Combustion Science and Technology, 86 (1-6) (1992) 67–85. doi:10.1080/00102209208947188.

[146] D. Riechelmann, T. Fujimori and J. Sato, Effect of dilution on extinction of methane diffusion flame in high temperature air up to 1500 K. Combustion Science and Technology, 174 (2) (2002) 23–46. doi:10.1080/714922614.

[147] A. Cavigiolo, M. A. Galbiati, A. Effuggi, D. Gelosa and R. Rota, Mild combustion in a laboratory-scale apparatus. Combustion Science and Technology, 175(8) (2003) 1347–1367. doi:10.1080/00102200302356.

[148] A. Effuggi, D. Gelosa, M. Derudi, and R. Rota, Mild combustion of methane-derived fuel mixtures: Natural gas and biogas, Combustion Science and Technology, 180 (3) (2008) 481–493. doi:10.1080/00102200701741368.

[149] M. Derudi, A. Villani and R. Rota, Sustainability of mild combustion of hydrogen-containing hybrid fuels, Proceedings of the Combustion Institute, 31(2) (2007) 3393 – 3400. doi:10.1016/j.proci.2006.08.107.

[150] M. Mancini, P. Schweppe, R. Weber and S. Orsino, On mathematical modelling of flameless combustion, Combustion and Flame, 150(1-2) (2007) 54–59. doi:10.1016/j.combustflame.2007.03.007.

[151] E.W. Grandmaison, I. Yimer, H. A. Becker and A. Sobiesiak, The strong-jet/weak-jet problem and aerodynamic modeling of the CGRI burner, Combustion and Flame, 114(3-4) (1998) 381 – 396. doi:10.1016/s0010-2180(97)00314-3.

[152] I. Yimer, H.A. Becker and E.W. Grandmaison, The strong-jet/weak-jet problem: new experiments and CFD, Combustion and Flame, 124(3) (2001) 481–502. doi: 10.1016/S0010-2180(00)00216-9.

[153] Charles E. Baukal Jr, in Industrial Combustion Testing, Taylor & Francis Group, (2010), p. 487-504, doi: 10.1201/EBK1420085280-c24.

[154] G. Li, D. Stankovic, N. Overman, M. Cornwell, E. Gutmark and L. Fuchs, Experimental Study of Flameless Combustion in Gas Turbine Combustors, 44th AIAA Aerospace Sciences Meeting and Exhibit, (2006), Reno, Nevada. doi:10.2514/6.2006-546

[155] https://www.engr.colostate.edu/~marchese/abc2.html

[156] H.K. Chelliah, C.K. Law, T. Ueda, M.D. Smooke and F.A. Williams, An experimental and theoretical investigation of the dilution, pressure and flow-field effects on the extinction condition of methane-air-nitrogen diffusion flames. Symposium (International) on Combustion, 23(1) (1991) 503–511. doi:10.1016/s0082-0784(06)80297-3.

[157] P. Papas, J. W. Fleming and R. S. Shein son, 26th Symposium (International) on Combustion, The Combustion Institute, pp.l405-1412, 1996.

[158] K. Seshadri and F. A. Williams, Laminar flow between parallel plates with injection of a reactant at high reynolds number, International Journal of Heat and Mass Transfer, 21(2) (1978) 251–253. doi:10.1016/0017-9310(78)90230-2

[159] IK. Puri, K. Seshadri, Extinction of diffusion flames burning diluted methane and diluted propane in diluted air, Combustion and Flame, 65(2) (1986) 137–150. doi:10.1016/0010-2180(86)90015-5.

[160] R. J. Kee, J. A. Miller, and G. H. Evans, in Proceedings of the 22ND Symposium (International) on Combustion, The Combustion Institute, Pittsburgh, Pennsylvania, 1479 (1988).

[161] T. Von. Karman, NACA Tech. Mem. 1092 (1921).

[162] A. Mameri and F. Tabet, Numerical investigation of counter-flow diffusion flame of biogas–hydrogen blends: Effects of biogas composition, hydrogen enrichment and scalar dissipation rate on flame structure and emissions. Int J Hydrogen Energy, 41(3) (2016) 2011–22. doi:10.1016/j.ijhydene.2015.11.035.

[163] A. Mameri, F. Tabet and A. Hadef, Numerical investigation of biogas diffusion flames characteristics under several operation conditions in counter-flow configuration with an emphasis on thermal and chemical effects of CO_2 in the fuel mixture, Heat Mass Transfer, 53(8) (2017) 2701–2710. doi:10.1007/s00231- 017-2017-4.

[164] A. Mameri, S. Boussetla, R. Belalmi and Z. Aouachria, Combustion characterization of the mixtures biogas-syngas, strain rate and ambient pressure effects, International Journal of Hydrogen Energy, 44(39) (2019) 22478–91. doi:10. 1016/j.ijhydene.2019.05.142

[165] https://www.sandia.gov/TNF/radiation.html

[166] X.L. Zhu and J.P. Gore, The Effects of self-absorption of radiation on an opposed flow partially premixed flame, Combustion and Flame, 129(3) (2002) 42–5, doi:10. 1016/S0010-2180(02)00341-3.

[167] R.S. Barlow, A.N. Karpetis and J.H. Frank, Scalar profiles and NO formation in laminar opposed-flow partially premixed methane/air flames. Combustion and Flame, 127(3) (2001) 2102–2118. doi:10.1016/S0010-2180(01)00313-3.

[168] R.J Kee, J. Warnatz and J.A. Miller, A Fortran computer code package for the evaluation of gas-phase viscosities and diffusion coefficients, (1983), Sandia National Laboratories, SAND83-8209

[169] R.J. Kee, J.A. Miller and T.H. Jefferson, A general-purpose transportable Fortran chemical kinetics code package, (1980), Sandia National Laboratories, SAND80-8003.

[170] F.A. Williams, Combustion theory, Addison Wesley Publishing Company, (1965), Inc London.

[171] J.O. Hirschfelder, C. F. Curtis and R. B. Bird, Molecular Theory of Gases and Liquids, John Wiley, (1954), New York.

[172] M. Barriere and R. Prud'homme, Equations Fondamentales de l'Aerothermochimie, (1973), Masson.

[173] F.A. Williams, Combustion Theory**,** The Fundamental Theory of Chemically Reacting Flow Systems, (1965), Addison-Wesley.

[174] J.O. Olsson and L.L. Andersson, Sensitivity analysis based on an efficient brute-force method, applied to an experimental CH_4/O_2 premixed laminar flame. Combustion and Flame, 67(2) (1987) 99–109. doi:10.1016/0010-2180(87)90143-x

[175] R. Borghi and M. Destriau, Combustion and Flames Edition Technip, (1995), Paris.

[176] J. Lim, J. Gore and R. Viskanta, A study of the effects of air preheat on the structure of methane/air counterflow diffusion flames, Combustion and Flame, 121(1-2) (2000) 262-74. doi:10.1016/S0010-2180 (99)00137-6.

[177] A. Bhattacharya and S. Basu, An investigation into the heat release and emissions from counterflow diffusion flames of methane/dimethyl ether/hydrogen blends in air, International Journal of Hydrogen Energy, 44 (39) (2019) 22328-46. doi:10.1016/j.ijhydene.2019.06.190. 0360-3199.

[178] Y. Tu, S. Xu, M. Xu, H. Liu and W. Yang, Numerical study of methane combustion under moderate or intense low-oxygen dilution regime at elevated pressure conditions up to 8 atm. Energy, 197 (2020) 117158. doi:10.1016/ j.energy.2020.117158.

[179] G. Rozenchan, D.L. Zhu, C.K. Law and S.D. Tse, Outward propagation, burning velocities and chemical effects of methane flames up to 60 ATM. Proceeding Combustion Institute, 29(2) (2002) 1461–70. doi:10.1016/S1540-7489(02)80179-1.

[180] T. Takeno and M. Nishioka, Species conservation and emission indices for flames described by similarity solutions, Combustion and Flame, 92(4) (1993) 465–468. doi:10.1016/0010-2180(93)90157-x.

[181] J. Park, K. Lee and E. Lee, Effects of ambient pressure on flame structure of $CO/H_2/N_2$ counterflow diffusion flame, International Journal of Energy Research, 25(3) (2001) 187-205. doi:10.1002/er.671.

[182] Y. He, C. Zou, Y. Song, Y. Liu and C. Zheng, Numerical study of characteristics on NO formation in methane MILD combustion with simultaneously hot and diluted oxidant and fuel (HDO/HDF), Energy, 112 (2016) 1024–35. doi:10.1016/j.energy.2016.07.020.

[183] K. Safer, F. Tabet and M. Safer, A numerical investigation of structure and NO emissions of turbulent syngas diffusion flame in counter-flow configuration, International Journal of Hydrogen Energy, 41(4) (2016) 3208-21. doi: 10.1016/j.ijhydene.2015.12.154.

[184] R. Selfarski, J. Sacha and P. Grzymislavski, Combustion of mixtures of biogases and syngases with methane in strong swirl flow, 6th European Combustion Meeting, (2013), Lund, Sweden.